NEW SOLUTIONS OF HALF-SPACE CONTACT PROBLEMS USING POTENTIAL THEORY, SURFACE ELASTICITY AND STRAIN GRADIENT ELASTICITY

A Dissertation

by

SONGSHENG ZHOU

Submitted to the Office of Graduate Studies of
Texas A&M University
in partial fulfillment of the requirements for the degree of

DOCTOR OF PHILOSOPHY

December 2011

Major Subject: Mechanical Engineering

New Solutions of Half-Space Contact Problems Using Potential Theory, Surface Elasticity and Strain Gradient Elasticity

NEW SOLUTIONS OF HALF-SPACE CONTACT PROBLEMS USING POTENTIAL THEORY, SURFACE ELASTICITY AND STRAIN GRADIENT ELASTICITY

A Dissertation

by

SONGSHENG ZHOU

Submitted to the Office of Graduate Studies of
Texas A&M University
in partial fulfillment of the requirements for the degree of

DOCTOR OF PHILOSOPHY

Approved by:

Chair of Committee,	Xin-Lin Gao
Committee Members,	Miladin Radovic
	Steve Suh
	Theofanis Strouboulis
Head of Department,	Jerald A. Caton

December 2011

Major Subject: Mechanical Engineering

ABSTRACT

New Solutions of Half-Space Contact Problems Using Potential Theory, Surface Elasticity and Strain Gradient Elasticity. (December 2011)

Songsheng Zhou, B.Sc.; M.Sc., Wuhan University of Technology

Chair of Advisory Committee: Dr. Xin-Lin Gao

Size-dependent material responses observed at fine length scales are receiving growing attention due to the need in the modeling of very small sized mechanical structures. The conventional continuum theories do not suffice for accurate descriptions of the exact material behaviors in the fine-scale regime due to the lack of inherent material lengths. A number of new theories/models have been propounded so far to interpret such novel phenomena. In this dissertation a few enriched-continuum theories – the adhesive contact mechanics, surface elasticity and strain gradient elasticity – are employed to study the mechanical behaviors of a semi-infinite solid induced by the boundary forces.

A unified treatment of axisymmetric adhesive contact problems is developed using the harmonic functions. The generalized solution applies to the adhesive contact problems involving an axisymmetric rigid punch of arbitrary shape and an adhesive interaction force distribution of any profile, and it links existing solutions/models for axisymmetric non-adhesive and adhesive contact problems like the Hertz solution, Sneddon's solution, the JKR model, the DMT model and the M-D model.

The generalized Boussinesq and Flamant problems are examined in the context of the surface elasticity of Gurtin and Murdoch (1975, 1978), which treats the surface as a negligibly thin membrane with material properties differing from those of the bulk. Analytical solution is derived based on integral transforms and use of potential functions. The newly derived solution applies to the problems of an elastic half-space (half-plane as well) subjected to prescribed surface tractions with consideration of surface effects. The newly derived results exhibit substantial deviations from the classical predictions near the loading points and converge to the classical ones at a distance far away from those points. The size-dependency of material responses is clearly demonstrated and material hardening effects are predicted.

The half-space contact problems are also studied using the simplified strain gradient elasticity theory which incorporates material microstructural effects. The solution is obtained by taking advantage of the displacement functions of Mindlin (1964) and integral transforms. Significant discrepancy between the current and the classical solutions is seen to exist in the immediate vicinity of the loading area. The discontinuity and singularity exist in classical solution are removed, and the stress and displacement components change smoothly through the solid body.

DEDICATION

To my parents and grandparents

for their love, guidance and encouragement.

ACKNOWLEDGEMENTS

I wish to express my gratitude to my advisor, Dr. Xin-Lin Gao for his support and guidance throughout the duration of my Ph.D. study.

I am most grateful to my parents for their consistent support and encouragement.

I also would like to express my love and gratitude to my dear friends.

This work would not have been possible without the support and encouragement from all of you. Thank you.

Songsheng Zhou

Texas A&M University

December 2011

TABLE OF CONTENTS

LIST OF FIGURES

LIST OF TABLES

1. INTRODUCTION

1.1 Technical Advances and Challenges

The past century has witnessed the rapid development of micro/nano-technologies, which deal with structures or components of extremely small sizes. This technical advance has brought about revolutionary devices that are of cutting-edge interest. To realize the full potential of the emerging micro/nano-industry it is essential that relevant studies be conducted to gain a fundamental understanding of the material behaviors at small length scales.

Numerious experimental studies have indicated that the classical continuum theories are inadequate to accurately describe the material response at micron and nano-meter scales, where materials are frequently reported to exhibit increased stiffness with decreasing sample size, e.g. torsion stiffness of wires (e.g., Flect and Hutchinson, 1993), bending stiffness of plates and bars (Miller and Shenoy, 2000), indentation hardness (e.g., Stelmashenko *et al*., 1993; De Guzman *et al.*, 1993; Ma and Clarke, 1995), tensile strength of ultra-thin films (e.g., Judelewicz *et al*., 1994; Hong and Weil, 1996; Read, 1998; Zhang *et al*., 2008;). The classical continuum mechanics cannot describe this microstructure-dependent size effect due to the lack of inherent material length parameters. Hence, higher order continuum theories that contain material length scale parameters are needed to capture the size and other effects at the micron and nanometer scales.

This dissertation follows the style of Journal of the Mechanics and Physics of Solids.

1.2 Review of Existing Studies

1.2.1 Adhesive Contact

Forces at interfaces are familiar to colloid and surface chemists. For a long time relevant studies and measurements have been mainly confined to liquids. It is not until 1930s that considerable efforts were made to the understanding of the surface interaction forces between solids and particular between colloids. The dispersion forces were first explained by London in 1930 (Maugis, 1992; Tabor, 1977) and the London theory of Van der Waals was later applied by Bradley (1932), Derjaguin (1934), de Boer (1936) and Hamaker (1937) to the problem of forces between macroscopic bodies.

Surface forces can make a significant contribution to the contact equilibrium under conditions of light loading between elastic solids, e.t. contact at the micron and submicron scales. In the later 1960s, experimental contradictions to the famous Hertz theory (Hertz, 1882) were reported by Roberts (1968) and Kendall (1969), which revealed that the contact area between elastic bodies is considerably larger than the Hertz result at low loads. In addition, the contact area does not vanish upon the removal of loads, and a mechanical load is required to separate two solid bodies in intimate contact (e.g. Adamson, 1967; Tabor and Winterton, 1969). These and other evidence suggested that attractive forces act between solids close together and their influence on the material response cannot be neglected at low loads (Johnson *et al*., 1971).

The concept of adhesive forces between elastic solids in contact was propound in the 1960s and improved understanding of the adherence of solids was gained with the introduction of the energy balance concept by Kendall (1971) and Johnson *et al*. (1971).

Their energy balance approach was successfully applied to problems of peeling (Kendall, 1973, 1975b), adherence of spheres (Johnson *et al*., 1971), composite (Kendall, 1975a, 1976) and etc. The adhesive contact model of Johnson *et al*. (1971) (known as the JKR model) accounts for the adhesion inside the contact zone and the surface energy is included in the energy balance involving the strain energy and potential energy additionally. An extensive experimental investigation regarding the energy release rate and system stability was later conducted by Maugis and Barquins (1978).

Not long after the publication of the paper of Johnson *et al*. (1971), Derjaguin *et al*. (1975) proposed a model (called DMT model) that considers the molecular attractions in a ring-shaped zone right outside the contact area (the non-contact adhesion). The two theories – JKR and DMT – are essentially different from each other although they are both evolved from Hertz's solution and both give an equilibrium contact area larger than Hertz's result. The sharp differences between these two landmarked models led to a long and heated debate in the 1980s (e.g., Muller *et al*., 1980, 1982, 1983; Greenwood and Johnson, 1981; Pashley, 1984) and the controversy was finally resolved by Maugis' (1992) transition model (called the M-D model) based on the Dugdale cohesive zone model and the Griffith energy criterion in fracture mechanics.

The Maugis' (1992) work bridges the JKR and DMT models via a transition parameter similar to Tabor's number (Tabor, 1977) and thereby greatly clarifies the distinctions between the two theories. The JKR model and DMT models are found to be two limiting cases of the general M-D model. It is now widely acknowledged that the

former is accurate for soft solids having high surface energy whereas the latter is suitable for hard materials with low surface energy (e.g., Tabor, 1977; Hughes and White, 1979; Muller *et al*., 1980; Johnson and Greenwood, 1997; Yao *et al*., 2007; Barthel, 2008; Zhou *et al*., 2011).

These three monumental models – JKR, DMT and M-D – have been receiving growing attention due to the need of knowledge in micro-/nano-contact. The M-D adhesive contact model involving a spherical punch and a constant cohesive stress has been extended by Barthel (1998) and Greenwood and Johnson (1998) to more general surface interactions and by Goryacheva and Makhovskaya (2001) and Zheng and Yu (2007) to arbitrary axisymmetric punch profiles. The M-D model has also been generalized to the non-slipping adhesive contact of an elastic cylinder with a stretched substrate by Chen and Gao (2006a). Recently, a potential function based treatment was provided by Zhou *et al*. (2011) which unifies existing solutions/models for axisymmetric non-adhesive and adhesive contact problems in one framework.

The interaction surface forces used in the aforementioned references were infinitesimal-range forces. Finite-range interaction forces were employed by Attard and Parker (1992) and Attard (2000) to consider the interaction of spherical bodies. In addition, Graham *et al*. (2010) analyzed the nano-indentation problems involving sphero-concical tips due to realistic, finite-range surface forces.

1.2.2 Surface Elasticity

In classical continuum mechanics, the material properties of the solid surfaces are regarded to be the same as those of the bulk material. This ignores the fact that the

near surface physical properties are sensibly different from those of the bulk interior. The reason for such difference is that the nature of the chemical bonding of the surface atoms differs from that of the interior atoms and the surface atomic structure changes relative to the bulk so that the structure equilibrium is maintained (Thomson *et al*., 1986; Cammarata, 1994).

Mechanical work is required to create a new surface. The concept of surface energy is defined as the reversible work to isothermally create an element area of a new surface (Cammarata and Sieradzki, 1994; Maugis 2000, pp28). It has been known that the surface energy is identical to the surface tension for a fluid (Dupré, 1869), but they are not equal for solids as was first shown by Gibbs (1876). The presence of the surface stress is predicted from microscopic considerations whenever a new surface is created (Shuttleworth, 1950; Herring, 1951; Orawan, 1970). It was verified experimentally by Nicolson (1955) that certain crystals exhibit a surface stress when cleaved.

The studiess of Shuttleworth (1950) and Herring (1951) firstly connect the surface tension to the surface energy of a solid. Their seminal findings were elaborated by the subsequent researchers (e.g., Cammarata, 1994; Cammarata and Sieradzki, 1994) and were successfully applied to cases such as crystal surface morphology (Shchukin and Bimberg, 1999) and thin films (e.g., Koch, 1994; Streitz *et al*. 1994).

The surface free energy is associated with only a few layers of atoms near the surface and is typically neglected in traditional continuum mechanics (Dingreville *et al*., 2005). For a solid of macro-dimension its surface energy is relatively negligible when compared to its bulk energy. However, the surface energy is appreciable at small length

scales and the influence of surface stress on the material behavior is significant, especially for dimensions below 10 nm (Cammarat, 1994).

Blinowski (1970, cf. Povstenko (1993)) suggested a constitutive equation that incorporates the surface stresses, but his formulation lacks mathematical rigor. It is due to Gurtin and Murdoch (1975, 1978) that a rigorous theory for surface elasticity was established. In the Gurtin-Murdoch model, the surface is treated as a negligibly thin membrane adhering to the underlying bulk without slipping. This model is quite general in the sense that it allows the surface to possess its own elastic constants and stress by an additional constitutive law. The model was later extended by Gurtin *et al*. (1998) to treat interfacial stress. As noted in Gurtin and Murdoch (1978), their general theory can also be applied to describe the mechanical behaviors of an elastic substrate coated with thin film of another material.

The special importance of the theory of Gurtin and Murdoch (1975, 1978) is that it contains intrinsic material lengths arisen from the surface effects and thereby it offers an explanation for size effects at fine scales, especially when the associated solid has a large surface to bulk ratio. This theory has received a lot of attention in recent years due to the progress in micro-/nano-materials and devices. In particular, simplified versions (by retaining only the surface residual stress) of the Gurtin-Murdoch theory have been used to analyze responses of nano-structures (Miller and Shenoy, 2000; Shenoy, 2002), deformation of semi-infinite solids (He and Lim, 2006; Wang and Feng, 2007; Zhao and Rajapakse, 2009), deflections of thin films (He *et al*., 2004) and inclusion problems (Sharma *et al*., 2003; Sharma and Ganti, 2004). All these studies show that the presence

of surface/interface stresses results in size-dependent elastic responses.

1.2.3 Higher-Order Strain Gradient Theories

The micro-structural effects are important at small length scales, particularly for materials like polymer, polycrystalline and granular materials. A common approach to incorporating the microstructural effects is to enrich the classical constitutive equations with additional higher-order derivatives.

In the early 20^{th} century, the Cosserat brothers (Cosserat and Cosserat, 1909) generalized Cauchy's model to include additionally the micro-rotation in an elastic solid and thereby included the couple stress (energetically conjugated to the micro-rotation) in the equilibrium equations. It was not until 1960s that this higher order continuum approach received serious attention. Casal (1961) formulated a simple linear continuum theory that incorporates material microstructures. The framework for gradient theories was latter established by Mindlin and his associates (1964, 1965; Mindlin and Tiersten 1962; Mindlin and Eshel, 1968), Toupin (1962, 1964) and Kioter (1964). Germain (1972, 1973a,b) later addressed several theoretical issues to strain gradient elasticity.

In gradient theories, material length scale parameters enter the constitutive equations through the strain energy density function. In a landmark paper, Mindlin (1964) introduced the idea of unit cell (or micro-media) in solids that are in themselves deformable media and considered micro-deformations in addition to macro-deformation. In its most general form, Mindlin's theory contains 18 material constants (two being Lam é constants) and was simplified to contain five additional material constants by himself (Mindlin, 1964).

Mindlin's original theories are general but complicated. One would face considerable difficulties attempting to solve even simple boundary value problems (BVPs) with these general theories (Georgiadis and Anagnostou, 2008). Besides, the experimental quantification of the associate material constants is a formidable task (Exadaktylos and Vardoulakis, 1998). As a result, the Mindlin's original theories have not found widespread applications in the modeling of size-dependent phenomena.

To progress from this situation, simplified strain gradient theories have been suggested (e.g., Vardoulakis *et al*., 1996; Exadaktylos *et al*., 1996; Altan and Aifantis, 1992, 1997). Vardoulakis' version contains volume and surface energy strain gradient terms, whereas Altan and Aifantis' includes one additional material constant. These simplified models are mathematically more tractable and have been adopted to analyze various problems, such as Kelvin's problems (Karlis *et al*., 2010), fracture (Exadaktylos, 1998; Shi *et al*., 2000; Georgiadis, 2003), mechanics of defects (Lazar and Maugin, 2005), thick-walled shell problem (Goa and Park, 2007; Gao *et al*., 2009) and Eshelby type inclusion problem (Gao and Ma, 2009, 2010a,b).

Despite the successful applications of strain gradient elasticity, the fundamental problems of a half-plane or half-space subjected to a concentrated force have not been well addressed in gradient elasticity.

1.3 Motivations and Objectives

As reviewed in the last section, the mechanisms of non-conventional behaviors at small length scales have not been fully understood and some fundamental issues have

not been thoroughly discussed. In this dissertation, several fundamental problems in contact mechanics are studied in the context of adhesive contact mechanics, surface elasticity and strain gradient elasticity.

The fundamental problems of an elastic isotropy subjected to a concentrated force are viewed as the most celebrated problems in the theory of elasticity. In classical doctrine, the problems of Kelvin (an elastic solid of infinite extend acted by a point force), Boussinesq/Cerruti (an elastic half-space subjected to surface normal/tangential force) and Mindlin (an elastic half-space under the action of a buried force) afford closed-form solutions and are of significant importance in the field of contact mechanics, tribology and soil mechanics. However, these fundamental problems have not been fully examined in the context of the newly proposed enriched continuum theories reviewed in the last section.

In this dissertation we shall be concerned with the small-scale elastic response of a homogeneous semi-infinite isotropy subjected to prescribed boundary tractions. The fundamental contact problems will be examined in the context of the three renowned theories outlined in the preceding section – adhesive contact mechanics, surface elasticity and gradient elasticity. It is expected that certain types of size-dependency be observed when each of these refined continuum theory is adopted. Special attentions shall be drawn to the possible deviation of the newly derived solutions from the classical ones.

The role of adhesive interaction forces is significant for the material responses of contact solid bodies under small load. A general model will be developed for

axisymmetric contact problems by using classical elasticity theory and incorporating the effect of adhesive interaction forces. This general model is expected to be applicable for adhesive contact problems with arbitrary punch profiles and adhesive interaction force distributions.

At small length scale the influences of material microstructural and surface energy effects on the mechanical behaviors of materials are non-negligible. The surface elasticity of Gurtin and Murdoch (1975, 1978) and strain gradient elasticity theory of Mindlin (1964) will be adopted to study the elastic field of a semi-infinite solid subjected to prescribed boundary tractions. For the fundamental problems of an elastic half-space, the existing surface elasticity-based (e.g., He and Lim, 2006; Wang and Feng, 2007; Zhao and Rajapakse, 2009) and strain gradient-based solutions (e.g., Zhou and Jin, 2003; Li *et al.*, 2004) involve certain simplifications/assumptions and thus these solutions are either incomplete or not exact. A complete formulation and exact solutions shall be pursued by using the two theories – surface elasticity and strain gradient elasticity – and the departure between the newly derived solutions and their classical counterparts will be examined and discussed.

2. A UNIFIED TREATMENT OF AXISYMMETRIC ADHESIVE CONTACT PROBLEMS*

2.1 Introduction

Contact of two elastic solids was first studied by Hertz (1882) using the theory of elasticity. Hertz's solution is for the frictionless non-adhesive contact of two elastic spheres under a pair of compressive forces, which was reviewed and elaborated by Johnson (1982) in a broad context. To account for the adhesion inside the contact zone, Johnson *et al*. (1971) extended Hertz's theory and developed an adhesive contact model (known as the JKR model) by including the surface energy in the energy balance involving the strain energy and potential energy additionally, which yields an equilibrium contact area larger than that given by the Hertz solution.

On the other hand, by considering the molecular attractions in a ring-shaped zone right outside the contact area, Derjaguin *et al*. (1975) proposed another model (called DMT model), which adopts Hertz's stress distribution and displacement field but predicts a larger contact radius than that predicted by Hertz's theory due to the incorporation of the non-contact adhesion in the ring-shaped zone. The JKR and DMT models are found to work well for two extreme cases, with the former being accurate for soft solids having high surface energy and the latter valid for hard materials with low surface energy (e.g., Tabor, 1977; Hughes and White, 1979; Muller *et al*., 1980; Johnson

---

* Reprint with permission from ''A unified treatment of axisymmetric adhesive contact problems using the harmonic potential function method'' by S.-S. Zhou, X.-L. Gao and Q.-C. He, 2011, *Journal of the Mechanics and Physics of Solids*, 59, 145-159, Copyright [2011] by Elsevier.

and Greenwood, 1997; Yao *et al*., 2007; Barthel, 2008).

The sharp differences between these two models were resolved by Maugis' (1992) transition model (called the M-D model) based on the Dugdale cohesive zone model and the Griffith energy criterion in fracture mechanics. The M-D adhesive contact model involving a spherical punch and a constant cohesive stress has been extended by Barthel (1998) and Greenwood and Johnson (1998) to more general surface interactions and by Goryacheva and Makhovskaya (2001) and Zheng and Yu (2007) to an 'arbitrary' axisymmetric punch represented by a power-law shape function. The M-D model for frictionless adhesive contact has also been generalized to the no-slipping adhesive contact of an elastic cylinder with a stretched substrate by Chen and Gao (2006a), who also extended the JKR model to no-slipping adhesive contact problems involving isotropic and transversely isotropic materials (Chen and Gao, 2006b, 2007).

The original M-D model and the subsequently modified models mentioned above are built on Sneddon's (1965) Hankel transform-based solution for the frictionless contact problem (involving an axisymmetric punch of arbitrary profile) and the solution of Lowengrub and Sneddon (1965) for an external crack problem. In this strain energy release rate-based approach (Maugis, 1992, 2000), evaluations of some crucial parameters, such as stress intensity factor and applied normal load, are quite challenging, and the interpretation of the energy balance in terms of the strain energy release rate can be difficult at times (Greenwood and Johnson, 1998).

On the other hand, the harmonic potential function method for axisymmetric elasticity problems developed by Green (1949) and Collins (1959, 1963) and elaborated

in Green and Zerna (1968) has been found to exhibit significant advantages in solving axisymmetric half space problems with mixed boundary conditions (e.g., Barber, 1983; Chaiyat *et al*., 2008; Jin *et al*., 2008). However, this method has not been systematically explored for its use in studying adhesive contact problems of axisymmetric elastic bodies, for which the JKR model, the DMT model, and the M-D model and its variants have been developed using the Hertz theory (1882) or Sneddon's (1965) solution. This motivated the current study.

In the present paper, a unified treatment of non-adhesive and adhesive axisymmetric contact problems is provided using the harmonic potential function method. Based on this method and the principle of superposition, a general solution for the adhesive contact problem involving an axisymmetric rigid punch of arbitrary shape and an adhesive interaction force distribution of any profile is derived, which gives analytical expressions for all non-zero displacement and stress components on the contact surface, differing from other solutions. It is demonstrated that Sneddon's axisymmetric punch solution, Boussinesq's flat punch solution, Hertz's spherical punch solution, the JKR model, the DMT model, the M-D model, and the M-D-*n* model, which were developed individually using various methods (other than the harmonic function method) over the years, can all be reduced from the current general solution as special/limiting cases.

2.2 Harmonic Potential Function Method

For an axisymmetric problem of a homogeneous, isotropic, linearly elastic

material, the general elasticity solution can be written in terms of a harmonic (potential) function $\phi = \phi(r, z)$ as (e.g., Green and Zerna, 1968)

$$\sigma_{rr} = z\frac{\partial^3\phi}{\partial r^2\partial z} + \frac{\partial^2\phi}{\partial r^2} + \frac{2\nu}{r}\frac{\partial\phi}{\partial r}, \quad \sigma_{\theta\theta} = -\frac{\partial^2\phi}{\partial z^2} - (1-2\nu)\frac{\partial^2\phi}{\partial r^2} + \frac{z}{r}\frac{\partial^2\phi}{\partial r\partial z}, \quad \sigma_{zz} = z\frac{\partial^3\phi}{\partial z^3} - \frac{\partial^2\phi}{\partial z^2},$$
$$\sigma_{r\theta} = 0, \quad \sigma_{\theta z} = 0, \quad \sigma_{rz} = z\frac{\partial^3\phi}{\partial r\partial z^2},$$
$$u_r = \frac{1}{2\mu}\left[z\frac{\partial^2\phi}{\partial r\partial z} + (1-2\nu)\frac{\partial\phi}{\partial r}\right], \quad u_\theta = 0, \quad u_z = \frac{1}{2\mu}\left[-2(1-\nu)\frac{\partial\phi}{\partial z} + z\frac{\partial^2\phi}{\partial z^2}\right], \tag{2.1}$$

where (r, θ, z) are the usual cylindrical coordinates, μ and ν are, respectively, the shear modulus and Poisson's ratio of the material, $\sigma_{ij} = \sigma_{ij}(r, z)$ are the stress components, and $u_i = u_i(r, z)$ are the displacement components.

In particular, on the plane $z = 0$, Eq. (2.1) gives

$$\sigma_{rr}\big|_{z=0} = \left.\frac{\partial^2\phi}{\partial r^2}\right|_{z=0} + \left.\frac{2\nu}{r}\frac{\partial\phi}{\partial r}\right|_{z=0}, \quad \sigma_{\theta\theta}\big|_{z=0} = -\left.\frac{\partial^2\phi}{\partial z^2}\right|_{z=0} - (1-2\nu)\left.\frac{\partial^2\phi}{\partial r^2}\right|_{z=0}, \quad \sigma_{zz}\big|_{z=0} = -\left.\frac{\partial^2\phi}{\partial z^2}\right|_{z=0},$$
$$\sigma_{r\theta}\big|_{z=0} = 0, \quad \sigma_{\theta z}\big|_{z=0} = 0, \quad \sigma_{rz}\big|_{z=0} = 0,$$
$$u_r\big|_{z=0} = \frac{1-2\nu}{2\mu}\left.\frac{\partial\phi}{\partial r}\right|_{z=0}, \quad u_\theta\big|_{z=0} = 0, \quad u_z\big|_{z=0} = -\frac{1-\nu}{\mu}\left.\frac{\partial\phi}{\partial z}\right|_{z=0}, \tag{2.2}$$

which show that all the shear stress components vanish on the $z = 0$ plane.

Clearly, the solution for a given axisymmetric problem hinges on the determination of the harmonic function $\phi(r, z)$. This will depend on the boundary conditions of the problem.

An illuminating discussion on using the harmonic function method to solve axisymmetric mixed boundary value problems and many useful expressions have been

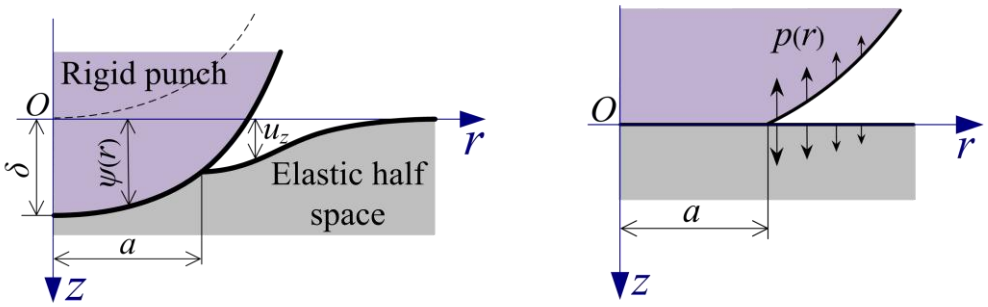

(a) Displacement prescribed inside (0, *a*)

(b) Traction prescribed outside (0, *a*)

Figure 2.1. Schematic of two different types of contact problems.

provided by Barber (1983). Also, some important contributions to fracture mechanics have recently been made by Chaiyat *et al*. (2008) and Jin *et al*. (2008) utilizing this method. The current formulation of non-adhesive and adhesive contact problems is greatly facilitated by the findings of these studies.

This harmonic potential function method has also been extended to solve non-axisymmetric elasticity problems by Keer (1964) and in other subsequent studies.

2.3 Two Types of Contact Problems

Consider the problem of a rigid axisymmetric punch of arbitrary shape in contact with an elastic half space. The following two types of boundary conditions (BCs) will be discussed: (1) displacement prescribed inside the contact zone, as shown in Figure 2.1a; (2) traction prescribed outside the contact zone, as illustrated in Figure 2.1b.

For the first type, the normal stresses inside and outside the contact zone and the

displacements outside it will be sought. An example of this type is Hertz's (1882) contact problem. For the second type, the displacements outside the contact zone and the normal stresses inside it are to be found. External circular crack problems in fracture mechanics belong to this type.

To solve the axisymmetric contact problems schematically shown in Figure 2.1, the following harmonic function is adopted:

$$\phi = -\int_0^\infty \frac{1}{\xi} A(\xi) e^{-z\xi} J_0(\xi r) d\xi, \tag{2.3}$$

where J_0 is the Bessel function of the first kind of the zeroth order, and

$$A(\xi) = \int_{r_i}^{r_o} g(t) \cos(\xi t) dt, \tag{2.4}$$

with $g(t)$ being an unknown function to be determined from boundary conditions, and r_i, r_o being the inner and outer radii of the axisymmetric circular area on the plane $z = 0$ under consideration. For the problems shown in Figure 2.1, $r_i = 0$ and $r_o = a$ inside the contact zone, and $r_i = a$ and $r_o = \infty$ outside it. It can be readily proved that $\phi = \phi(r, z)$ defined in Eqs. (2.3) and (2.4) satisfies Laplace's equation and is therefore a harmonic function. Equations (2.3) and (2.4) were recently used by Jin *et al*. (2008), with specified values of r_i and r_o, to solve an external circular crack problem. Equation (2.3) and an expression similar to Eq. (2.4) (containing $\sin(\xi t)$ rather than $\cos(\xi t)$) were employed earlier to solve penny-shaped and other internal crack problems (Kassir and Sih, 1975; Chen and Keer, 1993; Chaiyat *et al*., 2008). This harmonic function is adopted in the current study to solve non-adhesive and adhesive contact problems involving axisymmetric punches of arbitrary shapes and BCs of both types.

From Eqs. (2.3) and (2.4), the surface values of the derivatives of ϕ involved in Eq. (2.2) can be readily obtained. These are listed in Table 2.1 separately for the two different types of BCs shown in Figure 2.1.

In Table 2.1, ϕ_1 and ϕ_2 denote, respectively, the harmonic functions satisfying the first type of BCs and the second type of BCs, $H(x)$ is the Heaviside function defined by $H(x)=\begin{cases}0 & x<0\\ 1 & x\geq 0\end{cases}$, and $g_1(x)$ (for ϕ_1) and $g_2(x)$ (for ϕ_2) are the unknown functions to be determined from BCs in each problem.

It can be shown from Table 2.1 that the relation:

$$\left.\frac{\partial^2\phi}{\partial r^2}\right|_{z=0}=-\frac{1}{r}\left.\frac{\partial\phi}{\partial r}\right|_{z=0}-\left.\frac{\partial^2\phi}{\partial z^2}\right|_{z=0} \tag{2.5a}$$

holds for both types of BCs mentioned above. It then follows from Eqs. (2.2) and (2.5a) that the surface values of the radial and circumferential stress components can be expressed as

$$\sigma_{rr}\big|_{z=0}=-\frac{1-2\nu}{r}\left.\frac{\partial\phi}{\partial r}\right|_{z=0}+\sigma_{zz}\big|_{z=0},\quad \sigma_{\theta\theta}\big|_{z=0}=\frac{1-2\nu}{r}\left.\frac{\partial\phi}{\partial r}\right|_{z=0}+2\nu\sigma_{zz}\big|_{z=0}. \tag{2.5b,c}$$

Equations (2.5b,c) are applicable to both types of BCs and are valid in the entire domain, and they will be used to obtain the expressions of the two in-plane normal stresses.

From Table 2.1 and Eq. (2.2), the normal load (P) and the stress intensity factor (K_{I} for Mode I loading) at the periphery of the contact area (as the front of an external Mode I circular crack) can also be readily obtained. The relevant results are listed in Table 2.2, which are the same as those provided in Barber (1983) using more general harmonic potential functions.

Clearly, the normal load P and the stress intensity factor K_{I} will become immediately available once the unknown functions $g_1(x)$ and $g_2(x)$ have been determined from BCs.

Table 2.1 Surface values of derivatives of the harmonic functions for the two types of boundary conditions

		$r < a$	$r > a$
First type (Displacement prescribed inside the contact zone)	$\left.\frac{\partial \phi_1}{\partial r}\right\|_{z=0}$	$\frac{1}{r}\int_0^a g_1(t)dt - \frac{1}{r}\int_r^a \frac{tg_1(t)}{\sqrt{t^2-r^2}}dt$	$\frac{1}{r}\int_0^a g_1(t)dt$
	$\left.\frac{\partial \phi_1}{\partial z}\right\|_{z=0}$	$\int_0^r \frac{g_1(t)}{\sqrt{r^2-t^2}}dt$	$\int_0^a \frac{g_1(t)}{\sqrt{r^2-t^2}}dt$
	$\left.\frac{\partial^2 \phi_1}{\partial z^2}\right\|_{z=0}$	$-\frac{g_1(a)}{\sqrt{a^2-r^2}} + \int_r^a \frac{g_1'(t)}{\sqrt{t^2-r^2}}dt$	0
Second type (Traction prescribed outside the contact zone)	$\left.\frac{\partial \phi_2}{\partial r}\right\|_{z=0}$	$\frac{1}{r}\int_a^\infty \left[g_2(t) - \frac{tg_2(t)}{\sqrt{t^2-r^2}}\right]dt$	$\frac{1}{r}\int_a^\infty g_2(t)dt - \frac{1}{r}\int_r^\infty \frac{tg_2(t)}{\sqrt{t^2-r^2}}dt$
	$\left.\frac{\partial \phi_2}{\partial z}\right\|_{z=0}$	0	$\int_a^r \frac{g_2(t)}{\sqrt{r^2-t^2}}dt$
	$\left.\frac{\partial^2 \phi_2}{\partial z^2}\right\|_{z=0}$	$\frac{g_2(a)}{\sqrt{a^2-r^2}} + \int_a^\infty \frac{g_2'(t)}{\sqrt{t^2-r^2}}dt$	$\int_r^\infty \frac{g_2'(t)}{\sqrt{t^2-r^2}}dt$

Table 2.2 Normal load and stress intensity factor

	First type	Second type
$P = -\int_0^\infty 2\pi r \sigma_{zz}\|_{z=0}\, dr$	$-2\pi\int_0^a g_1(r)dr$	$-2\pi\int_a^\infty g_2(r)dr$
$K_{\mathrm{I}} = \lim_{r\to a^-}\left(\sqrt{a^2-r^2}\,\sigma_{zz}\|_{z=0}\right)$	$g_1(a)$	$-g_2(a)$

2.3.1 Problems with BCs of the First Type

Applying a normal load P^I on the rigid axisymmetric punch will lead to a rigid-body displacement δ (also known as the depth of penetration of the tip of the punch) and a circular contact area of radius a. The elastic half space after contact is schematically shown in Figure 2.1a. The BCs of the first type can be expressed as

$$\begin{aligned} &u_z = \psi(r) \equiv \delta - f(r), && z = 0, \quad r < a; \\ &\sigma_{zz} = 0, && z = 0, \quad r > a; \\ &\sigma_{rz} = \sigma_{\theta z} = 0, && z = 0, \quad 0 < r < \infty, \end{aligned} \tag{2.6a-c}$$

where $f(r)$ is the shape function of the axisymmetric punch. Note that Eq. (2.6c) is automatically satisfied by the general solution given in Eq. (2.2), irrespective of the expression of ϕ. Also, since $\partial^2\phi_1/\partial z^2 = 0$ outside the contact zone (i.e., $z = 0$, $r>a$) (see Table 2.1), it follows from Eq. (2.2) that Eq. (2.6b) is exactly met. Upon using Eq. (2.2) and $\partial\phi_1/\partial z$ (for $z = 0$, $r < a$) listed in Table 2.1, Eq. (2.6a), the only remaining boundary condition, has the form:

$$-\frac{1-\nu}{\mu}\int_0^r \frac{g_1(t)}{\sqrt{r^2 - t^2}}\,dt = \psi(r). \tag{2.7}$$

This integral equation can be solved by the inverse Abel transform (or using a direct procedure of integration and differentiation similar to that employed in Green and Zerna (1968)) to obtain

$$g_1(t) = -\frac{2\mu}{\pi(1-\nu)}\left[\psi(0) + \int_0^t \frac{t\psi'(x)}{\sqrt{t^2 - x^2}}\,dx\right]. \tag{2.8}$$

With $\psi(r) \equiv \delta - f(r)$ and $f(0) = 0$ (i.e., the origin of the cylindrical coordinate system coincides with the tip of the punch before indenting occurs), Eq. (2.8) becomes

$$g_1(t) = -\frac{2\mu}{\pi(1-\nu)}\left[\delta - \int_0^t \frac{tf'(x)}{\sqrt{t^2-x^2}}\,dx\right]. \tag{2.9}$$

Therefore, for given punch shape function $f(r)$ and penetration δ, the explicit expression of $g_1(t)$ can be readily obtained from Eq. (2.9).

Using Eq. (2.9) and the derivative expressions from Table 2.1 in Eq. (2.2) will then yield the out-of-plane displacement and normal stress components on the contact surface as

$$u_z^I\big|_{z=0} = \frac{2}{\pi}\left[\delta \sin^{-1}\frac{a}{r} - \sqrt{r^2-a^2}\int_0^a \frac{tf(t)}{(r^2-t^2)\sqrt{a^2-t^2}}\,dt\right], \quad r > a; \tag{2.10a}$$

$$\sigma_{zz}^I\big|_{z=0} = -\frac{2\mu}{\pi(1-\nu)}\left\{\frac{1}{\sqrt{a^2-r^2}}\left[\delta - \int_0^a \frac{af'(t)}{\sqrt{a^2-t^2}}\,dt\right] + \int_r^a \int_0^x \frac{[tf'(t)]'}{\sqrt{(x^2-t^2)(x^2-r^2)}}\,dtdx\right\}, \quad r < a. \tag{2.10b}$$

Also, it follows from Eq. (2.9) and Table 2.2 that the normal load is given by

$$P^I = \frac{4\mu}{1-\nu}\left[\delta a - \int_0^a f'(t)\sqrt{a^2-t^2}\,dt\right], \tag{2.11a}$$

and the stress intensity factor by

$$K_{\mathrm{I}}^I = -\frac{2\mu}{\pi(1-\nu)}\left[\delta - \int_0^a \frac{af'(t)}{\sqrt{a^2-t^2}}\,dt\right]. \tag{2.11b}$$

It can be readily shown that Eqs. (2.10a,b) and (2.11a) are the same as those obtained by Sneddon (1965) based on the Hankel transform method[†]. Physically, the problem studied in Sneddon (1965) is the indentation of an isotropic elastic half space by an

[†] Note that there was a typographical error in equation (5.2) of Sneddon (1965). That is, the sign in front of the second term on the right-hand side of his equation (5.2) should be negative (rather than positive).

axisymmetric rigid punch of arbitrary profile.

In particular, for a flat-ended cylindrical punch, $f(r) = 0$ and $f'(r) = 0$. It then follows from Eq. (2.9) that $g_1(t) = -2\delta\mu/[\pi(1-\nu)]$ (a constant), and from Eqs. (2.10a,b) and (2.11a) that

$$u_z^I\big|_{z=0} = \frac{2}{\pi}\delta \sin^{-1}\frac{a}{r}, \quad r > a; \tag{2.12a}$$

$$\sigma_{zz}^I\big|_{z=0} = -\frac{2\mu}{\pi(1-\nu)}\frac{\delta}{\sqrt{a^2-r^2}}, \quad r < a; \tag{2.12b}$$

$$P^I = \frac{4\mu a\delta}{1-\nu}. \tag{2.12c}$$

Equations (2.12a-c) are identical to those given by Boussinesq's solution (e.g., Sneddon, 1965; Maugis, 2000), which is for the indentation of a half space by a flat-ended cylindrical punch.

From Eq. (2.9) and Table 2.1 it follows that

$$\frac{\partial \phi_1}{\partial r}\bigg|_{z=0} = \begin{cases} -\dfrac{2\mu}{\pi(1-\nu)}\dfrac{1}{r}\left[\left(a-\sqrt{a^2-r^2}\right)\delta - \displaystyle\int_0^a f'(t)\sqrt{a^2-t^2}\,dt + \int_r^a\int_0^x \frac{x^2 f'(t)}{\sqrt{(x^2-t^2)(x^2-r^2)}}\,dtdx\right], & r < a; \\ -\dfrac{2\mu}{\pi(1-\nu)}\dfrac{1}{r}\left[a\delta - \displaystyle\int_0^a f'(t)\sqrt{a^2-t^2}\,dt\right], & r > a. \end{cases} \tag{2.13}$$

Using Eqs. (2.6b), (2.10b) and (2.13) in Eqs. (2.2) and (2.5b,c) then yields the in-plane displacement and normal stress components on the contact surface as

$$u_r^I\big|_{z=0} = \begin{cases} -\dfrac{1-2\nu}{\pi(1-\nu)}\dfrac{1}{r}\left[\left(a-\sqrt{a^2-r^2}\right)\delta - \displaystyle\int_0^a f'(t)\sqrt{a^2-t^2}\,dt + \int_r^a\int_0^x \frac{x^2 f'(t)}{\sqrt{(x^2-t^2)(x^2-r^2)}}\,dtdx\right], & r < a; \\ -\dfrac{1-2\nu}{\pi(1-\nu)}\dfrac{1}{r}\left[a\delta - \displaystyle\int_0^a f'(t)\sqrt{a^2-t^2}\,dt\right], & r > a; \end{cases} \tag{2.14a}$$

$$\sigma_{rr}^{I}\Big|_{z=0}=\frac{2\mu}{\pi(1-\nu)}\left\{-\int_0^a f'(t)\left[\frac{1-2\nu}{r^2}\sqrt{a^2-t^2}-\frac{a}{\sqrt{(a^2-t^2)(a^2-r^2)}}\right]dt\right.$$
$$\left.+\int_r^a\int_0^x\frac{\left[(1-2\nu)f(t)x^2/r^2-tf'(t)\right]'}{\sqrt{(x^2-t^2)(x^2-r^2)}}dtdx+\left[\frac{1-2\nu}{r^2}\left(a-\sqrt{a^2-r^2}\right)-\frac{1}{\sqrt{a^2-r^2}}\right]\delta\right\},\quad r<a; \tag{2.14b}$$

$$\sigma_{\theta\theta}^{I}\Big|_{z=0}=\frac{2\mu}{\pi(1-\nu)}\left\{\int_0^a f'(t)\left[\frac{1-2\nu}{r^2}\sqrt{a^2-t^2}+\frac{2\nu a}{\sqrt{(a^2-t^2)(a^2-r^2)}}\right]dt\right.$$
$$\left.-\int_r^a\int_0^x\frac{\left[(1-2\nu)f(t)x^2/r^2+2\nu tf'(t)\right]'}{\sqrt{(x^2-t^2)(x^2-r^2)}}dtdx-\left[\frac{1-2\nu}{r^2}\left(a-\sqrt{a^2-r^2}\right)+\frac{2\nu}{\sqrt{a^2-r^2}}\right]\delta\right\},\quad r<a; \tag{2.14c}$$

$$\sigma_{rr}^{I}\Big|_{z=0}=-\sigma_{\theta\theta}^{I}\Big|_{z=0}=\frac{2\mu(1-2\nu)}{\pi(1-\nu)}\frac{1}{r^2}\left[a\delta-\int_0^a f'(t)\sqrt{a^2-t^2}dt\right],\quad r>a. \tag{2.14d}$$

For a flat-ended cylindrical punch with $f(r) = 0$ and $f'(r) = 0$, Eqs. (2.14a-d) give

$$u_r^{I}\Big|_{z=0}=\begin{cases}-\dfrac{1-2\nu}{\pi(1-\nu)}\dfrac{1}{r}\left(a-\sqrt{a^2-r^2}\right)\delta, & r<a;\\ -\dfrac{1-2\nu}{\pi(1-\nu)}\dfrac{a}{r}\delta, & r>a;\end{cases} \tag{2.15a}$$

$$\sigma_{rr}^{I}\Big|_{z=0}=\frac{2\mu}{\pi(1-\nu)}\left[\frac{1-2\nu}{r^2}\left(a-\sqrt{a^2-r^2}\right)-\frac{1}{\sqrt{a^2-r^2}}\right]\delta,\quad r<a; \tag{2.15b}$$

$$\sigma_{\theta\theta}^{I}\Big|_{z=0}=-\frac{2\mu}{\pi(1-\nu)}\left[\frac{1-2\nu}{r^2}\left(a-\sqrt{a^2-r^2}\right)+\frac{2\nu}{\sqrt{a^2-r^2}}\right]\delta,\quad r<a; \tag{2.15c}$$

$$\sigma_{rr}^{I}\Big|_{z=0}=-\sigma_{\theta\theta}^{I}\Big|_{z=0}=\frac{2\mu(1-2\nu)}{\pi(1-\nu)}\frac{a}{r^2}\delta,\quad r>a. \tag{2.15d}$$

Note that at the periphery of the contact zone (i.e., at $r = a$) all the three normal stress components for the flat punch problem given in Eqs. (2.12b) and (2.15b,c) exhibit the same singularity as that of an external circular crack with the front at $r = a$, thereby confirming the analogy between the external crack problem and the flat punch contact

problem and validating the use of fracture mechanics concepts in solving contact problems.

For a spherical punch, the punch shape function can be approximately represented by $f(r) = r^2/(2R)$ (e.g., Barthel, 2008), which results from a Taylor's expansion (e.g., Gao *et al*., 2006; Gao, 2006a,b). Using this shape function in Eqs. (2.10 a,b) and (2.11a) then gives

$$\delta = \frac{1-\nu}{4\mu}\frac{P^I}{a} + \frac{a^2}{3R};$$

$$u_z^I\Big|_{z=0} = \frac{1}{\pi R}\left[\left(2R\delta - r^2\right)\sin^{-1}\frac{a}{r} + a\sqrt{r^2-a^2}\right], \quad r > a; \tag{2.16a-c}$$

$$\sigma_{zz}^I\Big|_{z=0} = -\frac{2\mu}{\pi(1-\nu)}\left[\frac{1}{\sqrt{a^2-r^2}}\left(\delta - \frac{a^2}{R}\right) + \frac{2}{R}\sqrt{a^2-r^2}\right], \quad r < a.$$

In order for σ_{zz} to be finite (non-singular) at $r = a$, it is required from Eq. (2.16c) that

$$\delta = \frac{a^2}{R}. \tag{2.17}$$

Using Eq. (2.17) in Eqs. (2.16a-c) then leads to

$$P^I = \frac{8\mu}{3(1-\nu)}\frac{a^3}{R};$$

$$u_z^I\Big|_{z=0} = \frac{a^2}{\pi R}\left[\left(2 - \frac{r^2}{a^2}\right)\sin^{-1}\frac{a}{r} + \sqrt{\frac{r^2}{a^2}-1}\right], \quad r > a; \tag{2.18a-c}$$

$$\sigma_{zz}^I\Big|_{z=0} = -\frac{4\mu}{\pi(1-\nu)}\frac{a}{R}\sqrt{1-\frac{r^2}{a^2}} = -\frac{3P^I}{2\pi a^2}\sqrt{1-\frac{r^2}{a^2}}, \quad r < a.$$

Equations (2.18a-c) are exactly those given by the Hertz solution for the indentation of a half space by a spherical punch (e.g., Maugis, 2000).

Similarly, using $f(r) = r^2/(2R)$ and Eq. (2.17) in Eqs. (2.14a-d) yields

$$u_r^I\Big|_{z=0} = \begin{cases} -\dfrac{2(1-2\nu)}{3\pi(1-\nu)}\dfrac{a^3}{Rr}\left[1-\left(1-\dfrac{r^2}{a^2}\right)^{3/2}\right], & r<a; \\ -\dfrac{2(1-2\nu)}{3\pi(1-\nu)}\dfrac{a^3}{Rr}, & r>a; \end{cases}$$

$$\sigma_{rr}^I\Big|_{z=0} = \frac{4\mu}{\pi(1-\nu)}\frac{a}{R}\left\{\frac{1-2\nu}{3}\frac{a^2}{r^2}\left[1-\left(1-\frac{r^2}{a^2}\right)^{3/2}\right]-\sqrt{1-\frac{r^2}{a^2}}\right\},\ r<a; \quad \text{(2.19a-d)}$$

$$\sigma_{\theta\theta}^I\Big|_{z=0} = -\frac{4\mu}{\pi(1-\nu)}\frac{a}{R}\left\{\frac{1-2\nu}{3}\frac{a^2}{r^2}\left[1-\left(1-\frac{r^2}{a^2}\right)^{3/2}\right]+2\nu\sqrt{1-\frac{r^2}{a^2}}\right\},\ r<a;$$

$$\sigma_{rr}^I\Big|_{z=0} = -\sigma_{\theta\theta}^I\Big|_{z=0} = \frac{4\mu(1-2\nu)}{3\pi(1-\nu)}\frac{a^3}{Rr^2},\quad r>a$$

as the in-plane displacement and normal stress components on the contact surface $z = 0$ for the spherical punch problem. Equations (2.18a-c) and (2.19a-d) are the same as those provided in Johnson (1985) using a different approach.

Note that in this spherical punch problem all the stress components remain finite in the entire contact zone. In particular, the normal stresses at $r = a$, $z = 0$ and $r = 0$, $z = 0$ are obtained from Eqs. (2.18c) and (2.19b-d) as

$$\begin{aligned} &\sigma_{zz}^I\Big|_{z=0,r=a} = 0,\quad \sigma_{rr}^I\Big|_{z=0,r=a} = -\sigma_{\theta\theta}^I\Big|_{z=0,r=a} = \frac{4\mu(1-2\nu)}{3\pi(1-\nu)}\frac{a}{R}, \\ &\sigma_{zz}^I\Big|_{z=0,r=0} = -\frac{4\mu}{\pi(1-\nu)}\frac{a}{R},\quad \sigma_{rr}^I\Big|_{z=0,r=0} = \sigma_{\theta\theta}^I\Big|_{z=0,r=0} = -\frac{2\mu(1+2\nu)}{\pi(1-\nu)}\frac{a}{R}. \end{aligned} \quad \text{(2.20a-d)}$$

2.3.2 Problems with BCs of the Second Type

With prescribed normal traction $p(r)$ outside the contact zone and zero out-of-plane displacement inside it, as shown in Figure 2.1b, the boundary conditions of the second type can be expressed as

$$\begin{aligned} &u_z = 0, && z = 0, \quad r < a; \\ &\sigma_{zz} = -p(r), && z = 0, \quad r > a; \\ &\sigma_{rz} = \sigma_{\theta z} = 0, && z = 0. \end{aligned} \tag{2.21a-c}$$

Again, Eq. (2.21c) is automatically satisfied by the general solution given in Eq. (2.2). Also, from Eq. (2.2) and $\partial\phi_2/\partial z = 0$ (for $z = 0$, $r < a$) given in Table 2.1, it follows that Eq. (2.21a) is exactly met. Hence, upon using Eq. (2.2) and $\partial^2\phi_2/\partial^2 z$ (for $z = 0$, $r > a$) listed in Table 2.1, Eq. (2.21b), the only remaining boundary condition, becomes

$$\int_r^\infty \frac{g_2'(t)}{\sqrt{t^2 - r^2}}\, dt = p(r). \tag{2.22}$$

By using the inverse Abel transform, Eq. (2.22) can be solved to get

$$g_2(t) = -\frac{2}{\pi}\int_t^\infty \frac{xp(x)}{\sqrt{x^2 - t^2}}\, dx. \tag{2.23}$$

For given $p(r)$, the explicit expression of $g_2(t)$ can be readily obtained from Eq. (2.23). By using Eq. (2.23) and the derivative expressions from Table 2.1 in Eq. (2.2), the out-of-plane displacement and normal stress components on the contact surface can then be determined as

$$\begin{aligned} u_z^{II}\big|_{z=0} &= \frac{2(1-\nu)}{\pi\mu}\int_a^r \int_x^\infty \frac{tp(t)}{\sqrt{(r^2 - x^2)(t^2 - x^2)}}\, dt dx, \quad r > a; \\ \sigma_{zz}^{II}\big|_{z=0} &= \frac{2}{\pi}\int_a^\infty \frac{tp(t)\sqrt{t^2 - a^2}}{(t^2 - r^2)\sqrt{a^2 - r^2}}\, dt, \quad r < a. \end{aligned} \tag{2.24a,b}$$

Also, it follows from Eq. (2.23) and Table 2.2 that the normal load is given by

$$P^{II} = 4\int_a^\infty tp(t)\cos^{-1}\frac{a}{t}\, dt, \tag{2.25a}$$

and the stress intensity factor by

$$K_{\mathrm{I}}^{II} = \frac{2}{\pi}\int_a^\infty \frac{tp(t)}{\sqrt{t^2-a^2}}\,dt. \tag{2.25b}$$

From Eq. (2.23) and Table 2.1, it follows that

$$\left.\frac{\partial \phi_2}{\partial r}\right|_{z=0} = \begin{cases} -\dfrac{2}{\pi}\dfrac{1}{r}\displaystyle\int_a^\infty tp(t)\left[\cos^{-1}\frac{a}{t} - \tan^{-1}\sqrt{\frac{a^2-t^2}{r^2-a^2}}\right]dt, & r<a; \\ -\dfrac{2}{\pi}\dfrac{1}{r}\left[\displaystyle\int_a^\infty tp(t)\cos^{-1}\frac{a}{t}\,dt - \frac{\pi}{2}\int_r^\infty tp(t)dt\right], & r>a. \end{cases} \tag{2.26}$$

Using Eqs. (2.21b), (2.24b) and (2.26) in Eqs. (2.2) and (2.5b,c) then yields the in-plane displacement and normal stress components on the contact surface as

$$u_r^{II}\Big|_{z=0} = \begin{cases} -\dfrac{1-2\nu}{\pi\mu}\dfrac{1}{r}\displaystyle\int_a^\infty tp(t)\left[\cos^{-1}\frac{a}{t} - \tan^{-1}\sqrt{\frac{a^2-t^2}{r^2-a^2}}\right]dt, & r<a; \\ -\dfrac{1-2\nu}{\pi\mu}\dfrac{1}{r}\left[\displaystyle\int_a^\infty tp(t)\cos^{-1}\frac{a}{t}\,dt - \frac{\pi}{2}\int_r^\infty tp(t)dt\right], & r>a; \end{cases} \tag{2.27a}$$

$$\sigma_{rr}^{II}\Big|_{z=0} = \begin{cases} \dfrac{2}{\pi}\displaystyle\int_a^\infty tp(t)\left[\frac{1-2\nu}{r^2}\left(\cos^{-1}\frac{a}{t} - \tan^{-1}\sqrt{\frac{a^2-t^2}{r^2-a^2}}\right) + \frac{\sqrt{t^2-a^2}}{(t^2-r^2)\sqrt{a^2-r^2}}\right]dt, & r<a; \\ \sigma_{rr}^{II}\Big|_{z=0} = \dfrac{2}{\pi}\dfrac{1-2\nu}{r^2}\left[\displaystyle\int_a^\infty tp(t)\cos^{-1}\frac{a}{t}\,dt - \frac{\pi}{2}\int_r^\infty tp(t)dt\right] + p(r), & r>a; \end{cases} \tag{2.27b}$$

$$\sigma_{\theta\theta}^{II}\Big|_{z=0} = \begin{cases} -\dfrac{2}{\pi}\displaystyle\int_a^\infty tp(t)\left[\frac{1-2\nu}{r^2}\left(\cos^{-1}\frac{a}{t} - \tan^{-1}\sqrt{\frac{a^2-t^2}{r^2-a^2}}\right) - \frac{2\nu\sqrt{t^2-a^2}}{(t^2-r^2)\sqrt{a^2-r^2}}\right]dt, & r<a; \\ -\dfrac{2}{\pi}\dfrac{1-2\nu}{r^2}\left[\displaystyle\int_a^\infty tp(t)\cos^{-1}\frac{a}{t}\,dt - \frac{\pi}{2}\int_r^\infty tp(t)dt\right] + 2\nu\,p(r), & r>a. \end{cases} \tag{2.27c}$$

Equations (2.24a,b), (2.25a,b) and (2.27a-c) provide the general solution for the frictionless axisymmetric punch problem with the boundary conditions of the second type.

As an example, consider the cohesive stress $p(r)$ ($a < r < \infty$) of the Dugdale type:

$$p(r) = \begin{cases} -\sigma_0, & a < r < c; \\ 0 & r > c, \end{cases} \tag{2.28}$$

where c is the outer radius of the adhesive interaction zone, and $\sigma_0 = 1.026w/z_0$ is the theoretical strength of the indented material chosen to match what is given by the Lennard-Jones potential (Maugis, 1992; Johnson and Greenwood, 1997; Zheng and Yu, 2007; Yao *et al*., 2007), with w being the Dupré energy of adhesion (also called surface energy or work of adhesion) and z_0 the equilibrium separation distance between atomic planes. Using Eqs. (2.21a,b) and (2.28) in Eqs. (2.24a,b) and (2.27a-c) then gives the displacement components on the contact surface as

$$u_z^{II}\big|_{z=0} = \begin{cases} 0, & r < a; \\ -\dfrac{2(1-\nu)\sigma_0}{\pi\mu}\displaystyle\int_a^r \sqrt{\frac{c^2-x^2}{r^2-x^2}}\,dx, & a < r < c; \\ -\dfrac{2(1-\nu)\sigma_0}{\pi\mu}\displaystyle\int_a^c \sqrt{\frac{c^2-x^2}{r^2-x^2}}\,dx, & r > c, \end{cases} \tag{2.29a}$$

$$u_z^{II}\big|_{z=0} = \begin{cases} -\dfrac{1-2\nu}{2\pi\mu}\dfrac{\sigma_0}{r}\left[\sqrt{c^2-a^2}\left(a-\sqrt{a^2-r^2}\right) - c^2\cos^{-1}\dfrac{a}{c} + \left(c^2-r^2\right)\tan^{-1}\sqrt{\dfrac{c^2-a^2}{a^2-r^2}}\right], & r < a; \\ \dfrac{1-2\nu}{2\mu}\dfrac{\sigma_0}{r}\left[\dfrac{r^2}{2} - \dfrac{1}{\pi}\left(a\sqrt{c^2-a^2} + c^2\sin^{-1}\dfrac{a}{c}\right)\right], & a < r < c; \\ -\dfrac{1-2\nu}{2\pi\mu}\dfrac{\sigma_0}{r}\left(a\sqrt{c^2-a^2} - c^2\cos^{-1}\dfrac{a}{c}\right), & r > c, \end{cases} \tag{2.29b}$$

and the normal stress components as

$$\sigma_{zz}^{II}\big|_{z=0} = -\frac{2\sigma_0}{\pi}\left[\frac{\sqrt{c^2-a^2}}{\sqrt{a^2-r^2}} - \tan^{-1}\frac{\sqrt{c^2-a^2}}{\sqrt{a^2-r^2}}\right], \quad r < a; \tag{2.29c}$$

$$\sigma_{rr}^{II}\Big|_{z=0} = \frac{1-2\nu}{\pi}\frac{\sigma_0}{r^2}\left[\sqrt{c^2-a^2}\left(a-\sqrt{a^2-r^2}\right)-c^2\cos^{-1}\frac{a}{c}\right] + \frac{\sigma_0}{\pi}\tan^{-1}\sqrt{\frac{c^2-a^2}{a^2-r^2}}\left[(1-2\nu)\frac{c^2}{r^2}+1+2\nu\right]-\frac{2\sigma_0}{\pi}\frac{\sqrt{c^2-a^2}}{\sqrt{a^2-r^2}},\ r<a; \tag{2.29d}$$

$$\sigma_{\theta\theta}^{II}\Big|_{z=0} = -\frac{1-2\nu}{\pi}\frac{\sigma_0}{r^2}\left[\sqrt{c^2-a^2}\left(a-\sqrt{a^2-r^2}\right)-c^2\cos^{-1}\frac{a}{c}\right] - \frac{\sigma_0}{\pi}\tan^{-1}\sqrt{\frac{c^2-a^2}{a^2-r^2}}\left[(1-2\nu)\frac{c^2}{r^2}-1-2\nu\right]-\frac{4\nu}{\pi}\sigma_0\frac{\sqrt{c^2-a^2}}{\sqrt{a^2-r^2}},\ r<a \tag{2.29e}$$

in the contact zone,

$$\sigma_{zz}^{II}\Big|_{z=0} = \sigma_0,\quad a<r<c;$$

$$\sigma_{rr}^{II}\Big|_{z=0} = \frac{1-2\nu}{\pi}\frac{\sigma_0}{r^2}\left(a\sqrt{c^2-a^2}+c^2\sin^{-1}\frac{a}{c}\right)+\frac{\sigma_0}{2}(1+2\nu),\quad a<r<c; \tag{2.29f-h}$$

$$\sigma_{\theta\theta}^{II}\Big|_{z=0} = -\frac{1-2\nu}{\pi}\frac{\sigma_0}{r^2}\left(a\sqrt{c^2-a^2}+c^2\sin^{-1}\frac{a}{c}\right)+\frac{\sigma_0}{2}(1+2\nu),\quad a<r<c$$

in the adhesive zone, and

$$\sigma_{zz}^{II}\Big|_{z=0} = 0,\quad \sigma_{rr}^{II}\Big|_{z=0} = -\sigma_{\theta\theta}^{II}\Big|_{z=0} = \frac{1-2\nu}{\pi}\frac{\sigma_0}{r^2}\left(a\sqrt{c^2-a^2}-c^2\cos^{-1}\frac{a}{c}\right),\quad r>c \tag{2.29i,j}$$

in the non-contact zone.

It is seen from Eqs. (2.29c-e) that the stress field is singular at the periphery of the contact zone where $r = a$.

2.4 Adhesive Contact Problems

As demonstrated in the previous section, by using the harmonic potential function method for solving axisymmetric mixed boundary value elasticity problems, the stress and displacement components, applied normal load, and stress intensity factor can

all be expressed in terms of $g(x)$ (see Eq. (2.4)) in a unified manner. This makes the harmonic potential function method very advantageous, particularly in treating adhesive contact problems.

In solving an adhesive contact problem, the stress intensity factor needs to be evaluated, and the normal load has to be computed. The determination of these quantities using Sneddon's (1965) solution for an axisymmetric punch problem based on the Hankel transform method tends to be complex, as reflected in the development of the M-D model (Maugis, 1992). However, finding these two quantities is rather straightforward when using the harmonic potential function method: both the normal load P and the stress intensity factor K_{I} can be easily obtained once $g(x)$ has been determined, as indicated in Table 2.2. This feature greatly facilitates the formulation of the adhesive contact problem, as demonstrated below.

Figure 2.2 schematically shows an axisymmetric adhesive contact problem with an arbitrary adhesive interaction force distribution in the deformed configuration. It is

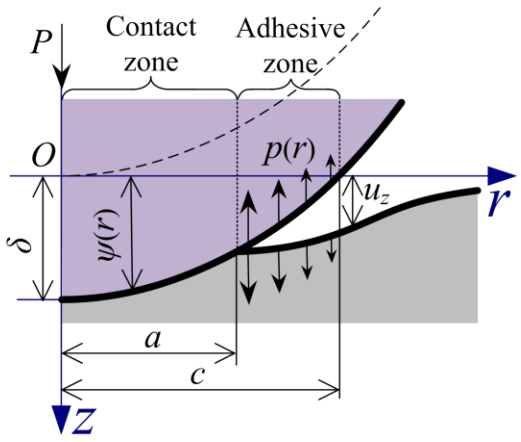

Figure 2.2. Schematic illustration of an adhesive contact problem.

assumed that the punch is rigid and the contact is frictionless. Inside the contact zone ($0 < r < a$) the out-of-plane displacement is a given function of r related to the punch shape (i.e., $\psi(r) = \delta - f(r)$), and in the adhesive zone ($a < r < c$) the surface adhesive interaction force is a known function of r (i.e., $p(r)$). Both $f(r)$ (and thus $\psi(r)$) and $p(r)$ can be arbitrary.

2.4.1 Solution by Superposition

The boundary conditions of the adhesive contact problem shown in Figure 2.2 can be expressed as

$$\begin{aligned} &u_z = \delta - f(r), \quad z = 0, \quad r < a; \\ &\sigma_{zz} = -p(r), \quad z = 0, \quad r > a; \\ &\sigma_{rz} = \sigma_{\theta z} = 0, \quad z = 0. \end{aligned} \tag{2.30a-c}$$

Based on the superposition principle, this axisymmetric mixed boundary value problem (BVP) of elasticity can be decomposed into two simpler BVPs, with the first BVP having the boundary conditions:

$$\begin{aligned} &u_z = \delta - f(r), \quad z = 0, \quad r < a; \\ &\sigma_{zz} = 0, \quad z = 0, \quad r > a; \\ &\sigma_{rz} = \sigma_{\theta z} = 0, \quad z = 0, \end{aligned} \tag{2.31a-c}$$

and the second BVP having the boundary conditions:

$$\begin{aligned} &u_z = 0, \quad z = 0, \quad r < a; \\ &\sigma_{zz} = -p(r), \quad z = 0, \quad r > a; \\ &\sigma_{rz} = \sigma_{\theta z} = 0, \quad z = 0. \end{aligned} \tag{2.32a-c}$$

Note that Eqs. (2.31a-c) and Eqs. (2.32a-c) are, respectively, the boundary conditions of the first type and of the second type discussed in the preceding section (see Eqs. (2.6a-c) and Eqs. (2.21a-c)). Hence, the solution of the first BVP is that given in Eqs. (2.10a,b),

(2.11a,b) and (2.14a-d), and the solution of the second BVP is that listed in Eqs. (2.24 a,b), (2.25a,b) and (2.27a-c). It then follows from the principle of superposition that the solution of the current adhesive contact problem with the boundary conditions expressed in Eqs. (2.30a-c) can be obtained from the solutions of the first BVP and the second BVP as

$$u_z\big|_{z=0} = u_z^I\big|_{z=0} + u_z^{II}\big|_{z=0} = \frac{2}{\pi}\delta\sin^{-1}\frac{a}{r} - \frac{2}{\pi}\int_0^a \frac{tf(t)\sqrt{r^2-a^2}}{(r^2-t^2)\sqrt{a^2-t^2}}dt + \frac{2(1-\nu)}{\pi\mu}\int_a^r\int_x^\infty \frac{tp(t)}{\sqrt{(r^2-x^2)(t^2-x^2)}}dtdx, \quad r>a; \tag{2.33a}$$

$$\sigma_{zz}\big|_{z=0} = \sigma_{zz}^I\big|_{z=0} + \sigma_{zz}^{II}\big|_{z=0} = -\frac{2\mu}{\pi(1-\nu)}\left\{\frac{1}{\sqrt{a^2-r^2}}\left[\delta - \int_0^a \frac{af'(t)}{\sqrt{a^2-t^2}}dt\right] + \int_r^a\int_0^x \frac{[tf'(t)]'}{\sqrt{(x^2-t^2)(x^2-r^2)}}dtdx\right\} + \frac{2}{\pi}\int_a^\infty \frac{tp(t)\sqrt{t^2-a^2}}{(t^2-r^2)\sqrt{a^2-r^2}}dt, \quad r<a; \tag{2.33b}$$

$$P = P^I + P^{II} = \frac{4\mu}{1-\nu}\left[a\delta - \int_0^a f'(t)\sqrt{a^2-t^2}dt\right] + 4\int_a^\infty tp(t)\cos^{-1}\frac{a}{t}dt, \tag{2.33c}$$

$$K_{\mathrm{I}} = K_{\mathrm{I}}^I + K_{\mathrm{I}}^{II} = -\frac{2\mu}{\pi(1-\nu)}\left[\delta - \int_0^a \frac{af'(t)}{\sqrt{a^2-t^2}}dt\right] + \frac{2}{\pi}\int_a^\infty \frac{tp(t)}{\sqrt{t^2-a^2}}dt. \tag{2.33d}$$

$$u_r\big|_{z=0} = u_r^I\big|_{z=0} + u_r^{II}\big|_{z=0} = -\frac{1-2\nu}{\pi\mu}\frac{1}{r}\left\{\frac{\mu}{1-\nu}\left[\left(a-\sqrt{a^2-r^2}\right)\delta - \int_0^a f'(t)\sqrt{a^2-t^2}dt + \int_r^a\int_0^x \frac{x^2f'(t)}{\sqrt{(x^2-t^2)(x^2-r^2)}}dtdx\right] + \int_a^\infty tp(t)\left(\cos^{-1}\frac{a}{t} - \tan^{-1}\sqrt{\frac{a^2-t^2}{r^2-a^2}}\right)dt\right\}, \quad r<a; \tag{2.33e}$$

$$u_r\big|_{z=0} = u_r^I\big|_{z=0} + u_r^{II}\big|_{z=0} = -\frac{1-2\nu}{\pi\mu}\frac{1}{r}\left\{\frac{\mu}{1-\nu}\left[a\delta - \int_0^a f'(t)\sqrt{a^2-t^2}dt\right] + \int_a^\infty tp(t)\cos^{-1}\frac{a}{t}dt - \frac{\pi}{2}\int_r^\infty tp(t)dt\right\}, \quad r>a; \tag{2.33f}$$

$$\sigma_{rr}\big|_{z=0}=\sigma_{rr}^{I}\big|_{z=0}+\sigma_{rr}^{II}\big|_{z=0}=\frac{2\mu}{\pi(1-\nu)}\left\{-\int_0^a f'(t)\left[\frac{1-2\nu}{r^2}\sqrt{a^2-t^2}-\frac{a}{\sqrt{(a^2-t^2)(a^2-r^2)}}\right]dt\right.$$
$$\left.+\int_r^a\int_0^x\frac{\left[(1-2\nu)f(t)x^2/r^2-tf'(t)\right]'}{\sqrt{(x^2-t^2)(x^2-r^2)}}dtdx+\left[\frac{1-2\nu}{r^2}\left(a-\sqrt{a^2-r^2}\right)-\frac{1}{\sqrt{a^2-r^2}}\right]\delta\right\}$$
$$+\frac{2}{\pi}\int_a^\infty tp(t)\left[\frac{1-2\nu}{r^2}\left(\cos^{-1}\frac{a}{t}-\tan^{-1}\sqrt{\frac{a^2-t^2}{r^2-a^2}}\right)+\frac{\sqrt{t^2-a^2}}{(t^2-r^2)\sqrt{a^2-r^2}}\right]dt,\quad r<a;$$
(2.33g)

$$\sigma_{rr}\big|_{z=0}=\sigma_{rr}^{I}\big|_{z=0}+\sigma_{rr}^{II}\big|_{z=0}=\frac{2(1-2\nu)}{\pi}\frac{1}{r^2}\left\{\frac{\mu}{1-\nu}\left[a\delta-\int_0^a f'(t)\sqrt{a^2-t^2}dt\right]\right.$$
$$\left.+\int_a^\infty tp(t)\cos^{-1}\frac{a}{t}dt-\frac{\pi}{2}\int_r^\infty tp(t)dt\right\}+p(r),\quad r>a;$$
(2.33h)

$$\sigma_{\theta\theta}\big|_{z=0}=\sigma_{\theta\theta}^{I}\big|_{z=0}+\sigma_{\theta\theta}^{II}\big|_{z=0}=\frac{2\mu}{\pi(1-\nu)}\left\{\int_0^a f'(t)\left[\frac{1-2\nu}{r^2}\sqrt{a^2-t^2}+\frac{2\nu a}{\sqrt{(a^2-t^2)(a^2-r^2)}}\right]dt\right.$$
$$\left.-\int_r^a\int_0^x\frac{\left[(1-2\nu)f(t)x^2/r^2+2\nu tf'(t)\right]'}{\sqrt{(x^2-t^2)(x^2-r^2)}}dtdx-\left[\frac{1-2\nu}{r^2}\left(a-\sqrt{a^2-r^2}\right)+\frac{2\nu}{\sqrt{a^2-r^2}}\right]\delta\right\}$$
$$-\frac{2}{\pi}\int_a^\infty tp(t)\left[\frac{1-2\nu}{r^2}\left(\cos^{-1}\frac{a}{t}-\tan^{-1}\sqrt{\frac{a^2-t^2}{r^2-a^2}}\right)-\frac{2\nu\sqrt{t^2-a^2}}{(t^2-r^2)\sqrt{a^2-r^2}}\right]dt,\quad r<a;$$
(2.33i)

$$\sigma_{\theta\theta}\big|_{z=0}=\sigma_{\theta\theta}^{I}\big|_{z=0}+\sigma_{\theta\theta}^{II}\big|_{z=0}=-\frac{2(1-2\nu)}{\pi}\frac{1}{r^2}\left\{\frac{\mu}{1-\nu}\left[a\delta-\int_0^a f'(t)\sqrt{a^2-t^2}dt\right]\right.$$
$$\left.+\int_a^\infty tp(t)\cos^{-1}\frac{a}{t}dt-\frac{\pi}{2}\int_r^\infty tp(t)dt\right\}+2\nu\,p(r),\quad r>a.$$
(2.33j)

2.4.2 General Solution of the Adhesive Contact Problem

The solution obtained above by superposition is not yet complete, and additional conditions are needed to close the solution. The "closure" conditions can be either stress (pressure profile) continuity (as in the DMT model) or energy minimization (as in the

JKR model), but the former is believed to be more natural (e.g., Barthel, 1998). Hence, the stress continuity is adopted here as the closure condition.

To eliminate the stress discontinuity (singularity) at the periphery of the contact zone (i.e., at $r = a$) explicitly shown in Eqs. (2.33b), (2.33g) and (2.33i), it is required that $K_I = 0$, as was done in Maugis (1992). This gives, upon using Eq. (2.33d),

$$\delta = \int_0^a \frac{af'(t)}{\sqrt{a^2 - t^2}}\, dt + \frac{1-\nu}{\mu} \int_a^\infty \frac{tp(t)}{\sqrt{t^2 - a^2}}\, dt. \tag{2.34}$$

Equation (2.34) relates the penetration δ to the punch shape function $f(r)$, the adhesive interaction force $p(r)$, the contact radius a, and the material properties μ and ν.

Then, using Eq. (2.34) in Eqs. (2.33b,c) leads to

$$\sigma_{zz}\big|_{z=0} = -\frac{2\mu}{\pi(1-\nu)} \int_r^a \int_0^x \frac{\left[tf'(t)\right]'}{\sqrt{(x^2 - t^2)(x^2 - r^2)}}\, dt dx - \frac{2}{\pi} \int_a^\infty \frac{tp(t)}{t^2 - r^2} \sqrt{\frac{a^2 - r^2}{t^2 - a^2}}\, dt, \quad r < a;$$

$$P = 4a \int_a^\infty \frac{tp(t)}{\sqrt{t^2 - a^2}}\, dt + \frac{4\mu}{1-\nu} \int_0^a \frac{t^2 f'(t)}{\sqrt{a^2 - t^2}}\, dt + 4 \int_a^\infty tp(t) \cos^{-1}\frac{a}{t}\, dt. \tag{2.35a,b}$$

Note that the normal stress component given in Eq. (2.35a) no longer has singularity at $r = a$.

Similarly, substituting Eq. (2.34) into Eqs. (2.33e-j) will result in the expressions of the in-plane displacement and normal stress components on the contact surface as

$$u_r\big|_{z=0} = -\frac{1-2\nu}{\pi\mu} \frac{1}{r} \left\{ \frac{\mu}{1-\nu} \left[\int_0^a \frac{t^2 - a\sqrt{a^2 - r^2}}{\sqrt{a^2 - t^2}}\, f'(t) dt + \int_r^a \int_0^x \frac{x^2 f'(t)}{\sqrt{(x^2 - t^2)(x^2 - r^2)}}\, dt dx \right] \right.$$
$$\left. + \int_a^\infty tp(t) \left[\frac{a - \sqrt{a^2 - r^2}}{\sqrt{t^2 - a^2}} + \cos^{-1}\frac{a}{t} - \tan^{-1}\sqrt{\frac{a^2 - t^2}{r^2 - a^2}} \right] dt \right\}, \quad r < a; \tag{2.35c}$$

$$u_r\big|_{z=0} = -\frac{1-2\nu}{\pi\mu}\frac{1}{r}\left[\frac{\mu}{1-\nu}\int_0^a \frac{t^2 f'(t)}{\sqrt{a^2-t^2}}dt + \int_a^\infty tp(t)\left(\frac{a}{\sqrt{a^2-t^2}} + \cos^{-1}\frac{a}{t}\right)dt - \frac{\pi}{2}\int_r^\infty tp(t)dt\right], \quad r > a; \tag{2.35d}$$

$$\sigma_{rr}\big|_{z=0} = \frac{2\mu(1-2\nu)}{\pi(1-\nu)}\left\{\int_0^a f'(t)\frac{t^2 - a\sqrt{a^2-r^2}}{r^2\sqrt{a^2-t^2}}dt + \int_r^a\int_0^x \frac{[(1-2\nu)f(t)x^2/r^2 - tf'(t)]'}{(1-2\nu)\sqrt{(x^2-t^2)(x^2-r^2)}}dtdx\right\}$$
$$+\frac{2}{\pi}\frac{1}{r^2}\int_a^\infty tp(t)\left[(1-2\nu)\left(\cos^{-1}\frac{a}{t} - \tan^{-1}\sqrt{\frac{a^2-t^2}{r^2-a^2}} + \frac{a}{\sqrt{t^2-a^2}}\right)\right.$$
$$\left. -\frac{\sqrt{a^2-r^2}}{\sqrt{t^2-a^2}}\left(\frac{t^2}{t^2-r^2} - 2\nu\right)\right]dt, \quad r < a; \tag{2.35e}$$

$$\sigma_{rr}\big|_{z=0} = \frac{2(1-2\nu)}{\pi r^2}\left[\frac{\mu}{1-\nu}\int_0^a \frac{t^2 f'(t)}{\sqrt{a^2-t^2}}dt + \int_a^\infty tp(t)\left(\frac{a}{\sqrt{t^2-a^2}} + \cos^{-1}\frac{a}{t}\right)dt - \frac{\pi}{2}\int_r^\infty tp(t)dt\right] + p(r), \quad r > a; \tag{2.35f}$$

$$\sigma_{\theta\theta}\big|_{z=0} = -\frac{2\mu(1-2\nu)}{\pi(1-\nu)}\left\{\int_r^a\int_0^x \frac{[(1-2\nu)f(t)x^2/r^2 + 2\nu tf'(t)]'}{(1-2\nu)\sqrt{(x^2-t^2)(x^2-r^2)}}dtdx\right.$$
$$\left. +\int_0^a f'(t)\frac{t^2 - a\sqrt{a^2-r^2}}{r^2\sqrt{a^2-t^2}}dt\right\} - \frac{2}{\pi}\frac{1}{r^2}\int_a^\infty tp(t)\left[\frac{\sqrt{a^2-r^2}}{\sqrt{t^2-a^2}}\left(\frac{2\nu t^2}{t^2-r^2} - 1\right)\right. \tag{2.35g}$$
$$\left. +(1-2\nu)\left(\cos^{-1}\frac{a}{t} - \tan^{-1}\sqrt{\frac{a^2-t^2}{r^2-a^2}} + \frac{a}{\sqrt{t^2-a^2}}\right)\right]dt, \quad r < a;$$

$$\sigma_{\theta\theta}\big|_{z=0} = -\frac{2(1-2\nu)}{\pi r^2}\left[\frac{\mu}{1-\nu}\int_0^a \frac{t^2 f'(t)}{\sqrt{a^2-t^2}}dt + \int_a^\infty tp(t)\left(\frac{a}{\sqrt{t^2-a^2}} + \cos^{-1}\frac{a}{t}\right)dt - \frac{\pi}{2}\int_r^\infty tp(t)dt\right] + 2\nu\, p(r), \quad r > a. \tag{2.35h}$$

Equations (2.35a-h) are the expressions of a general solution for the adhesive contact problem under consideration, which involves an axisymmetric rigid punch of

arbitrary shape (represented by $f(r)$) and an adhesive interaction force of any profile (described by $p(r)$). Clearly, when $p(r) \equiv 0$ for any value of r (i.e., no adhesion is present), Eqs. (2.35a-h) will reduce to those of the solution for the non-adhesive contact problem with the BCs of the first type given in Eqs. (2.10a,b), (2.11a,b) and (2.14a-d), which includes Sneddon's axisymmetric punch solution, Boussinesq's flat punch solution, and Hertz's spherical punch solution as special cases, as demonstrated in the previous section.

For the punch profile, consider a power-law function of the form (e.g., Zheng and Yu, 2007):

$$f(r) = \frac{r^n}{nQ}, \tag{2.36}$$

where n (>0) is a shape index, and Q (>0) is a shape parameter with the dimension of [length]$^{n-1}$. In particular, when $n = 1$, Eq. (2.36) represents a cone-shaped punch, with $Q = \tan\varphi$, where φ is the cone angle; when $n = 2$, Eq. (2.36) approximates a spherical punch, with $Q = R$, the radius of the spherical punch; when $n \to \infty$, Eq. (2.36) corresponds to a flat-ended cylindrical punch, with $Q = a^{n-1}$, where a is the radius of the contact area, which is the same as the radius of the cylindrical punch. The index n can take other positive values to represent other punch shapes (e.g., Segedin, 1957; Sneddon, 1965; Spence, 1968; Goryacheva and Makhovskaya, 2001; Borodich *et al.*, 2003; Woirgard *et al.*, 2008). Hence, this power-law shape function is also called an "arbitrary" shape function in the literature (e.g., Zheng and Yu, 2007).

Using Eq. (2.36) in Eqs. (2.33a), (2.34) and (2.35a-h) will result in

$$u_z\big|_{z=0} = \frac{2}{\pi}\delta \sin^{-1}\frac{a}{r} - \frac{r^n}{2\pi Q} B\left(\frac{n}{2},\frac{1}{2}\right) B\left(\frac{a^2}{r^2};\frac{n+1}{2},\frac{1}{2}\right) + \frac{2(1-\nu)}{\pi\mu}\int_a^r \int_x^\infty \frac{tp(t)}{\sqrt{(r^2-x^2)(t^2-x^2)}}\,dt dx, \quad r > a; \tag{2.37a}$$

$$\delta = \frac{a^n}{2Q} B\left(\frac{n}{2},\frac{1}{2}\right) + \frac{1-\nu}{\mu}\int_a^\infty \frac{tp(t)}{\sqrt{t^2-a^2}}\,dt, \tag{2.37b}$$

$$P = \frac{2\mu}{1-\nu}\frac{a^{n+1}}{Q} B\left(\frac{n}{2}+1,\frac{1}{2}\right) + 4\int_a^\infty tp(t)\left[\frac{a}{\sqrt{t^2-a^2}} + \cos^{-1}\frac{a}{t}\right]dt, \tag{2.37c}$$

$$\sigma_{zz}\big|_{z=0} = -\frac{\mu}{\pi(1-\nu)}\frac{n}{Q} B(\frac{n}{2},\frac{1}{2})\int_r^a \frac{t^{n-1}}{\sqrt{t^2-r^2}}\,dt - \frac{2}{\pi}\int_a^\infty \frac{tp(t)}{t^2-r^2}\sqrt{\frac{a^2-r^2}{t^2-a^2}}dt, \; r < a, \tag{2.37d}$$

$$u_r\big|_{z=0} = -\frac{1-2\nu}{\pi\mu}\frac{1}{r}\left\{\frac{\mu}{1-\nu}\frac{1}{2Q}\left[a^{n+1}B(\frac{n}{2}+1,\frac{1}{2}) - nB(\frac{n}{2},\frac{1}{2})\int_r^a x^{n-1}\sqrt{x^2-r^2}\,dx\right] + \int_a^\infty tp(t)\left[\frac{a-\sqrt{a^2-r^2}}{\sqrt{t^2-a^2}} + \cos^{-1}\frac{a}{t} - \tan^{-1}\sqrt{\frac{a^2-t^2}{r^2-a^2}}\right]dt\right\}, \quad r < a; \tag{2.37e}$$

$$u_r\big|_{z=0} = -\frac{1-2\nu}{\pi\mu}\frac{1}{r}\left[\frac{\mu}{1-\nu}\frac{a^{n+1}}{2Q} B(\frac{n}{2}+1,\frac{1}{2}) + \int_a^\infty tp(t)\left(\frac{a}{\sqrt{a^2-t^2}} + \cos^{-1}\frac{a}{t}\right)dt - \frac{\pi}{2}\int_r^\infty tp(t)dt\right], \quad r > a; \tag{2.37f}$$

$$\sigma_{rr}\big|_{z=0} = \frac{1}{Qr^2}\frac{\mu(1-2\nu)}{\pi(1-\nu)}\left\{a^{n+1}\left[B(\frac{n}{2}+1,\frac{1}{2}) - B(\frac{n}{2},\frac{1}{2})\sqrt{1-\frac{r^2}{a^2}}\right] + B(\frac{n}{2},\frac{1}{2})\int_r^a \frac{(1-2\nu)x^{n+1} - nx^{n-1}r^2}{(1-2\nu)\sqrt{x^2-r^2}}\,dx\right\} + \frac{2}{\pi}\frac{1}{r^2}\int_a^\infty tp(t)\left[(1-2\nu)\left(\cos^{-1}\frac{a}{t} - \tan^{-1}\sqrt{\frac{a^2-t^2}{r^2-a^2}} + \frac{a}{\sqrt{t^2-a^2}}\right) - \frac{\sqrt{a^2-r^2}}{\sqrt{t^2-a^2}}\left(\frac{t^2}{t^2-r^2} - 2\nu\right)\right]dt, \quad r < a; \tag{2.37g}$$

$$\sigma_{rr}\big|_{z=0} = \frac{2(1-2\nu)}{\pi r^2}\left[\frac{\mu}{1-\nu}\frac{a^{n+1}}{2Q} B(\frac{n}{2}+1,\frac{1}{2}) - \frac{\pi}{2}\int_r^\infty tp(t)dt + \int_a^\infty tp(t)\left(\frac{a}{\sqrt{t^2-a^2}} + \cos^{-1}\frac{a}{t}\right)dt\right] + p(r), \quad r > a; \tag{2.37h}$$

$$\sigma_{\theta\theta}\big|_{z=0} = -\frac{1}{Qr^2}\frac{\mu(1-2\nu)}{\pi(1-\nu)}\left\{a^{n+1}\left[B(\frac{n}{2}+1,\frac{1}{2}) - B(\frac{n}{2},\frac{1}{2})\sqrt{1-\frac{r^2}{a^2}}\right]\right.$$
$$\left. + B(\frac{n}{2},\frac{1}{2})\int_r^a \frac{(1-2\nu)x^{n+1} + 2\nu n x^{n-1}r^2}{(1-2\nu)\sqrt{x^2-r^2}}\,dx\right\} - \frac{2}{\pi}\frac{1}{r^2}\int_a^\infty tp(t)\left[(1-2\nu)\left(\cos^{-1}\frac{a}{t}\right.\right.$$
$$\left.\left. - \tan^{-1}\sqrt{\frac{a^2-t^2}{r^2-a^2}} + \frac{a}{\sqrt{t^2-a^2}}\right)dt + \frac{\sqrt{a^2-r^2}}{\sqrt{t^2-a^2}}\left(\frac{2\nu t^2}{t^2-r^2}-1\right)\right]dt, \quad r<a; \tag{2.37i}$$

$$\sigma_{\theta\theta}\big|_{z=0} = -\frac{2(1-2\nu)}{\pi r^2}\left[\frac{\mu}{1-\nu}\frac{a^{n+1}}{2Q}B(\frac{n}{2}+1,\frac{1}{2}) - \frac{\pi}{2}\int_r^\infty tp(t)dt\right.$$
$$\left. + \int_a^\infty tp(t)\left(\frac{a}{\sqrt{t^2-a^2}} + \cos^{-1}\frac{a}{t}\right)dt\right] + 2\nu\, p(r), \quad r>a, \tag{2.37j}$$

where $B(\,;\,)$ and $B(\,;\,;\,)$ are, respectively, the beta function and the incomplete beta function defined by

$$B(\alpha,\beta) \equiv \int_0^1 t^{\alpha-1}(1-t)^{\beta-1}dt, \quad B(x;\alpha,\beta) \equiv \int_0^x t^{\alpha-1}(1-t)^{\beta-1}dt, \tag{2.37k,l}$$

with the real parts of α and β being positive.

Equations (2.37a-j) provide explicit expressions of the general solution for the penetration, applied load, and non-zero displacement and stress components on the contact surface in the frictionless adhesive contact of a power-law axisymmetric rigid punch with an elastic half space involving an arbitrary adhesive interaction force. The existing models of adhesive contact reviewed in Section 2.1 can all be recovered by this general solution as specific/limiting cases, as shown next.

2.4.3 Reduction from the General Solution

In the M-D model (Maugis, 1992) and the M-D-*n* model (Zheng and Yu, 2007), the adhesive interaction force distribution of the Dugdale type given in Eq. (2.28) is used

to obtain analytical expressions.

Substituting Eq. (2.28) into Eqs. (2.37a-d) leads to

$$u_z\big|_{z=0} = \begin{cases} \dfrac{2}{\pi}\delta\sin^{-1}\dfrac{a}{r} - \dfrac{r^n}{2\pi Q}B\left(\dfrac{n}{2},\dfrac{1}{2}\right)B\left(\dfrac{a^2}{r^2};\dfrac{n+1}{2},\dfrac{1}{2}\right) - \dfrac{2(1-\nu)\sigma_0}{\pi\mu}\displaystyle\int_a^r \frac{\sqrt{c^2-x^2}}{\sqrt{r^2-x^2}}dx, & a < r < c; \\ \dfrac{2}{\pi}\delta\sin^{-1}\dfrac{a}{r} - \dfrac{r^n}{2\pi Q}B\left(\dfrac{n}{2},\dfrac{1}{2}\right)B\left(\dfrac{a^2}{r^2};\dfrac{n+1}{2},\dfrac{1}{2}\right) - \dfrac{2(1-\nu)\sigma_0}{\pi\mu}\displaystyle\int_a^c \frac{\sqrt{c^2-x^2}}{\sqrt{r^2-x^2}}dx, & r > c; \end{cases} \tag{2.38a}$$

$$\delta = \frac{a^n}{2Q}B\left(\frac{n}{2},\frac{1}{2}\right) - \frac{(1-\nu)\sigma_0 a}{\mu}\sqrt{\left(\frac{c}{a}\right)^2 - 1}, \tag{2.38b}$$

$$P = \frac{2\mu}{1-\nu}\frac{a^{n+1}}{Q}B\left(\frac{n}{2}+1,\frac{1}{2}\right) - 2\sigma_0 a^2\left[\left(\frac{c}{a}\right)^2\sec^{-1}\left(\frac{c}{a}\right) + \sqrt{\left(\frac{c}{a}\right)^2 - 1}\right], \tag{2.38c}$$

$$\sigma_{zz}\big|_{z=0} = -\frac{\mu}{\pi(1-\nu)}\frac{n}{Q}B(\frac{n}{2},\frac{1}{2})\int_r^a \frac{t^{n-1}}{\sqrt{t^2-r^2}}dt + \frac{2\sigma_0}{\pi}\tan^{-1}\sqrt{\frac{c^2-a^2}{a^2-r^2}},\ r < a. \tag{2.38d}$$

Note that after contact the separation distance (also called the air gap) between the punch and the deformed half space surface at $r = c$ is given by

$$h(c) = f(c) + u_z\big|_{z=0,r=c} - \delta. \tag{2.39}$$

Using Eqs. (2.36), (2.38a) and (2.38b) in Eq. (2.39) then leads to

$$\begin{aligned} h(c) = \frac{a^n}{nQ}\left\{m^n - \frac{n}{2\pi}B\left(\frac{n}{2},\frac{1}{2}\right)\left[m^n B\left(\frac{1}{m^2};\frac{n+1}{2},\frac{1}{2}\right) + 2\sec^{-1}m\right]\right\} \\ + \frac{2(1-\nu)\sigma_0 a}{\pi\mu}\left(1 - m + \sqrt{m^2-1}\sec^{-1}m\right), \end{aligned} \tag{2.40}$$

where $m \equiv c/a$.

The surface energy w, also called the Dupré energy of adhesion as defined near Eq. (2.28), represents the work required to separate two surfaces to infinity (Greenwood

and Johnson, 1998). That is,

$$w = -\int_0^\infty p dh \tag{2.41}$$

where $h = h(r)$ is the separation distance between the two surfaces at position r, and $p = p(h)$ is the cohesive stress at r (with $p > 0$ for a surface pressure as shown in Figure 2.1b and Figure 2.2). Using the Dugdale cohesive stress expression (see Eq. (2.28)) in Eq. (2.41) then yields, with $h(r) = 0$ (i.e., no air gap) in the contact area (i.e., $0 \le r \le a$),

$$w = \int_a^c \sigma_0 \frac{dh}{dr} dr = \sigma_0 h(c), \tag{2.42}$$

where σ_0 is the theoretical strength defined near Eq. (2.28). Note that Eq. (2.42) can also be obtained using the Griffith energy criterion, as was done in Maugis (1992). However, the current approach is more direct and less confusing than the method based on the strain energy release rate (Greenwood and Johnson, 1998; Kim *et al*., 1998).

Substituting Eq. (2.40) into Eq. (2.42) results in

$$\begin{aligned} w = \frac{a^n \sigma_0}{nQ} \left\{ m^n - \frac{n}{2\pi} B\left(\frac{n}{2}, \frac{1}{2}\right) \left[m^n B\left(\frac{1}{m^2}; \frac{n+1}{2}, \frac{1}{2}\right) + 2\sec^{-1} m \right] \right\} \\ + \frac{2(1-\nu)\sigma_0{}^2 a}{\pi\mu} \left(1 - m + \sqrt{m^2 - 1} \sec^{-1} m\right), \end{aligned} \tag{2.43}$$

which provides a relation among the punch shape parameters n and Q, the material properties of the indented half space μ, ν and σ_0, the contact radius a, and the radius of the adhesive interaction zone c. Equation (2.43) can be used to determine the value of c when the other parameters are known.

Equations (2.38b,c) and (2.43) are identical to those provided by the M-D-*n* model of Zheng and Yu (2007), who also employed Sneddon's (1965) Hankel

transform-based solution for an axisymmetric punch problem. That is, the general solution obtained in Eqs. (2.37a-j) has recovered the M-D-*n* model. The M-D-*n* model extends the M-D model of Maugis (1992) for the adhesive indentation of a half space by a spherical punch to that by an arbitrary punch represented by a power-law shape function.

Furthermore, when $n = 2$ and $Q = R$, Eqs. (2.38a-d) and (2.43) become

$$\delta = \frac{a^2}{R} - \frac{(1-\nu)\sigma_0 a}{\mu}\sqrt{m^2-1}, \tag{2.44a}$$

$$P = \frac{8\mu}{3(1-\nu)}\frac{a^3}{R} - 2\sigma_0 a^2\left[m^2 \sec^{-1} m + \sqrt{m^2-1}\right], \tag{2.44b}$$

$$u_z\big|_{z=0} = \begin{cases} \dfrac{2}{\pi}\left[\left(\delta - \dfrac{r^2}{2R}\right)\sin^{-1}\dfrac{a}{r} + \dfrac{a}{2R}\sqrt{r^2-a^2}\right] - \dfrac{2(1-\nu)\sigma_0}{\pi\mu}\displaystyle\int_a^r \frac{\sqrt{c^2-x^2}}{\sqrt{r^2-x^2}}dx, & a < r < c; \\ \dfrac{2}{\pi}\left[\left(\delta - \dfrac{r^2}{2R}\right)\sin^{-1}\dfrac{a}{r} + \dfrac{a}{2R}\sqrt{r^2-a^2}\right] - \dfrac{2(1-\nu)\sigma_0}{\pi\mu}\displaystyle\int_a^c \frac{\sqrt{c^2-x^2}}{\sqrt{r^2-x^2}}dx, & r > c; \end{cases} \tag{2.44c}$$

$$\sigma_{zz}\big|_{z=0} = -\frac{4\mu}{\pi(1-\nu)}\frac{1}{R}\sqrt{a^2-r^2} + \frac{2\sigma_0}{\pi}\tan^{-1}\sqrt{\frac{c^2-a^2}{a^2-r^2}}, \quad r < a; \tag{2.44d}$$

$$w = \frac{\sigma_0 a^2}{\pi R}\left[\sqrt{m^2-1} + \left(m^2-2\right)\sec^{-1} m\right] + \frac{2(1-\nu)\sigma_0{}^2 a}{\pi\mu}\left(1 - m + \sqrt{m^2-1}\sec^{-1} m\right), \tag{2.44e}$$

where use has been made of the results:

$$B(1,\frac{1}{2}) = 2, \;\; B(2,\frac{1}{2}) = \frac{4}{3}, \;\; B(\frac{1}{m^2};\frac{3}{2},\frac{1}{2}) = \frac{\pi}{2} - \sec^{-1} m - \frac{\sqrt{m^2-1}}{m^2} \tag{2.45}$$

which are computed from Eqs. (2.37k,l).

Equation (2.44e) can be rewritten in a non-dimensional form as

$$\frac{1}{2}\lambda A^2\left[\sqrt{m^2-1}+\left(m^2-2\right)\sec^{-1}m\right]+\frac{4}{3}\lambda^2 A\left(1-m+\sqrt{m^2-1}\sec^{-1}m\right)=1, \quad (2.46)$$

where

$$A\equiv\frac{a}{[3\pi wR^2/(8E^*)]^{1/3}}, \quad \lambda\equiv\frac{2\sigma_0}{[64\pi w(E^*)^2/(9R)]^{1/3}}, \quad (2.47a,b)$$

are non-dimensional parameters, with $E^*\equiv\mu/(1-\nu)$. These two expressions are taken to be the same as those introduced by Maugis (1992) to facilitate a direct comparison. The parameter λ is directly related to Tabor's parameter μ_T through $\lambda = 1.16\,\mu_T$, thereby having the same physical interpretation as that of μ_T (i.e., it is a measure of the ratio of the surface elastic deformation to the range of surface forces). The parameter λ has been used to construct adhesion maps (Johnson and Greenwood, 1997; Yao *et al*., 2007; Zheng and Yu, 2007). However, non-dimensional parameters differing from λ or μ_T have also been used by others, and no agreement seems to have been reached about the best form of such a parameter (Greenwood, 1997).

Equations (2.44a,b) and (2.46) are identical to those of the M-D model derived in Maugis (1992) (see his Eq. [5.9], Eq. [6.17] and Eq. [6.18]). Hence, the M-D model for the adhesive indentation of a half space by a spherical punch has been recovered by the general solution given in Eqs. (2.37a-j).

Moreover, when σ_0 is small and $m\to\infty$, Eq. (2.44e) gives $w\approx\frac{\sigma_0 c^2}{2R}$. Using this result in Eqs. (2.44a,b,d) then leads to

$$\delta\approx\frac{a^2}{R}, \quad P\approx\frac{8\mu}{3(1-\nu)}\frac{a^3}{R}-2\pi wR, \quad \sigma_{zz}\big|_{z=0}\approx-\frac{4\mu}{\pi(1-\nu)}\frac{1}{R}\sqrt{a^2-r^2}+\sigma_0, \quad (2.48a\text{-}c)$$

which are the DMT results (modified) (Maugis, 1992), including the Hertzian pressure distribution as a limiting case as $\sigma_0 \to 0$ (see Eq. (2.18c)). This shows that the DMT model has been reduced from the current general solution as a limiting case with small λ and very large m.

On the other hand, when σ_0 is large and $m \to 1$, Eq. (2.44e) yields $w \approx \frac{\sigma_0^{\,2}(1-\nu)}{\pi\mu}\frac{c^2-a^2}{a}$. Accordingly, substituting this result into Eqs. (2.44a,b,d) gives

$$\begin{aligned} &\delta \approx \frac{a^2}{R} - \sqrt{\frac{1-\nu}{\mu}\pi w a}, \quad P \approx \frac{8\mu}{3(1-\nu)}\frac{a^3}{R} - 4\sqrt{\frac{\mu}{1-\nu}\pi w a^3}, \\ &\sigma_{zz}\big|_{z=0} \approx -\frac{4\mu}{\pi(1-\nu)}\frac{1}{R}\sqrt{a^2-r^2} + 2\sqrt{\frac{\mu}{1-\nu}}\frac{a\sqrt{w}}{\sqrt{\pi a}\sqrt{a^2-r^2}}, \end{aligned} \tag{2.49a-c}$$

which are the JKR results (Maugis, 1992; Zheng and Yu, 2007). Thus, the JKR model has been recovered from the general solution provided in Eqs. (2.37a-j) as a limiting case with large σ_0 and $m \to 1$.

Finally, when $m = 1$, Eqs. (2.44a) and (2.44b) reduce to Eqs. (2.17) and (2.18a), respectively. That is, when there is no adhesive zone, the Hertz model is reduced from the current general solution. This agrees with what is discussed earlier in Sections 2.3.1 and 2.4.2.

For general punch profiles (that is n is arbitrary), similar to the normalization introduced in Eq. (2.47) we can define the following non-dimensional parameters as was done in (Zheng and Yu, 2007):

$$\begin{aligned} &\bar{a} \equiv \frac{a}{[wQ^2(1-\nu)/(2\mu)]^{1/(2n-1)}}, \quad \bar{\delta} \equiv \frac{\delta}{[w^n Q(1-\nu)^n/(2\mu)^n]^{1/(2n-1)}}, \\ &\bar{P} \equiv \frac{P}{\pi[w^{n+1}Q^3(1-\nu)^{n-2}/(2\mu)^{n-2}]^{1/(2n-1)}}, \quad \Lambda \equiv \sigma_0[w^{1-n}Q(1-\nu)^n/(2\mu)^n]^{1/(2n-1)}. \end{aligned} \tag{2.50}$$

Then Eqs. (2.38b,c) and (2.43) can be rewritten as

$$\bar{\delta} = \frac{1}{2} B\left(\frac{n}{2}, \frac{1}{2}\right) - 2\Lambda \bar{a} \sqrt{m^2 - 1},$$

$$\bar{P} = \frac{1}{\pi} \bar{a}^{n+1} B\left(\frac{n}{2} + 1, \frac{1}{2}\right) - \frac{2}{\pi} \Lambda \bar{a}^2 \left(m^2 \sec^{-1} m + \sqrt{m^2 - 1}\right),$$

$$\frac{1}{n} \Lambda \bar{a}^n \left\{ m^n \left[1 - \frac{B\left(\frac{1}{m^2}; \frac{n+1}{2}, \frac{1}{2}\right)}{B\left(\frac{n+1}{2}, \frac{1}{2}\right)} \right] - \frac{n}{\pi} B\left(\frac{n}{2}, \frac{1}{2}\right) \sec^{-1} m \right\} + \frac{4}{\pi} \Lambda^2 \bar{a} \left(1 - m + \sqrt{m^2 - 1} \sec^{-1} m\right) = 1. \quad (2.51a\text{-}c)$$

The above equations provide the relation between the load and depth of penetration (all be normalized) for arbitrary punch profiles and this general model is called M-D-*n* model in literature (Zheng and Yu, 2007). Apparently, the above equations regenerate the Maugis' solution when $n = 2$ and they further reduces to the solutions by DMT and JKR model when the parameter Λ approaches zero and infinite, respectively. The corresponding results for DMT and JKR model with arbitrary *n* can be readily obtained simply by setting $\Lambda = 0$ and $\Lambda \to \infty$, respectively, in Eq. (2.51).

2.4.4 Numerical Results

Last section shows, analytically, the connections between the generalized DMT, JKR and M-D models. Here we are going to demonstrate the transition between the DMT-*n* and JKR-*n* models by using the established M-D-*n* model for different values of the transition parameter Λ. Firstly, we solve Eq. (2.51c) to obtain the value of *m* numerically (the values of the rest parameters in this equation need to be specified first) and then substitute the obtained value for *m* into Eq. (2.51a,b) to evaluate the values of $\bar{\delta}$ and $\bar{P}$.

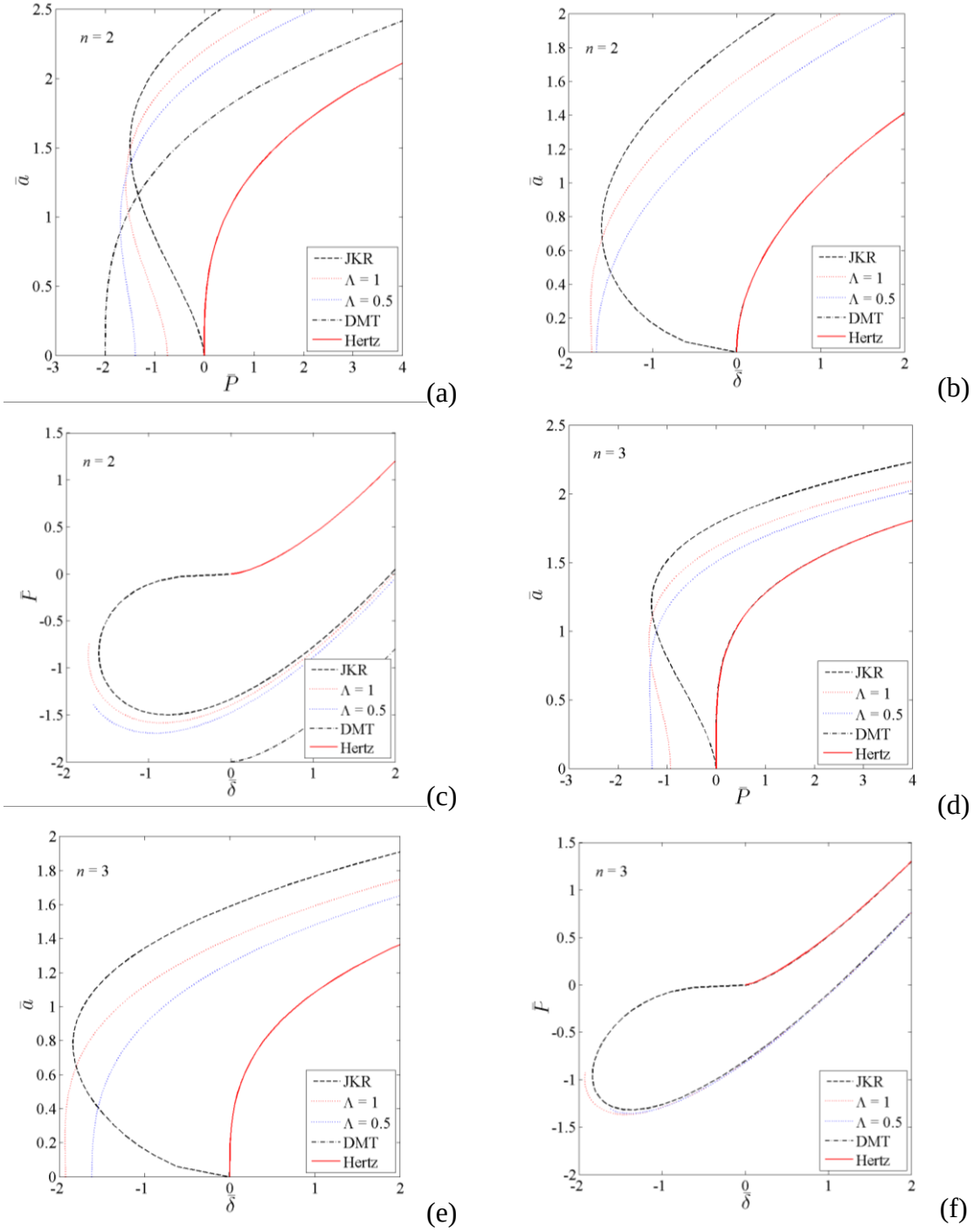

Figure 2.3. Relations between $\bar{a}$, $\bar{P}$ and $\bar{\delta}$ for variou values of Λ with n = 2 in (a), (b), and (c) and n = 3 in (d), (e) and (f). Note in (b), (d), (e) and (f) the Hertz's results and DMT's are indistinguishible.

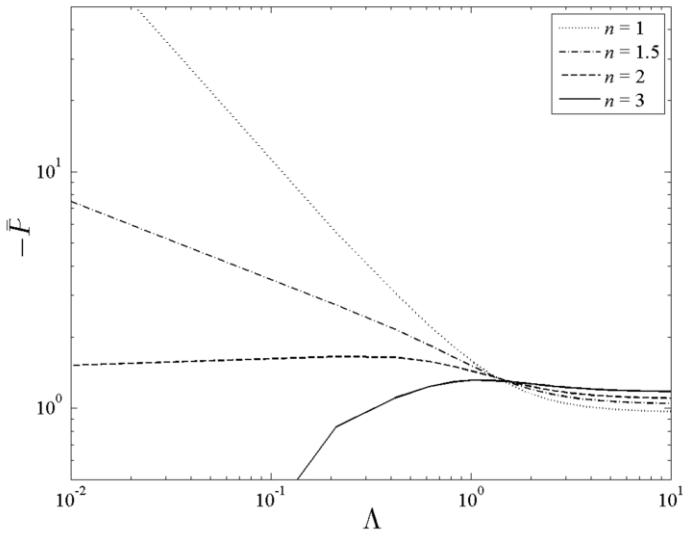

Figure 2.4. Variation of normalized load as function of parameter Λ for different punch shapes.

The relations between $\bar{a}$, $\bar{P}$ and $\bar{\delta}$ for two types of punch profiles (n = 2 and 3) are depicted in Figure 2.3. The transition from the JKR model to DMT model is clearly observed: with the value of Λ increasing from zero to infinite the M-D-n results deviate from the DMT's and gradually approach the results by JKR model. It is also noticed that the discrepancies between the three models (DMT, JKR and M-D) are smaller when the punch profile index n is larger.

Figure 2.4 shows the normalized load $\bar{P}$ as function of parameter Λ for various values of punch shape index, n. As we seen from Figure 2.4, the difference between the $\bar{P}$-Λ curves is remarkable when Λ < 1 and is insignificant for Λ > 1.

2.5 Summary

A unified treatment of axisymmetric adhesive contact problems is provided using the harmonic potential function method for axisymmetric elasticity problems. It is shown that this method enables straightforward calculations of the normal load and stress intensity factor and leads to a simpler and more consistent formulation of non-adhesive and adhesive contact problems.

A general solution is derived using the harmonic potential function method and the superposition principle for the adhesive contact problem involving an axisymmetric punch of arbitrary shape and an adhesive interaction force distribution of any profile. This solution furnishes analytical expressions for all non-zero displacement and stress components on the contact surface, which is different from other solutions.

The newly obtained solution unifies existing solutions/models for axisymmetric non-adhesive and adhesive contact problems in one framework and reveals the connections and differences among these solutions/models developed by different people using various methods over a long period of time. Specifically, it is shown that the current general solution explicitly recovers Sneddon's solution for the frictionless axisymmetric punch problem, Boussinesq's solution for the flat-ended cylindrical punch problem, the Hertz solution for the spherical punch problem, the JKR model, the DMT model, the M-D model, and the M-D-*n* model.

Finally, it should be pointed out that in the current formulation the adhesive normal traction outside the contact area is taken to be an explicit function of position r (i.e., $p = p(r)$). Since the determination of the surface energy w requires knowing the

surface separation $h = h(r)$, the Dugdale cohesive zone model with a constant cohesive stress that corresponds to a linear interaction potential is used in order to obtain the analytical solution. But the present formulation can be extended to more general separation laws by following the self-consistent approach of Barthel (1998) who employed a non-linear interaction potential and generalized the M-D model. However, the resulting solutions based on such non-linear interaction potentials would inevitably be numerical.

3. SEMI-INFINITE INDENTATION PROBLEMS WITH SURFACE EFFECTS

3.1 Introduction

The non-conventional behaviors of solids of very small volume is receiving growing interest nowadays, e.g. small volume torsion wires (Fleck and Hutchinson, 1993), plates and bars (Miller and Shenoy, 2000), thin film (Doerner and Nix, 1986; Lim and He, 2004) and nano-composites (Duan *et al*., 2005, Yvonnet *et al*., 2008). Micro/nano-indentation tests have become a widespread technique used to determine the material properties at small length scales (Fargesa and Degouta, 1989; McElhaney *et al*., 1998; Bei *et al*., 2005) and the related experiments show that the measured material hardness increases with decreasing indenter size (e.g. Stelmashenko *et al*., 1993; De Guzman *et al*., 1993; Ma and Clarke, 1995; Huang *et al*., 2010). The classical continuum theories cannot explain the indentation size effect (ISE) due to the lack of intrinsic material length scale parameters. Other factors such as work hardening, indenter pile-up and indenter tip radius effect (see Xue *et al*. (2002) for a review in this respect) are viewed to be partially responsible for the ISE and their effects should be taken into account for accurate predictions of material responses taking place at fine scales.

The theory of strain gradient plasticity pioneered by Fleck and Hutchinson (1993) is one dominating approach widely adopted to explain the ISEs and the material hardening is attributed to the geometrically necessary dislocations (GNDs) in the bulk. The depth-dependent indentation hardness is successfully addressed in a well-cited model of Nix and Gao (1998). This model works well for micro-indentation hardness

data but overestimates the hardness when indentation depth is at nano-level (e.g. Swadener *et al*., 2002; Feng and Nix, 2004; Qu *et al*., 2004; Huang *et al*., 2006). Other evidence (e.g. Tymiak *et al*., 2001; Gerberich *et al*., 2002) indicates that the strain gradient plasticity based theories is insufficient to describe ISEs at very shallow depth.

The surface energy of solids of macro-dimension is relatively negligible when compared to their bulk energy and hence is typically neglected in traditional continuum mechanics. However, the ratio of surface energy to bulk energy becomes appreciable for fine-scale contact problems and the influence of surface stress on the material responses is significant, especially for dimensions below 10 nm (Cammarat, 1994). The theory of surface elasticity originated by Gurtin and Murdoch (1975, 1978) accounts for the surface effects and contains intrinsic material length scale parameters. Therefore, it can be employed to model size effects, particularly when the surface to bulk ratio of the associated solid is large. This Gurtin and Murdoch model is quite general in a sense that it allows the surface to possess its own elastic constants and stresses by an additional constitutive law. Simplified versions of Gurtin and Murdoch model have been used in literature to analyze contact problems of a half-space (He and Lim, 2006), of a half-plane (Wang and Feng, 2007) and of an elastic layer (Zhao and Rajapakse, 2009).

The present work is intended to examine the contact problems in the context of theory of surface elasticity and thereby interpret the ISEs from a viewpoint of incorporating surface effects. General models for both the two-dimensional (2D) and three-dimensional (3D) contact problem are developed using the complete version of surface elasticity of Gurtin and Murdoch (1975, 1978).

3.2 Surface Elasticity

The nature of chemical bonding of the surface atoms differs from that of interior atoms and the surface atomic structure changes relative to the bulk so that the structural equilibrium is maintained (Thomson *et al*., 1986; Cammarata, 1994). As a result, the physical properties near a surface are sensibly different from those of the bulk interior. Surface energy, which is the reversible work to isothermally create an element area of a new surface (Cammarata and Sieradzki, 1994; Maugis, 2000, pp28), is used as a measurement of chemical bonding near a surface. For a fluid, surface energy is identical to surface tension, but they are not equal for solids unless the surface energy is deformation independent. An equation that relates the surface tension to the surface energy Γ (energy per unit area) of a solid was first suggested by Shuttleworth (1950) and Herring (1951), which now has the following form (Cammarata, 1994; Cammarata and Sieradzki, 1994)

$$\tau_{\alpha\beta} = \Gamma \delta_{\alpha\beta} + \frac{\partial \Gamma}{\partial \varepsilon_{\alpha\beta}}. \tag{3.1}$$

Therein, $\tau_{\alpha\beta}$ and $\varepsilon_{\alpha\beta}$ are, respectively, the components of surface stress and infinitesimal surface strain, and $\delta_{\alpha\beta}$ is Kronecker delta. Throughout the paper, the usual summation convention is adopted for repeated indices with the Greek indices running from 1 to 2 and the Latin ones taking 1 through 3, unless otherwise indicated.

A constitutive equation that incorporates the surface stress was proposed by Gurtin and Murdoch (1975). According to the Gurtin and Murdoch model, the surface is treated as a negligibly thin membrane with distinct material properties that adheres to the

underlying bulk material without slipping. This general theory is also applicable to describe the mechanical behaviors of an elastic substrate coated with a thin film of another material (Gurtin and Murdoch, 1978).

The classical theory of elasticity holds valid for the bulk solid, that is, the equilibrium and constitutive equations read:

$$\begin{aligned} \sigma_{ij,j} + b_i &= 0, \\ \sigma_{ij} &= \lambda \varepsilon_{kk} \delta_{ij} + 2\mu \varepsilon_{ij}, \end{aligned} \tag{3.2}$$

where b_i is the body force, ε_{ij} is the infinitesimal strain given by

$$\varepsilon_{ij} = \frac{1}{2}\left(u_{i,j} + u_{j,i}\right), \tag{3.3}$$

with u_i being the displacement components, and μ and λ are the standard Lam é constants related to elastic modulus E and Poisson's ratio ν by

$$\mu \equiv \frac{E}{2(1+\nu)}, \quad \lambda \equiv \frac{\nu E}{(1+\nu)(1-2\nu)}. \tag{3.4}$$

According to the surface elasticity of Gurtin and Murdoch (1975, 1978), the classical governing equations are coupled with surface equations, resulting in non-standard boundary conditions (BCs) involving the surface stresses which have the following form (Miller and Shenoy, 2000; Koguchi, 2003; Wang and Feng, 2007; Zhao and Rajapakse, 2009)[‡]:

$$\begin{aligned} \sigma_{\beta\alpha} n_\beta &= -\tau_{\beta\alpha,\beta}, \\ \sigma_{ij} n_i n_j &= \tau_{\beta\alpha} k_{\beta\alpha}, \end{aligned} \tag{3.5}$$

[‡] This two equations can be found in Zhao and Rajapakse (2009) and Wang and Feng (2007) and similar equations are also seen in Miller and Shenoy (2000, Eq. (4)), Yang (2004) and Koguchi (2003).

on the free surface of the substrate. In Eq. (3.5) $\boldsymbol{k}$ is the surface curvature tensor, $\boldsymbol{n}$ is the outward unit normal to the surface/interface and the surface stress components $\tau_{\alpha\beta}$ are given by (Gurtin and Murdoch, 1975, Eq. (L); 1978, Eq. (2))

$$\boldsymbol{\tau} = \tau_0 \mathbf{I} + 2(\mu_0 - \tau_0)\mathbf{I}\boldsymbol{\varepsilon}^S + (\lambda_0 + \tau_0) tr(\boldsymbol{\varepsilon}^S)\mathbf{I} + \tau_0 \nabla_S \mathbf{u}. \tag{3.6}$$

Therein, μ_0 and λ_0 are the surface Lamé constants, τ_0 is the residual surface stress, and $\boldsymbol{\varepsilon}^S$ is the surface strain tensor given by (Povstenko, 1993)[§]

$$\boldsymbol{\varepsilon}^S = \frac{1}{2}\left(\mathbf{I} - \mathbf{n}\otimes\mathbf{n}\right)\left[\nabla_S \mathbf{u} + (\nabla_S \mathbf{u})^T\right], \tag{3.7}$$

with $\mathbf{I}$ being the identity tensor and ∇_S the surface gradient operator[**]. By using the standard index notation, one can rewrite Eqs. (3.6) and (3.7) as

$$\begin{aligned} \tau_{ij} &= \tau_0\delta_{ij} + 2(\mu_0 - \tau_0)\varepsilon_{ij}^S + (\lambda_0 + \tau_0)\varepsilon_{kk}^S\delta_{ij} + \tau_0(u_{i,j} - n_j n_k u_{i,k}), \\ \varepsilon_{ij}^S &= \frac{1}{2}\left(\delta_{ik} - n_i n_k\right)\left[u_{k,j} + u_{j,k} - n_l\left(n_j u_{k,l} + n_k u_{j,l}\right)\right]. \end{aligned} \tag{3.8}$$

In general, the surface elastic moduli (namely, μ_0 and λ_0) vary over the surface with the change in surface tension (Povstenko, 1993). For simplicity, they are assumed to be constant in this work.

For an elastic body occupying the half-space ($x_3 > 0$), the surface equilibrium equations and the surface stress components given by Eq. (3.8) are (e.g., Gurtin and Murdoch, 1978)

[§] This definition differs from that provided in Gurtin and Murdoch (1975). However, both of them lead to Eq. (3.9b).

[**] The surface gradient of a scalar is given by: $\nabla_S u = \nabla u - \mathbf{n}(\mathbf{n}\cdot\nabla u)$.

$$\sigma_{i3} = -\tau_{i\alpha,\alpha},$$
$$\tau_{\alpha\beta} = [\tau_0 + (\lambda_0 + \tau_0)u_{\gamma,\gamma}]\delta_{\alpha\beta} + \mu_0(u_{\alpha,\beta} + u_{\beta,\alpha}) - \tau_0 u_{\beta,\alpha}, \tag{3.9}$$
$$\tau_{3\alpha} = \tau_0 u_{3,\alpha}.$$

Equation (3.9b) with $\mu_0 = \lambda_0 = 0$ is the simplified surface constitutive equation employed by He and Lim (2006) to derive fundamental solutions for an elastic half-space.

It follows from Eq. (3.9) that the conventional traction-free BCs for a semi-infinite solid are

$$\sigma_{33}\big|_{x_3=0} = -\tau_0\, u_{3,\alpha\alpha}\big|_{x_3=0},$$
$$\sigma_{\alpha 3}\big|_{x_3=0} = -(\mu_0 + \lambda_0)\, u_{\beta,\beta\alpha}\big|_{x_3=0} - \mu_0\, u_{\alpha,\beta\beta}\big|_{x_3=0}, \tag{3.10}$$

and they become (by setting the partial derivatives with respective to x_2 as zero)

$$\sigma_{33}\big|_{x_3=0} = -\tau_0\, u_{3,11}\big|_{x_3=0},$$
$$\sigma_{13}\big|_{x_3=0} = -(2\mu_0 + \lambda_0)\, u_{1,11}\big|_{x_3=0}, \tag{3.11}$$

in the case of a semi-infinite plane. In arriving at Eqs. (3.10) and (3.11), it has been assumed that parameters μ_0, λ_0 and τ_0 are deformation independent. These BCs can be easily modified to include prescribed boundary tractions.

Equations (3.10) and (3.11) provide, respectively, the general BCs for an elastic half-space and half-plane with free surfaces in the context of surface elasticity of Gurtin and Murdoch (1975, 1978). BCs other than Eq. (3.10) have been used in literature, e.g., He and Lim (2006), Wang and Feng (2007) and Zhao and Rajapakse (2009). The models employed by He and Lim (2006) and Wang and Feng (2007) only include the residual surface stress and lead to the same BCs for the problem of a semi-infinite medium, i.e.,

$\sigma_{\alpha 3} = 0$ and $\sigma_{33} = -\tau_0 u_{3,\alpha\alpha}$. On the other hand, the surface moduli (μ_0 and λ_0) are included in the formulations in Zhao and Rajapakse (2009). However, the surface curvature $u_{3,\alpha\alpha}$ is assumed to be zero as was done in Miller and Shenoy (2000).

Note that in each of the aforementioned models certain simplifications were made and the BCs are not exact. In the current work, the general BCs are formulated using the general surface elasticity theory of Gurtin and Murdoch (1975) and the only assumption being made is that μ_0, λ_0 and τ_0 are deformation independent.

3.3 Papkovitch-Neuber Potential Functions

The technique of integral transforms is very desirable in attacking higher order partial differential equations (PDEs) in that it enables one to obtain the solutions by manipulating algebraic equations in the transformed domain. This method is particularly powerful when associated with the used of potential functions. A monograph on the development of assorted potential functions is presented in Sternberg (1960) and the readers can refer to Truesdell (1959) for the bibliography of stress functions as well as a short note by Mindlin (1936) for the relations between different types of potential functions. The Papkovitch-Neuber (P-N) representation which contains a vector potential $\mathbf{\Psi}$ and scalar potential Φ is employed to solve the current half-space problem.

The displacement field in terms of P-N functions is given by (e.g., Ling *et al.*, 2002, pp71)

$$u_i = \Psi_i - \frac{1}{4(1-\nu)}(x_j \Psi_j + \Phi)_{,i}. \tag{3.12}$$

Upon use of Eq. (3.12) it can be shown that the Navier's equation is reduced to

$$\mu\nabla^2\Psi_i = -b_i, \tag{3.13}$$

so far as the scalar function Φ satisfies

$$\mu\nabla^2\Phi = x_i b_i, \tag{3.14}$$

where **x** is the position vector of a field point. Apparently, Ψ_i and Φ are harmonic functions when the body forces are absent, i.e.,

$$\nabla^2\Psi_i = 0 \text{ and } \nabla^2\Phi = 0. \tag{3.15}$$

The problems of a half-plane and of a half-space subjected to boundary normal forces are illustrated in Figure 3.1. The body forces are assumed to be absent through the discussion. The coordinate system is chosen such that the *xy*-plane coincides with the top bounding surface and its origin is at the geometry center of the distributed load.

For a semi-infinite solid subjected to a normal force, the vector potential **Ψ** takes

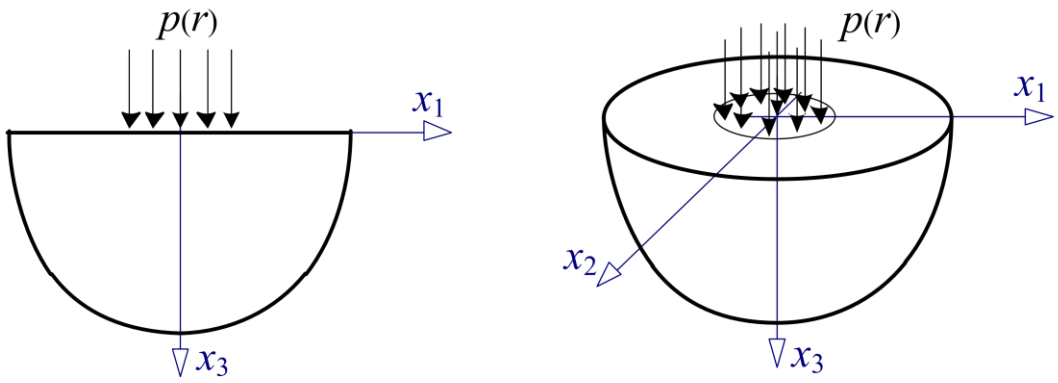

(a) (b)

Figure 3.1. An elastic half-plane (a) and an elastic half-space (b) subject to the distributed normal forces.

the form (0, 0, Ψ_3) and consequently, we have from Eq. (3.12)

$$u_\alpha = -\frac{1}{4(1-\nu)}\left(x_3\Psi_{3,\alpha} + \Phi_{,\alpha}\right),$$
$$u_3 = -\frac{1}{4(1-\nu)}\left[(-3+4\nu)\Psi_3 + x_3\Psi_{3,3} + \Phi_{,3}\right]. \tag{3.16}$$

Using Eq. (3.16) in Eq. (3.2b) then gives the stress components as

$$\sigma_{\alpha\beta} = \frac{\mu}{2(1-\nu)}\left(-x_3\Psi_{3,\alpha\beta} - \Phi_{,\alpha\beta}\right), \quad \alpha \neq \beta,$$
$$\sigma_{\alpha\alpha} = \frac{\mu}{2(1-\nu)}\left(2\nu\Psi_{3,3} - x_3\Psi_{3,\alpha\alpha} - \Phi_{,\alpha\alpha}\right),$$
$$\sigma_{3\alpha} = \frac{\mu}{2(1-\nu)}\left[(1-2\nu)\Psi_{3,\alpha} - x_3\Psi_{3,\alpha 3} - \Phi_{,\alpha 3}\right], \tag{3.17}$$
$$\sigma_{33} = \frac{\mu}{2(1-\nu)}\left[2(1-\nu)\Psi_{3,3} - x_3\Psi_{3,33} - \Phi_{,33}\right],$$

where summation is not applied on α in Eq. (3.17b) and Eq. (3.15) has been used in arriving at Eq. (3.17).

Similarly, using Eq. (3.16) and Eq. (3.15) one obtains

$$u_{3,\alpha\alpha} = \frac{1}{4(1-\nu)}\left[(-3+4\nu)\Psi_{3,33} + x_3\Psi_{3,333} + \Phi_{,333}\right],$$
$$(\mu_0+\lambda_0)u_{\beta,\beta\alpha} + \mu_0 u_{\alpha,\beta\beta} = \frac{2\mu_0+\lambda_0}{4(1-\nu)}\left(x_3\Psi_{3,33\alpha} + \Phi_{,33\alpha}\right). \tag{3.18}$$

Then by using Eqs. (3.17) and (3.18) in Eq. (3.10) whilst taking $x_3 = 0$, the non-standard BCs are expressed in terms of potential functions as

$$2(1-\nu)\Psi_{3,3} - \Phi_{,33} = \frac{\eta}{2}\left[(3-4\nu)\Psi_{3,33} - \Phi_{,333}\right] - \frac{2(1-\nu)}{\mu}\,p,$$
$$(1-2\nu)\Psi_3 - \Phi_{,3} = -\frac{\chi}{2}\Phi_{,33}, \tag{3.19}$$

where it is defined that

$$\eta = \frac{\tau_0}{\mu}, \quad \chi = \frac{2\mu_0 + \lambda_0}{\mu}, \tag{3.20}$$

and p denotes the normal pressure function and is positive for compressive forces. Integration with respect to x_α has been performed in arriving at Eq. (3.19b) and the constant of integration is taken to be zero[††]. It is of practical interest to note that both η and χ have dimensions of length characterized by the surface mechanical properties (τ_0, λ_0 and μ_0) and thus can be interpreted as intrinsic material length scale parameters.

Equation (3.19) provides the general BCs for semi-infinite contact problems in terms of the P-N functions and applies to the problems of a half-plane and of a half-space subjected to boundary normal forces.

3.4 Fourier Transform

The method of Fourier transform is widely used in literature to solve boundary value problems in solid mechanics. A successful treatment of axisymmetric contact problems was presented by Harding and Sneddon (1945) using Hankel transform and a biharmonic function (known as Love function or Galerkin vector). Recently, this Hankel transform based formulation was adopted by Zhao and Rajapakse (2009) to solve contact problems with consideration of surface effects.

The Fourier transforms and P-N functions are employed in the current approach to formulate the semi-infinite contact problems. The standard Fourier transform and

[††] Analogous argument can be found in Ling *et al*. (2002, pp84).

double Fourier transform are used, respectively, for the half-plane and half-space contact problems.

The standard Fourier transform pair is

$$\begin{aligned} \overline{f}(\xi) &= \int_{-\infty}^{\infty} f(x) e^{-\mathrm{i}\xi x} dx, \\ f(x) &= \frac{1}{2\pi} \int_{-\infty}^{\infty} \overline{f}(\xi) e^{\mathrm{i}\xi x} d\xi, \end{aligned} \tag{3.21}$$

whereas the double Fourier transform pair reads

$$\begin{aligned} \overline{f}(\xi_1, \xi_2) &= \int_{-\infty}^{\infty} \int_{-\infty}^{\infty} f(x_1, x_2) e^{-\mathrm{i}\xi_\alpha x_\alpha} dx_1 dx_2, \\ f(x_1, x_2) &= \frac{1}{4\pi^2} \int_{-\infty}^{\infty} \int_{-\infty}^{\infty} \overline{f}(\xi_1, \xi_2) e^{\mathrm{i}\xi_\alpha x_\alpha} d\xi_1 d\xi_2, \end{aligned} \tag{3.22}$$

where the overhead bar denotes a function in the transformed space.

For the harmonic functions Ψ_3 and Φ, the application of Fourier transform leads to

$$\frac{\partial^2}{\partial x_3^{\,2}} \overline{\Psi}_3 - \xi^2 \overline{\Psi}_3 = 0, \quad \frac{\partial^2}{\partial x_3^{\,2}} \overline{\Phi} - \xi^2 \overline{\Phi} = 0, \tag{3.23}$$

whose general solutions are

$$\overline{\Psi}_3 = A e^{-x_3|\xi|} + A' e^{x_3|\xi|}, \quad \overline{\Phi} = B e^{-x_3|\xi|} + B' e^{x_3|\xi|}. \tag{3.24}$$

Herein $\xi^2 = \xi_\alpha \xi_\alpha$ and equals to ξ^2 and $\xi_1^2 + \xi_2^2$ for 2D and 3D contact problems, respectively. The unknowns A, B, A', and B', in general, are functions of ξ and are to be determined from the BCs. Since it has been of our attention to solve semi-infinite problems, we should have

$$\overline{\Psi}_3 = A e^{-x_3|\xi|}, \quad \overline{\Phi} = B e^{-x_3|\xi|} \tag{3.25}$$

such that $\bar{\Psi}_3$ and $\bar{\Phi}$ converge at $x_3 \to \infty$. The potential functions Ψ_3 and Φ are then obtained by using the inverse Fourier transform to be

$$\Psi_3 = \frac{1}{2\pi}\int_{-\infty}^{\infty} A e^{\mathrm{i}\xi x_1 - x_3|\xi|} d\xi, \quad \Phi = \frac{1}{2\pi}\int_{-\infty}^{\infty} B e^{\mathrm{i}\xi x_1 - x_3|\xi|} d\xi \tag{3.26}$$

as for the half-plane problems, and

$$\Psi_3 = \frac{1}{4\pi^2}\int_{-\infty}^{\infty}\int_{-\infty}^{\infty} A e^{\mathrm{i}\xi_\alpha x_\alpha - x_3|\xi|} d\xi_1 d\xi_2, \quad \Phi = \frac{1}{4\pi^2}\int_{-\infty}^{\infty}\int_{-\infty}^{\infty} B e^{\mathrm{i}\xi_\alpha x_\alpha - x_3|\xi|} d\xi_1 d\xi_2 \tag{3.27}$$

as for half-space problems.

As shown in the Appendix, simpler integral forms can be obtained for double inverse Fourier transforms when the coordinate transform is used along with Bessel functions.

When $\bar{f}$ is θ-independent, it can be shown that

$$F^{-1}[\bar{f}(\xi)] = \frac{1}{2\pi}\int_0^{\infty} \bar{f}(\xi)\xi J_0(\xi r) d\xi, \tag{3.28a}$$

$$F^{-1}[\bar{f}(\xi)\xi_\alpha] = \mathrm{i}\frac{x_\alpha}{2\pi r}\int_0^{\infty} \bar{f}(\xi)\xi^2 J_1(\xi r) d\xi. \tag{3.28b}$$

where $r^2 = x_\alpha x_\alpha$. Also, one can show that

$$F^{-1}[\bar{f}(\xi)\xi_1\xi_2] = -\frac{x_1 x_2}{2\pi r^2}\int_0^{\infty} \bar{f}(\xi)\xi^3 J_2(\xi r) d\xi, \tag{3.28c}$$

$$F^{-1}[\bar{f}(\xi)\xi_\alpha^2] = \frac{1}{4\pi}\int_0^{\infty} \bar{f}(\xi)\xi^3 \left[J_0(\xi r) - \left(2x_\alpha^2 r^{-2} - 1\right) J_2(\xi r) \right] d\xi. \tag{3.28d}$$

Equation (3.28) provides the link between Fourier transforms and Hankel transforms and is used to evaluate the displacements and stresses in the space domain. Note that Eqs. (3.28c,d) are used to calculate $\sigma_{\alpha\beta}$, which are not discussed in this work.

3.5 General Solutions

The general solution for a semi-infinite medium subjected to a prescribed surface pressure is sought by using the BCs in Eq. (3.19) and the potential functions given in Eqs. (3.26) and (3.27).

Substituting Eq. (3.27) into Eq. (3.19) yields

$$\begin{aligned} -2(1-\nu)|\xi|A-\xi^2 B &= \frac{\eta}{2}\left[(3-4\nu)\xi^2 A+|\xi|^3 B\right]-\frac{2(1-\nu)}{\mu}\bar{p}, \\ (1-2\nu)A+|\xi|B &= -\frac{\chi}{2}\xi^2 B, \end{aligned} \tag{3.29}$$

the solution of which is given by

$$A=\frac{(1-\nu)(2+\chi|\xi|)}{\mu|\xi|\left(1+\kappa_1|\xi|+\kappa_2\xi^2\right)}\bar{p}, \quad B=-\frac{2(1-\nu)(1-2\nu)}{\mu\xi^2\left(1+\kappa_1|\xi|+\kappa_2\xi^2\right)}\bar{p}, \tag{3.30}$$

where

$$\begin{aligned} \kappa_1 &= (1-\nu)(\eta+\chi)=\frac{1-\nu}{\mu}\left(\tau_0+2\mu_0+\lambda_0\right), \\ \kappa_2 &= \left(\tfrac{3}{4}-\nu\right)\eta\chi=\frac{3-4\nu}{4\mu^2}\tau_0\left(2\mu_0+\lambda_0\right). \end{aligned} \tag{3.31}$$

If A and B are to be well-defined in the entire Fourier domain it is then required that $\tau_0 \geq 0$ and $2\mu_0+\lambda_0 \geq 0$.

The expression for $\bar{p}$ can be readily obtained once the surface pressure is given. For instance, $\bar{p}=P$ when the imposed boundary load is a concentrated force of magnitude P, i.e., $p(\mathbf{x}) = P\delta(\mathbf{x})$; and

$$\bar{p}=\begin{cases} 2q_0\xi^{-1}\sin(a\xi), & 2D \\ 2\pi q_0 a\xi^{-1}J_1(a\xi), & 3D \end{cases} \tag{3.32}$$

when a uniformly distributed pressure of intensity q_0 is applied over the region $|x_1| \le a$ (as for 2D) and $r \le a$ (for 3D), respectively.

In case of symmetric (2D case) or axisymmetric (3D case) loading, $\bar{p}$ is an even function of ξ. Accordingly, A and B given in Eq. (3.30) are even functions of ξ. This permits the use of Fourier cosine transform for potential functions:

$$\begin{aligned}\Psi_3 &= \frac{1-\nu}{\pi\mu}\int_0^\infty \frac{(2+\chi\xi)\bar{p}e^{-x_3\xi}}{\xi\left(1+\kappa_1\xi+\kappa_2\xi^2\right)}\cos(\xi x_1)d\xi,\\ \Phi &= -\frac{2(1-\nu)(1-2\nu)}{\pi\mu}\int_0^\infty \frac{\bar{p}e^{-x_3\xi}}{\xi^2\left(1+\kappa_1\xi+\kappa_2\xi^2\right)}\cos(\xi x_1)d\xi.\end{aligned} \tag{3.33}$$

Similarly, for the axisymmetric contact problems use of Eq. (3.28a) gives

$$\begin{aligned}\Psi_3 &= \frac{1-\nu}{2\pi\mu}\int_0^\infty \frac{(2+\chi\xi)\bar{p}e^{-x_3\xi}}{1+\kappa_1\xi+\kappa_2\xi^2}J_0(\xi r)d\xi,\\ \Phi &= -\frac{(1-\nu)(1-2\nu)}{\pi\mu}\int_0^\infty \frac{\bar{p}e^{-x_3\xi}}{\xi\left(1+\kappa_1\xi+\kappa_2\xi^2\right)}J_0(\xi r)d\xi.\end{aligned} \tag{3.34}$$

Then it follows from Eqs. (3.16) and (3.17) that the displacement and stress field are

$$\begin{aligned}u_1 &= \int_0^\infty h_1(x_3,\xi)\bar{p}(\xi)\sin(\xi x_1)d\xi,\\ u_3 &= \int_0^\infty h_2(x_3,\xi)\bar{p}(\xi)\cos(\xi x_1)d\xi,\\ \sigma_{31} &= \int_0^\infty h_3(x_3,\xi)\bar{p}(\xi)\sin(\xi x_1)d\xi,\\ \sigma_{33} &= \int_0^\infty h_4(x_3,\xi)\bar{p}(\xi)\cos(\xi x_1)d\xi,\end{aligned} \tag{3.35}$$

for the 2D contact problem with symmetrical load distribution, and

$$
\begin{aligned}
u_\alpha &= \frac{x_\alpha}{2r}\int_0^\infty h_1(x_3,\xi)\bar{p}(\xi)\xi J_1(\xi r)d\xi,\\
u_3 &= \frac{1}{2}\int_0^\infty h_2(x_3,\xi)\bar{p}(\xi)\xi J_0(\xi r)d\xi,\\
\sigma_{3\alpha} &= \frac{x_\alpha}{2r}\int_0^\infty h_3(x_3,\xi)\bar{p}(\xi)\xi J_1(\xi r)d\xi,\\
\sigma_{33} &= \frac{1}{2}\int_0^\infty h_4(x_3,\xi)\bar{p}(\xi)\xi J_0(\xi r)d\xi,
\end{aligned}
\tag{3.36}
$$

for the axisymmetric contact problems, where

$$
\begin{aligned}
h_1(x_3,\xi) &= -\frac{2(1-2\nu)-2x_3\xi-x_3\chi\xi^2}{4\pi\mu\xi\left(1+\kappa_1\xi+\kappa_2\xi^2\right)}e^{-x_3\xi},\\
h_2(x_3,\xi) &= \frac{4(1-\nu)+(3-4\nu)\chi\xi+x_3(2+\chi\xi)\xi}{4\pi\mu\xi\left(1+\kappa_1\xi+\kappa_2\xi^2\right)}e^{-x_3\xi},\\
h_3(x_3,\xi) &= -\frac{(1-2\nu)\chi\xi+x_3(2+\chi\xi)\xi}{2\pi\left(1+\kappa_1\xi+\kappa_2\xi^2\right)}e^{-x_3\xi},\\
h_4(x_3,\xi) &= -\frac{1+(1-\nu)\chi\xi+\frac{1}{2}x_3(2+\chi\xi)\xi}{\pi\left(1+\kappa_1\xi+\kappa_2\xi^2\right)}e^{-x_3\xi}.
\end{aligned}
\tag{3.37}
$$

As seen from Eqs. (3.36) and (3.37), the 2D and 3D solutions given in integral forms are analogous – with $\sin(\xi x_1)$ corresponding to $\xi J_1(\xi r)$ and $\cos(\xi x_1)$ to $\xi J_0(\xi r)$. This correspondence property enables one to attack the 2D and 3D problems of similar kind in a unified manner.

Equations (3.35) and (3.36) provide, respectively, the general solutions for contact problems of an elastic half-plane and of an elastic half-space based on the surface elasticity of Gurthin and Murdoch (1975). These results apply to symmetric (as in 2D cases) and axisymmetric (as in 3D cases) contact problems, and the classical solutions can be recovered from the newly derived solution as special cases wherein the

surface effects are neglected.

In contact mechanics, the surface displacements and stresses are of prime interest and are therefore examined. By setting $x_3 = 0$ in Eq. (3.35) and (3.36), we find on the surface $x_3 = 0$ of a half-plane the current results deviate from its classical counterparts by

$$\begin{aligned}
u_1^s\big|_{x_3=0} &= u_1\big|_{x_3=0} - u_1^c\big|_{x_3=0} = \int_0^\infty g_1(\xi)\,\bar{p}(\xi)\sin(\xi x_1)d\xi,\\
u_3^s\big|_{x_3=0} &= u_3\big|_{x_3=0} - u_3^c\big|_{x_3=0} = \int_0^\infty g_2(\xi)\,\bar{p}(\xi)\cos(\xi x_1)d\xi,\\
\sigma_{3\alpha}^s\big|_{x_3=0} &= \sigma_{3\alpha}\big|_{x_3=0} = \int_0^\infty g_3(\xi)\,\bar{p}(\xi)\xi\sin(\xi x_1)d\xi,\\
\sigma_{33}^s\big|_{x_3=0} &= \sigma_{33}\big|_{x_3=0} - \sigma_{33}^c\big|_{x_3=0} = \int_0^\infty g_4(\xi)\,\bar{p}(\xi)\xi\cos(\xi x_1)d\xi,
\end{aligned} \tag{3.38}$$

and for the problems of a half-space they become

$$\begin{aligned}
u_\alpha^s\big|_{z=0} &= \frac{x_\alpha}{2r}\int_0^\infty g_1(\xi)\,\bar{p}(\xi)\xi J_1(\xi r)d\xi,\\
u_3^s\big|_{z=0} &= \frac{1}{2}\int_0^\infty g_2(\xi)\,\bar{p}(\xi)\xi J_0(\xi r)d\xi,\\
\sigma_{3\alpha}^s\big|_{z=0} &= \frac{x_\alpha}{2r}\int_0^\infty g_3(\xi)\,\bar{p}(\xi)\xi^2 J_1(\xi r)d\xi,\\
\sigma_{33}^s\big|_{z=0} &= \frac{1}{2}\int_0^\infty g_4(\xi)\,\bar{p}(\xi)\xi^2 J_0(\xi r)d\xi,
\end{aligned} \tag{3.39}$$

where

$$\begin{aligned}
g_1(\xi) &= \frac{1-2\nu}{2\pi\mu}\frac{\kappa_1+\kappa_2\xi}{1+\kappa_1\xi+\kappa_2\xi^2},\\
g_2(\xi) &= -\frac{1-\nu}{\pi\mu}\frac{-\frac{3-4\nu}{4(1-\nu)}\chi+\kappa_1+\kappa_2\xi}{1+\kappa_1\xi+\kappa_2\xi^2} = -\frac{1-\nu}{\pi\mu}\frac{\frac{(1-2\nu)^2}{4(1-\nu)}\chi+(1-\nu)\eta+\kappa_2\xi}{1+\kappa_1\xi+\kappa_2\xi^2},
\end{aligned} \tag{3.40a,b}$$

$$g_3(\xi) = -\frac{(1-2\nu)\chi}{2\pi\left(1+\kappa_1\xi+\kappa_2\xi^2\right)},$$
$$g_4(\xi) = \frac{-(1-\nu)\chi+\kappa_1+\kappa_2\xi}{\pi\left(1+\kappa_1\xi+\kappa_2\xi^2\right)} = \frac{(1-\nu)\eta+\kappa_2\xi}{\pi\left(1+\kappa_1\xi+\kappa_2\xi^2\right)}. \quad (3.40c,d)$$

In Eqs. (3.38) and (3.39) the superscripts '*c*' and '*s*' denote, respectively, the classical solution and the departure between the newly derived solution and its classical counterpart. Clearly, $g_i(\xi) = 0$ (i = 1, 2, 3, 4) in the absence of the surface effects and the surface elasticity-based solution becomes identical to the classical one.

Provided $\tau_0 \geq 0$ and $2\mu_0 + \lambda_0 \geq 0$, one shall have from Eqs. (3.38)-(3.40) that $g_1(\xi) > 0$, $g_2(\xi) < 0$, $g_3(\xi) < 0$ and $g_4(\xi) > 0$, which imply that incorporating surface effects results in smaller displacements and normal stress, but non-vanishing shear stresses on the bounding surface. Besides, the influence of surface effects are more pronounced when the values of τ_0 and $2\mu_0 + \lambda_0$ larger.

3.6 Illustrative Examples

Representative problems are selected for demonstration of the potential applications of the current solution as well as to assess the influence of the surface effects on the responses of the semi-infinite solids.

3.6.1 Concentrated Vertical Force

Determination of the stress state in an isotropic elastic half-space subjected to a concentrated force acting normally to the plane surface was first studied by Boussinesq (1885). The Boussinesq problem is one of the most celebrated problems in classical

elasticity, and as a fundamental solution has found numerous applications in contact mechanics. Different approaches have been made to solve the Boussinesq problem, such as potential theory, combinations of dipoles and integral transform techniques (Selvadurai, 2007).

As mentioned near Eq. (3.32), $\bar{p} = P$ when p represents a concentrated force of magnitude P. By setting $\chi = \kappa_1 = \kappa_2 = 0$ and $\bar{p} = P$ in Eq. (3.34) one obtains the classical solutions of P-N functions for Boussinesq problem as

$$\begin{aligned} \Psi_3^c &= \frac{(1-\nu)P}{\pi\mu}\int_0^\infty e^{-x_3\xi} J_0(\xi r)d\xi = \frac{(1-\nu)P}{\pi\mu}\frac{1}{R}, \\ \Phi^c &= -\frac{(1-\nu)(1-2\nu)P}{\pi\mu}\int_0^\infty \xi^{-1} e^{-x_3\xi} J_0(\xi r)d\xi = \frac{(1-\nu)(1-2\nu)P}{\pi\mu}\ln(R+x_3), \end{aligned} \tag{3.41}$$

where $R^2 = r^2 + x_3^2 = x_i x_i$. The solution given by Eq. (3.41) is in agreement with the known results obtained by Mindlin (1953) using a different approach. The displacement field and state of stress for Bousinessq problem are readily obtained by using Eq. (3.41) in Eq. (3.17).

In the presence of surface effects, by replacing $\bar{p}$ with P in Eq. (3.36) we have

$$\begin{aligned} u_\alpha &= \frac{Px_\alpha}{2r}\int_0^\infty h_1(x_3,\xi)\xi J_1(\xi r)d\xi, \\ u_3 &= \frac{P}{2}\int_0^\infty h_2(x_3,\xi)\xi J_0(\xi r)d\xi, \end{aligned} \tag{3.42}$$

for the Boussinesq Problem. The displacements on the plane $x_3 = 0$ can be subsequently deduced by setting $x_3 = 0$ in Eq. (3.42).

Equation (3.42) provide the fundamental solution to the Boussinesq problem based on the theory of surface elasticity. Unlike the classical solution, the displacement

field now is dependent on the surface parameters through functions $h_i(x_3, \xi)$ given in Eq. (3.37). Besides, the displacement field obtained by He and Lim (2006) can be recovered from Eq. (3.42) as a special case with $\chi = 0$ and $\nu = 0.5$.

The surface effects on the elastic field are then examined for η and χ taking different values and the results are displayed in Figure 3.2. The solid blue lines with $\eta = \chi = 0$ correspond to the classical elastic solution which does not consider surface effects. The well-known displacement singularity and discontinuity at the point of the application of force are alleviated when the surface effects are incorporated and the magnitudes of displacements near the loading point are markedly smaller than the corresponding classical results. The current prediction of vanishing in-plane displacements at the loading point is more physical than the classical solution (e.g., Georgiadis and Anagnostou, 2008).

It is further noticed that the influence of the surface parameter χ is significant on

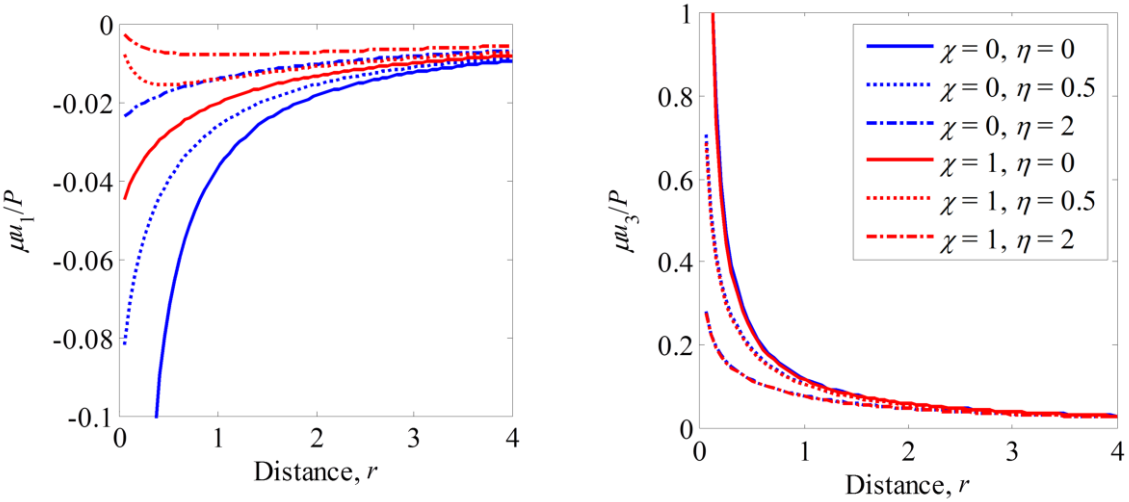

(*a*) (*a*)

Figure 3.2. Surface effects on the surface displacements for the Bausinessq's problem.

the in-plane displacements, but is negligible on the out-of-plane displacement. On the contrary, all surface displacements rely heavily on the residual surface stress τ_0 and their magnitudes drop considerably with increasing τ_0.

3.6.2 Uniformly Distributed Pressure

Next we consider a semi-infinite elastic solid subjected to a uniformly distributed normal load over the region $r < a$ on the plane $x_3 = 0$. Substituting Eqs. (3.32a) and (3.32 b) respectively into Eqs. (3.35) and (3.36) gives

$$\begin{aligned} u_1 &= 2q_0\int_0^\infty h_1(x_3,\xi)\xi^{-1}\sin(a\xi)\sin(\xi x_1)d\xi, \\ u_3 &= 2q_0\int_0^\infty h_2(x_3,\xi)\xi^{-1}\sin(a\xi)\cos(\xi x_1)d\xi, \\ \sigma_{13} &= 2q_0\int_0^\infty h_3(x_3,\xi)\xi^{-1}\sin(a\xi)\sin(\xi x_1)d\xi, \\ \sigma_{33} &= 2q_0\int_0^\infty h_4(x_3,\xi)\xi^{-1}\sin(a\xi)\cos(\xi x_1)d\xi \end{aligned} \tag{3.43}$$

for the half-plane problem, and

$$\begin{aligned} u_\alpha &= \pi q_0 a\frac{x_\alpha}{r}\int_0^\infty h_1(x_3,\xi)J_1(a\xi)J_1(\xi r)d\xi, \\ u_3 &= \pi q_0 a\int_0^\infty h_2(x_3,\xi)J_1(a\xi)J_0(\xi r)d\xi, \\ \sigma_{13} &= \pi q_0 a\frac{x_\alpha}{r}\int_0^\infty h_2(x_3,\xi)J_1(a\xi)J_1(\xi r)d\xi, \\ \sigma_{33} &= \pi q_0 a\int_0^\infty h_4(x_3,\xi)J_1(a\xi)J_0(\xi r)d\xi \end{aligned} \tag{3.44}$$

for the half-space problem.

In a similar fashion one can recover the classical solution for the half-plane problem considered here by setting $\chi = \kappa_1 = \kappa_2 = 0$ in Eq. (3.43) and by knowing (e.g., Georgiadis and Anagnostou, 2008)

$$\int_0^\infty \frac{\sin(xt)}{t}\,dt = \frac{\pi}{2}\,\mathrm{sgn}(x) \text{ and } \int_0^\infty \frac{\cos(xt)}{t}\,dt = -\ln|x| + \text{Const.}, \tag{3.45}$$

where sgn( ) is the signum function. In addition, the solution derived by Wang and Feng (2007) is reproduced as a particular case in which the surface elastic moduli (μ_0 and λ_0) are treated as zero.

The classical solution for the associated half-space problem can be regenerated from Eq. (3.44). For instance, along the x_3-axis ($r = 0$) one finds $u_\alpha = 0$ and

$$\begin{aligned} u_3^c\big|_{r=0} &= \frac{(1-\nu)q_0 a}{\mu}\int_0^\infty \frac{1}{\xi} e^{-x_3\xi} J_1(a\xi)\,d\xi + \frac{q_0 a}{2\mu}\int_0^\infty x_3 e^{-x_3\xi} J_1(a\xi)\,d\xi \\ &= \frac{(1-\nu)q_0}{\mu}\left(\sqrt{a^2+x_3^2} - x_3\right) + \frac{q_0}{2\mu}\left[x_3 - x_3^2(a^2+x_3^2)^{-1/2}\right], \\ \sigma_{33}^c\big|_{r=0} &= -q_0 a\int_0^\infty (1+x_3\xi)e^{-x_3\xi} J_1(a\xi)\,d\xi = -\left[1 - x_3^3(a^2+x_3^2)^{-2/3}\right]q_0, \end{aligned} \tag{3.46}$$

which are in agreement with the known classical solution (e.g., Ling *et al*., 2000, pp90).

Figure 3.3 shows the surface displacements and stresses of a half-plane subjected to a uniformly distributed load and those for the half-space are displayed in Figure 3.4. Various values of η and χ are taken to assess their influences on the mechanical response. One can conclude from these figures that:

1) The sharp edges encountered in classical results disappear when the surface effects are considered, and u_1 and σ_{33} change smoothly across the loading boundary.

2) Inside and near the loading zone, the magnitudes of the out-of-plane displacement (u_3) and stress (σ_{33}) decrease noticeably as the value of η increases. However, their dependences on χ are seen to be insignificant.

3) The magnitude of σ_{33} is considerably smaller inside the loading area and larger near the contact zone when it is compared with the classical result. Such difference is

mainly attributed to the residual surface stress included in the current model.

4) Surface shear stresses do not vanish in case $\chi \neq 0$ and under this condition their magnitudes decrease with increasing values of η.

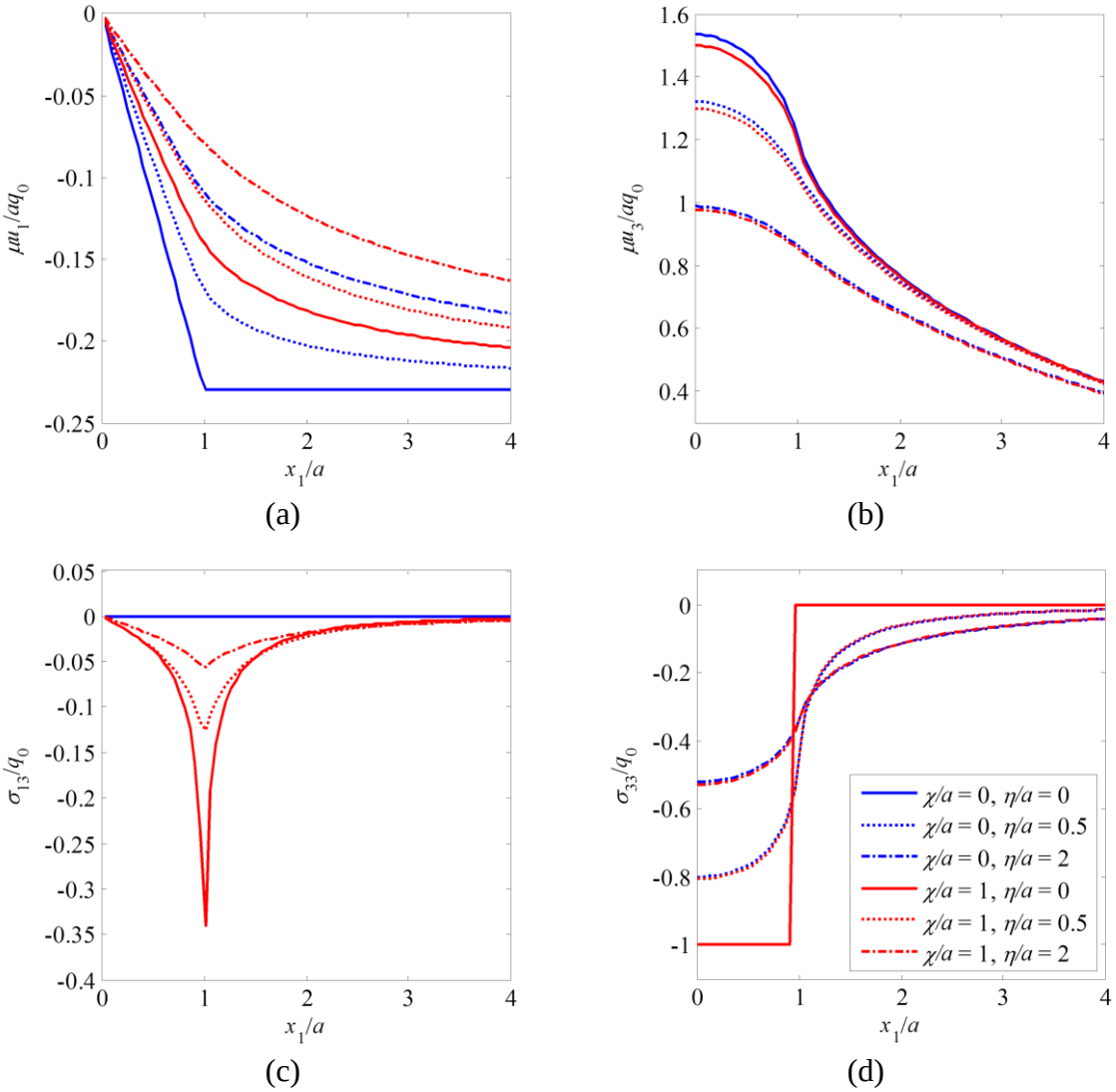

Figure 3.3. Surface displacements and stresses of a half-plane acted by a uniform pressure of intensity q_0 on the region of $-a < x_1 < a$.

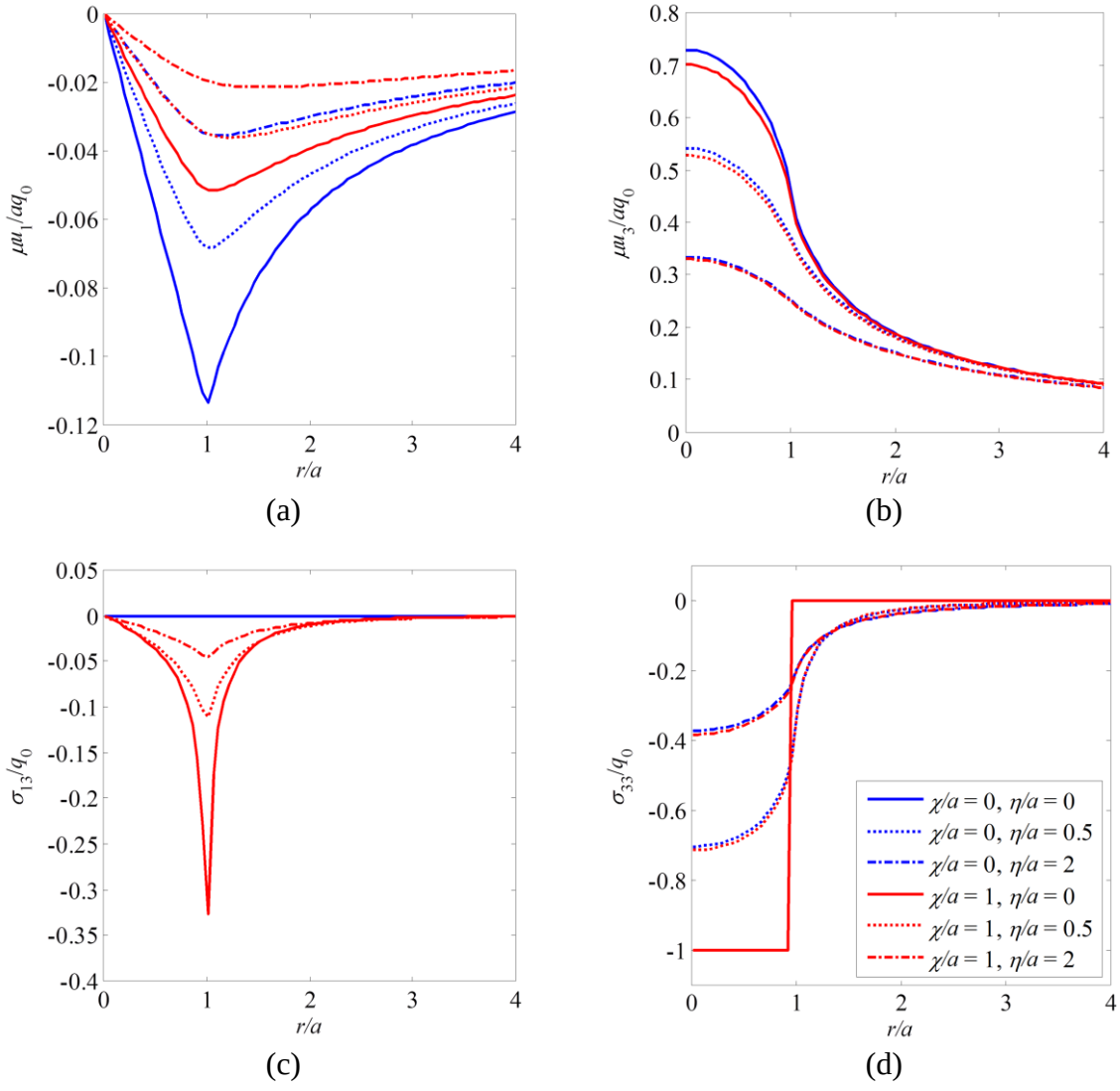

Figure 3.4. Surface displacements and stresses of a half-space acted by a uniform pressure of intensity q_0 on a circular region of radius a.

3.7 Axisymmetric Contact Problems with Surface Effects

Axisymmetric contact problems have been extensively studied since the investigations conducted by Boussinesq (1885) and Herzt (1882) in the late 1800s. A

landmark achievement was made by Sneddon (1965) who obtained explicit solutions for the problems of contact between a semi-infinite solid and a punch of arbitrary profile by means of the Hankel transform and the theory of dual integral equations.

3.7.1 Boussinesq's Flat-Ended Punch Problem

The state of stress in an elastic half-space indented by a rigid punch was first studied by Boussinesq (1885) using the method of potential theory. According to his solution, the contact pressure under the flat-ended punch has the form

$$p_\infty(r) = q_0(a^2 - r^2)^{-1/2}, \tag{3.47}$$

and is undefined at the periphery of the contact zone. Herein, the subscript '∞' is used to denote the flat-ended profile (related discussion can be found in S.-S Zhou *et al*. (2011)). Then we find

$$\bar{p}_\infty(\xi) = 2\pi q_0 \xi^{-1} \sin(a\xi), \tag{3.48}$$

with the knowledge of the integral identity $\int_0^a (a^2 - r^2)^{-1/2} r J_0(r) dr = \sin a$.

The displacement and stress fields can be readily obtained by inserting Eq. (3.48) into Eq. (3.36). The surface displacements and stresses can be subsequently computed by setting $x_3 = 0$ in the obtained results. For contact problems, the depth of penetration of the punch tip δ (also called indentation depth) is an important quantity (e.g. S.-S Zhou *et al*., 2011). Substituting Eq. (3.48) into Eq. (3.36b) while taking with $x_3 = 0$ and $r = 0$ yields

$$\delta_\infty = \pi q_0 \int_0^\infty h_2(0, \xi) \sin(a\xi) d\xi. \tag{3.49}$$

3.7.2 Spherical Punch – Hertz Problem

Contact of two elastic solids was first studied by Hertz (1882) using classical elasticity. Hertz's solution for the frictionless and non-adhesive contact of two elastic spheres has led to numerous applications in contact mechanics.

The profile of the spherical indenter can be approximated by $f(r) = r^2/2R$ if its radius is considerably larger than the contact radius a, and the pressure distribution under the indenter is given by (e.g., Barber, 2002)

$$p_2(r) = q_0\sqrt{a^2 - r^2}. \tag{3.50}$$

It is not difficult to show that

$$\bar{p}_2(\xi) = 2\pi q_0 \xi^{-3}\left[\sin(a\xi) - a\xi\cos(a\xi)\right] \tag{3.51}$$

by knowing $\int_0^a r\sqrt{a^2 - r^2}\,J_0(r)dr = \sin a - a\cos a$.

The elastic field are readily obtained by use of Eq. (3.51) in Eq. (3.36). Setting $r = 0$ in the obtained expression for u_3, one finds

$$\delta_2 = \pi q_0 \int_0^\infty h_2(0,\xi)\xi^{-2}\left[\sin(a\xi) - a\xi\cos(a\xi)\right]d\xi. \tag{3.52}$$

3.7.3 Conical Punch

For a conical shaped punch, the pressure distribution inside the contact zone has the form (e.g. Sneddon, 1965)

$$p_1(r) = q_0 \cosh^{-1}\frac{a}{r}. \tag{3.53}$$

The Fourier transform then yields

$$\bar{p}_1(\xi) = 2\pi q_0 \xi^{-2}\left[1 - \cos(\xi a)\right], \tag{3.54}$$

arriving at which the definition of $\cosh^{-1} x = \ln[x + (x^2 - 1)^{1/2}]$, integration by parts and the integral identity $\int_0^a a(a^2 - t^2)^{-1/2} J_1(t)dt = 1 - \cos a$ has been used.

Similarly, we find

$$\delta_1 = \pi q_0 \int_0^\infty h_2(0,\xi)\xi^{-1}\left[1 - \cos(\xi a)\right]d\xi. \tag{3.55}$$

For the aforementioned punch problems, their respective classical solutions for the surface displacements and stresses can be reproduced with the aid of integral identities (e.g., Maugis, 2000, pp403):

$$\begin{aligned} &\int_0^\infty \sin(\xi t)J_0(\xi r)d\xi = \frac{H(t-r)}{\sqrt{t^2 - r^2}}, \quad \int_0^\infty \cos(\xi t)J_0(\xi r)d\xi = \frac{H(r-t)}{\sqrt{r^2 - t^2}}, \\ &\int_0^\infty \sin(\xi t)J_1(\xi r)d\xi = \frac{tH(r-t)}{r\sqrt{r^2 - t^2}}, \quad \int_0^\infty \cos(\xi t)J_1(\xi r)d\xi = \frac{1}{r} - \frac{tH(t-r)}{r\sqrt{t^2 - r^2}}. \end{aligned} \tag{3.56}$$

Variation of displacements and stresses on the surface for different punch profiles are depicted in Figures 3.5, 3.6 and 3.7. The classical solution is recovered from the newly derived solution as a particular case with η = χ = 0 and is provide for comparison purpose. Similar observations to those discussed in the previous section are made: the newly derived solution predicts smaller surface displacements and a smoother normal stress profile; the current results converge to the classical ones at far distance away from the loading area; and the parameter η has a more significant impact on the mechanical response than χ does.

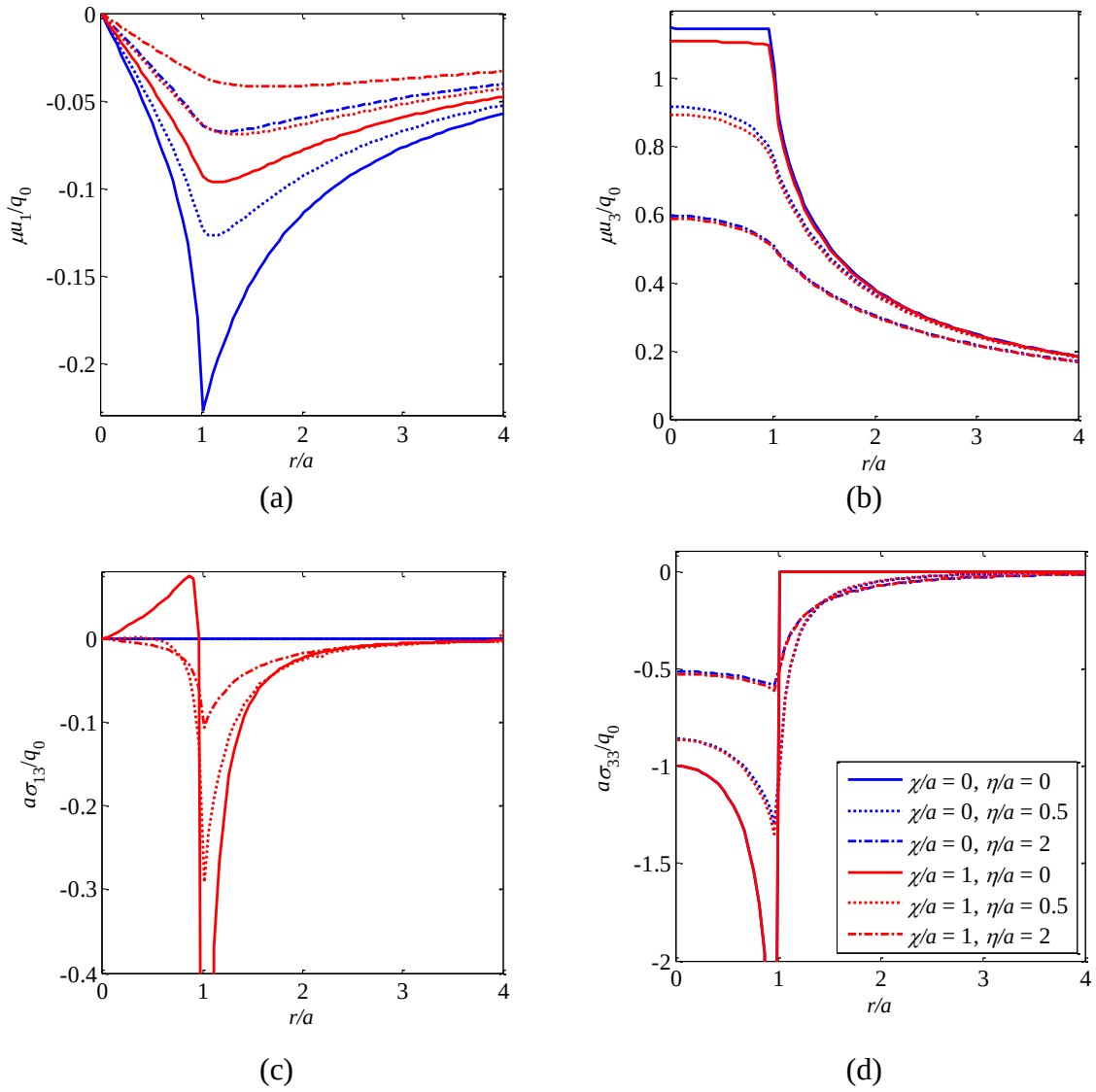

Figure 3.5. Surface displacements and stresses of a half-space subjected to the Boussinesq pressure distribution.

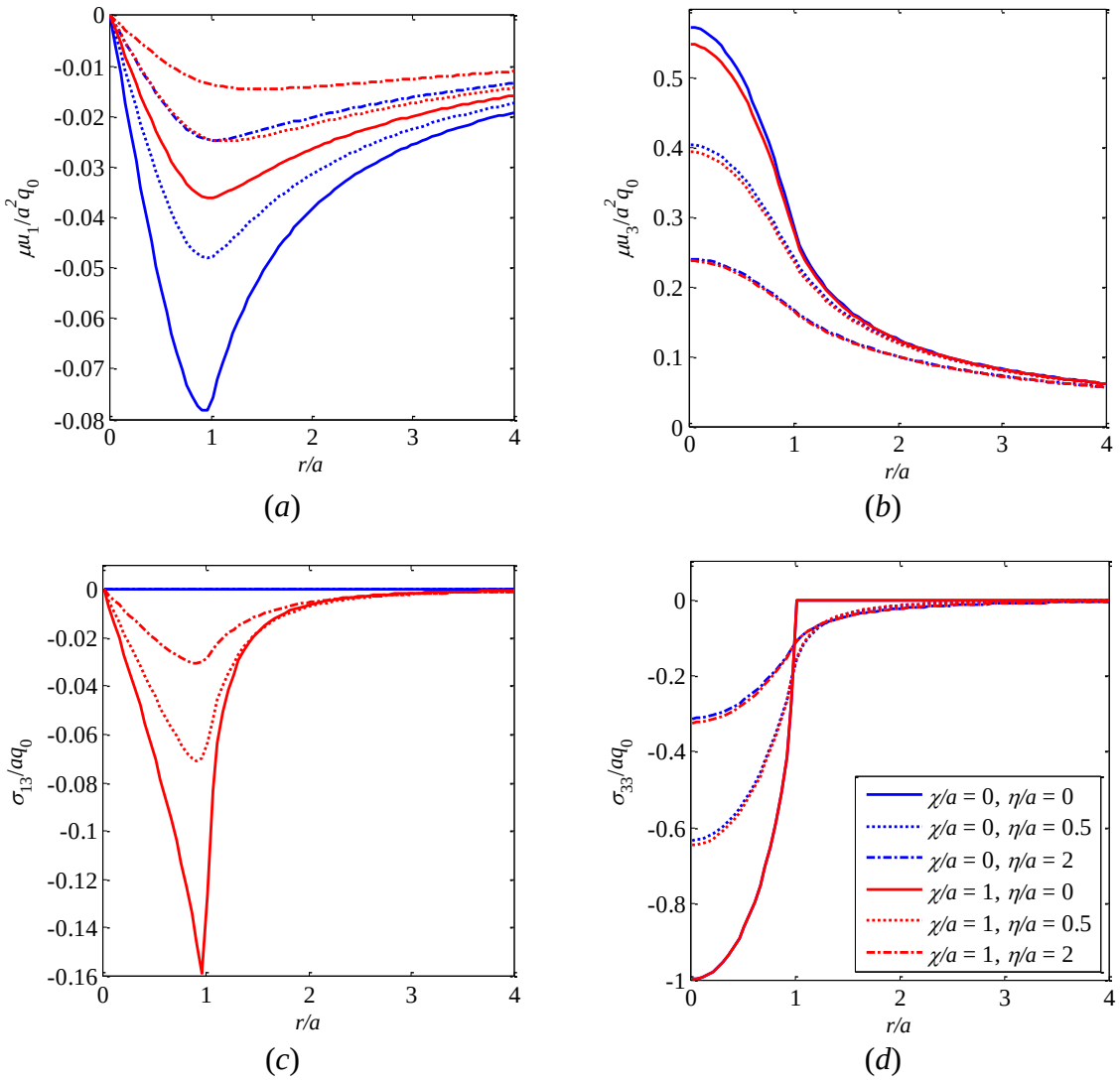

Figure 3.6. Surface displacements and stresses of a half-space subjected to the Hertzian pressure distribution.

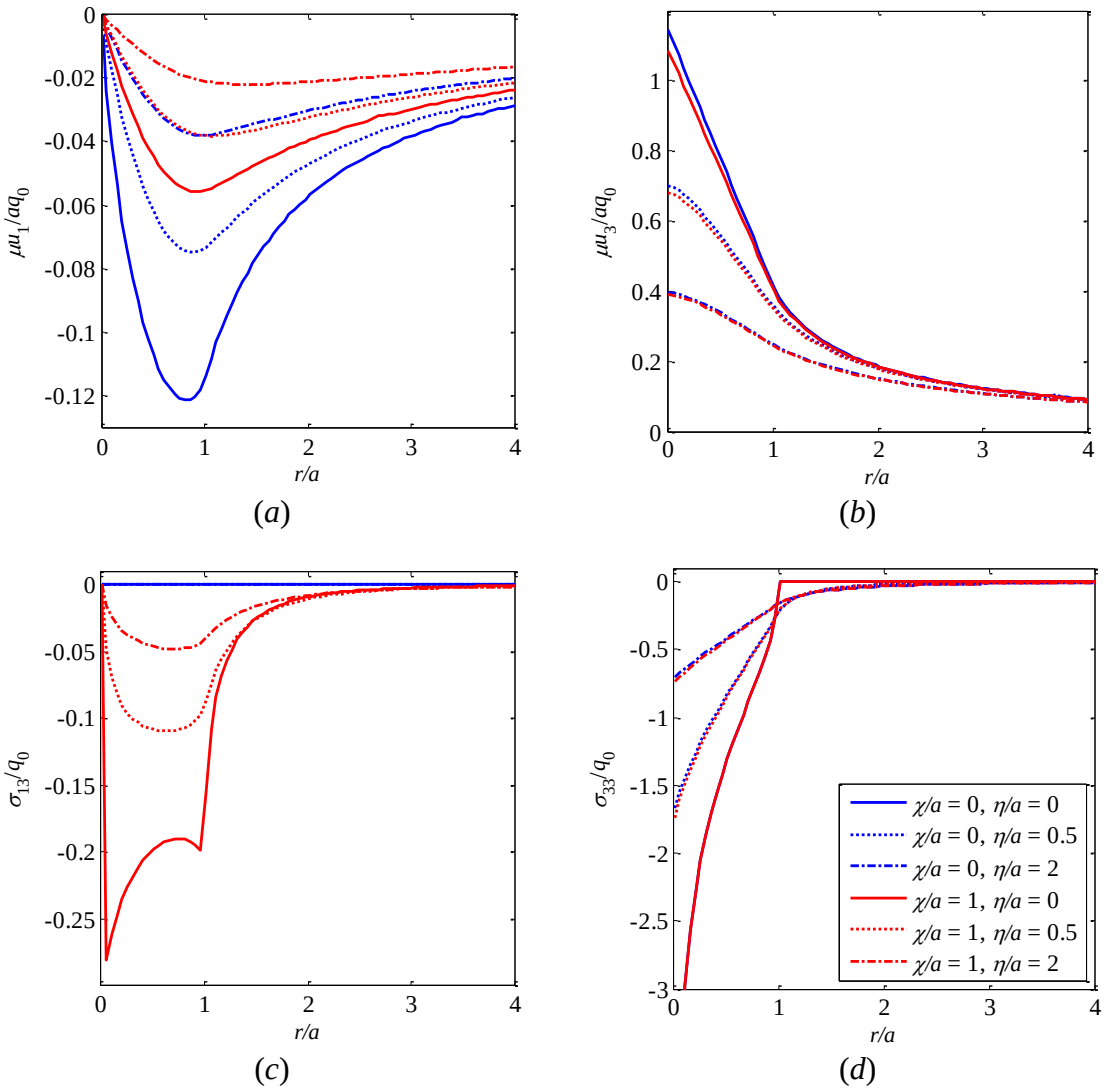

Figure 3.7. Surface displacements and stresses of a half-space subjected to the conical punch pressure distribution.

3.7.4 Depth-Dependent Hardness

Indentation depth δ and total applied load P are important factors in the analysis of contact problems. For axisymmetric pressure distribution the applied load can be evaluated by

$$P = 2\pi \int_0^a p(r) r dr. \tag{3.57}$$

For Boussinesq pressure distribution (flat-ended punch), Hertzian pressure profile (spherical punch) and conical punch pressure distribution, the applied loads are obtained to be

$$P_\infty = 2\pi a q_0,\ P_2 = \frac{2}{3}\pi a^3 q_0 \text{ and } P_1 = \pi a^2 q_0. \tag{3.58}$$

The indentation hardness is usually defined as the mean pressure exerted by the indenter at the maximum load (e.g., Fargesa and Degouta, 1989; McElhaney *et al*., 1998; Qu *et al*., 2004). Here, the parameter defined as (e.g., Wang and Feng, 2007)

$$H = \frac{P}{\delta} \tag{3.59}$$

is adopted as a measure of the hardness of the indented material.

If the surface effects are ignored, use of Eq. (3.49), (3.52) or (3.55) in Eq. (3.59) leads to

$$H_\infty^c = \frac{4\mu a}{1-\nu},\quad H_2^c = \frac{8\mu a}{3(1-\nu)},\quad H_1^c = \frac{2\mu a}{1-\nu}. \tag{3.60}$$

Upon reaching Eq. (3.60) use has been made of the following integral identities:

$$\int_0^\infty \frac{1}{t}\sin t dt = \frac{\pi}{2},\quad \int_0^\infty \frac{1}{t^2}(1-\cos t)dt = \frac{\pi}{2} \text{ and } \int_0^\infty \frac{1}{t^3}(\sin t - t\cos t)dt = \frac{\pi}{4}. \tag{3.61}$$

When the surface effects are accounted, the indentation hardness for each of the three pressure profiles is found to be related to the conventional results by

$$\frac{H_\infty^c}{H_\infty} = 1 - \frac{2}{\pi}\int_0^\infty \varphi(a,t)\sin t dt \tag{3.62a}$$

for the Boussinesq pressure distribution,

$$\frac{H_2^c}{H_2} = 1 - \frac{4}{\pi}\int_0^\infty \varphi(a,t)t^{-2}(\sin t - t\cos t)dt \tag{3.62b}$$

for the Hertzian pressure profile, and

$$\frac{H_1^c}{H_1} = 1 - \frac{2}{\pi}\int_0^\infty \varphi(a,t)t^{-1}(1-\cos t)dt \tag{3.62c}$$

for the conical punch pressure distribution, where

$$\varphi(a,t) = \frac{-\frac{3-4\nu}{4(1-\nu)}\frac{\chi}{a} + \frac{\kappa_1}{a} + \frac{\kappa_2}{a^2}t}{1 + \frac{\kappa_1}{a}t + \frac{\kappa_2}{a^2}t^2}. \tag{3.63}$$

By Eq. (3.63) we have $\varphi(a,t) \to 0$ if the contact radius a is considerably larger than the parameters η and χ, which are typically on the order of microns, and hence the formulae given in Eq. (3.62) become identical to the classical ones. However, when the magnitude of a is close to those of η or χ, the integrals on the right hand side of Eq. (3.62) become significant, thereby leading to an indentation hardness H that deviates substantially from the classical one.

The size-dependency of indentation hardness is clearly demonstrated in Figures 3.8 and 3.9. Including surface effects leads to a significant increase in the indentation hardness for all pressure profiles considered when the contact radius is small. Residual surface stress is found to have a dominant effect on H-curves, while the influence of the parameter χ is negligible. The profile of the H-curve shown in Figure 3.8 is in good agreement with the trends exhibited by experimental data presented in Ma and Clark (1995), Tymiak *et al*. (2001) and Gerberich *et al*. (2002).

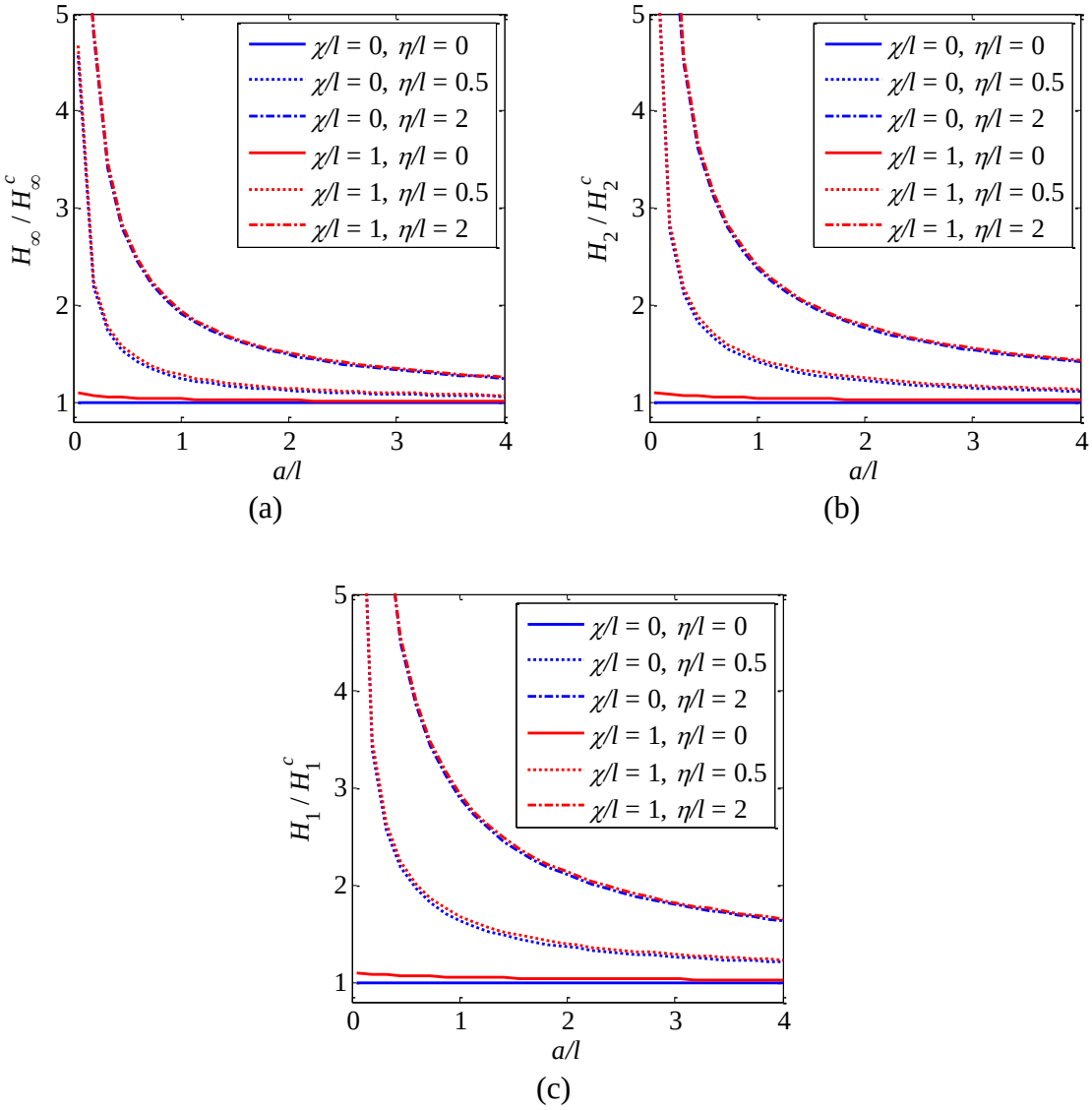

Figure 3.8. Variation of the indentation hardness with the contact radius for different pressure profiles: (a) flat-end, (b) spherical and (c) conical.

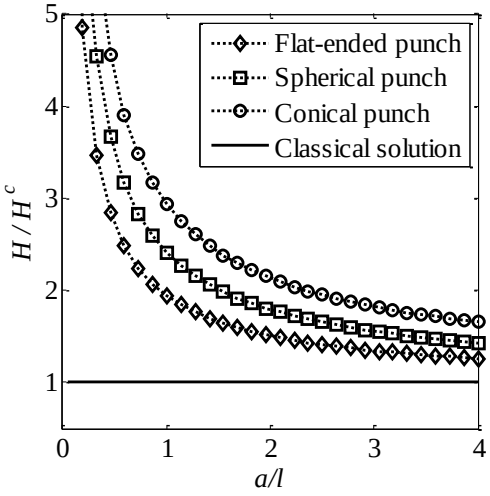

Figure 3.9. *H*-curves for different punch profiles (with $\chi = 0$ and $\eta / l = 2$).

3.8 Conclusions

A general solution for the problems of an elastic half-space with prescribed boundary pressure distribution is derived using the surface elasticity of Gurtin and Murdoch (1975, 1978). This approach is based on the use of Fourier transform method and Papkovitch-Neuber functions. The current solution incorporates the surface effects and applies to the 2D and 3D contact problems. It is demonstrated that the classical solutions for a number of contact problems can be reproduced from the newly derived solution, e.g., the solutions of the Flamant, Boussinesq and Hertz problems.

A few axisymmetric contact problems are used to examine the influence of the presence of surface effects on the elastic fields, such as the Boussinesq flat-ended punch problem, the Hertz spherical punch problem and the conical punch problem. The material response predicted by the current model deviates significantly from the classical result and such departure is most noticeable inside and near the loading area. The

displacement discontinuity and singularity existed in the classical solutions are alleviated when the surface effects are incorporated. The in-plane displacements decrease remarkably as parameter χ increases. However, the out-of-plane displacement and stress components remain largely unaffected as χ changes, which indicates that the simplified models considering the residual surface stress (e.g., He and Lim, 2006; Wang and Feng, 2007) can be satisfactorily applied to calculate out-of-plane displacement and stress.

The well-known indenter size effect at fine scale is predicted by the current solution. It is demonstrated that including the surface effects results in increased indentation hardness as indenter size decreases and the trend of the profile of the hardness curves are in good agreement with existing experimental observations.

4. GENERALIZED CERRUTI'S PROBLEM WITH SURFACE EFFECTS

4.1 Introduction

The size-dependency of material responses at small length scales has become an important research area, such as the indentation size effect observed in micro/nano-indentation tests (e.g. Stelmashenko *et al*., 1993; De Guzman *et al*., 1993; Ma and Clarke, 1995). Size-dependent behaviors cannot be satisfactorily explained by classical elasticity based models due to the lack of material length scale parameters. A number of new theories/models have thus been proposed to simulate the small-scale structures, like the JKR adhesive contact theory (Johnson *et al*., 1971), surface elasticity (Gurtin and Murdoch, 1975, 1978), and higher order elasticity theories (Toupin, 1962; Koiter, 1964; Mindlin, 1964). Unlike the classical scale-free continuum theories, the afore-mentioned theories contain inherent material lengths and can account for the size effects.

The Cerruti's problem is a fundamental problem in solid mechanics that deals with the deformation of a semi-infinite elastic solid loaded by a concentrated tangential force on its bounding surface. This problem has been extensively studied by different lines of approach in the context of classical elasticity (e.g., Johnson, 1985, pp68-70). The nonlocal Cerruti's problem was solved by Nowinki (1992) using the twin gradient theory of Westergaard (e.g., Ling *et al*., 2002) and the existing nonlocal solution of Kelvin's point force problem. Recently, the classical Boussinesq's and Cerruti's problems were extended by Barbot and Fialko (2010) to include a restoring buoyancy condition at the surface.

The theory of surface elasticity of Gurtin and Murdoch (1975, 1978) has been successfully implemented to interpret the size dependent deformation of solids (e.g. He and Lim, 2006; Wang and Feng, 2007; Zhao and Rajapakse, 2009). The problem of Cerruti was studied for an incompressible medium by He and Lim (2006) using a simplified version of the surface elasticity that retains only the surface residual stress.

In the present study, the Cerruti's problem is solved by using the original surface elasticity theory of Gurtin and Murdoch (1975, 1978). The resulting solution is valid for both incompressible and compressible materials.

4.2 Problem Statement

In this work we shall be concerned with the analysis of the stress and displacement fields in a half-space induced by uni-directional surface tangential forces, as illustrated in Figure 4.1. A Cartesian coordinate system is introduced and, as a

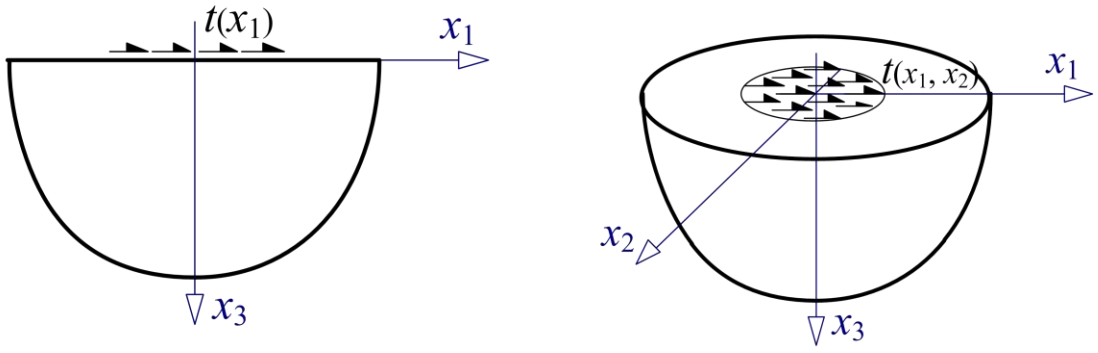

(a) (b)

Figure 4.1. Schematics of the generalized Cerruti's problem: (a) two-dimensional and (b) three-dimensional.

convention, the x_3-axis is taken as the axis of revolution of the solid and the x_1x_2-plane as the free surface. Without loss of generality, it is assumed that the surface tangential forces act in the x_1-direction. Through the discussion, stress components will be denoted by σ_{ij} while the components of displacement will be taken as u_i. The Einstein summation convention is adopted for repeated indices, with each Greek index running from 1 to 2 and the Latin one from 1 to 3, unless otherwise indicated.

The framework for elastic deformations with surface effects was established by Gurtin and Murdoch (1975, 1978), who treated the surface as a two-dimensional membrane with its material properties differing from those of the bulk material. The influence of surface effects on the material response is most pronounced when the surface energy to the bulk energy ratio of the associated solid is large (Cammarat, 1994). For macroscopic structures the stresses and strains attributable to the surface effects are negligible and the surface effects are typically ignored.

The non-standard boundary conditions (BCs) in the context of surface elasticity has been discussed in Section 3 and for a half-space (occupying $x_3 > 0$) subjected to prescribed traction $\boldsymbol{t}$ on the bounding surface the corresponding BCs can be written as

$$\begin{aligned} \sigma_{33}\big|_{x_3=0} &= -\tau_0\, u_{3,\alpha\alpha}\big|_{x_3=0} - t_3, \\ \sigma_{\alpha 3}\big|_{x_3=0} &= -(\mu_0+\lambda_0)\, u_{\beta,\beta\alpha}\big|_{x_3=0} - \mu_0\, u_{\alpha,\beta\beta}\big|_{x_3=0} - t_\alpha, \end{aligned} \tag{4.1}$$

which become

$$\begin{aligned} \sigma_{33}\big|_{x_3=0} &= -\tau_0\, u_{3,11}\big|_{x_3=0} - t_3, \\ \sigma_{13}\big|_{x_3=0} &= -(2\mu_0+\lambda_0)\, u_{1,11}\big|_{x_3=0} - t_1 \end{aligned} \tag{4.2}$$

for the cases of a half-plane occupying $x_3 > 0$. In Eqs. (4.1) and (4.2), τ_0 is the surface residual stress, μ_0 and λ_0 are the surface Lam é constants.

4.3 Two-Dimensional Cerruti's Problem

Consider the elastostatic deformation of a half-plane subjected to a surface tangential traction $t(x_1)$, as shown in Figure 4.1*a*. The Airy's stress function is very preferable in attacking two-dimensional elastic problem in that it breaks the very problem to a tractable potential problem (Barber, 2002, pp42-43). The stresses and displacements can all be expressed in terms of the Airy's stress function G (a biharmonic potential) as (e.g., Selvadurai, 2000, pp131-132) ‡‡

$$
\begin{aligned}
u_1 &= \frac{\mathrm{i}}{4\pi\mu}\int_{-\infty}^{\infty}\left[(1-\nu)\xi^{-1}\frac{d^2\bar{G}}{dx_3^2}+\nu\xi\bar{G}\right]e^{-\mathrm{i}\xi x_1}d\xi,\\
u_3 &= \frac{1}{4\pi\mu}\int_{-\infty}^{\infty}\left[(1-\nu)\xi^{-2}\frac{d^3\bar{G}}{dx_3^3}-(2-\nu)\frac{d\bar{G}}{dx_3}\right]e^{-\mathrm{i}\xi x_1}d\xi,\\
\sigma_{13} &= \frac{\mathrm{i}}{2\pi}\int_{-\infty}^{\infty}\xi\frac{d\bar{G}}{dx_3}e^{-\mathrm{i}\xi x_1}d\xi,\\
\sigma_{33} &= -\frac{1}{2\pi}\int_{-\infty}^{\infty}\xi^2\bar{G}e^{-\mathrm{i}\xi x_1}d\xi,
\end{aligned}
\tag{4.3}
$$

where ν is Poisson's ratio, μ and λ are Lam é constants of the bulk material, and variables with overhead bars indicate that the Fourier transforms has been applied.

Vanishing stresses at $x_3 \to \infty$ requires that the solution of the biharmoic function in the Fourier domain take the form

‡‡ Note that the form of the Fourier transform pair used in Selvadurai (2000) is different from that adopted in Section 3.

$$\bar{G} = (A + Bx_3)e^{-x_3|\xi|}, \tag{4.4}$$

where the unknowns A and B are either arbitrary functions of ξ or constants to be determined from the BCs.

Substituting Eqs. (4.3) and (4.4) into the BCs listed in Eq. (4.2) (with $t_2 = t_3 = 0$, $t_1 = t$) gives

$$\begin{aligned} A &= -\frac{\eta}{2}\left[(1-2\nu)B + A|\xi|\right], \\ -A|\xi| + B &= \frac{\chi}{2}\left[A\xi^2 - 2(1-\nu)B|\xi|\right] - \frac{1}{\mathrm{i}\xi}\bar{t}, \end{aligned} \tag{4.5}$$

where

$$\eta = \frac{\tau_0}{\mu}, \quad \chi = \frac{2\mu_0 + \lambda_0}{\mu}. \tag{4.6}$$

Note that each of the two material constants, η and χ, has a dimension of length characterized by four elastic properties of the solid (one from the bulk and three from the surface) and therefore can be regarded as intrinsic material length scale parameters.

The solution of Eq. (4.5) is given by

$$\begin{aligned} A &= -\frac{(1-2\nu)\eta}{2\xi\left(1 + \kappa_1|\xi| + \kappa_2\xi^2\right)}\mathrm{i}\bar{t}, \\ B &= \frac{2 + \eta|\xi|}{2\xi\left(1 + \kappa_1|\xi| + \kappa_2\xi^2\right)}\mathrm{i}\bar{t}, \end{aligned} \tag{4.7}$$

with

$$\kappa_1 = (1-\nu)(\eta + \chi), \quad \kappa_2 = (\tfrac{3}{4} - \nu)\eta\chi. \tag{4.8}$$

In order to take advantage of the Fourier cosine/sine series it is natural to

consider the cases wherein the magnitude of surface tangential load is symmetric. The expressions for A and B given in Eq. (4.7) are seen to be odd functions of ξ under this condition. Consequently, using Eqs. (4.4) and (4.7) in Eq. (4.3) and applying the Fourier cosine/sine transforms yield

$$\begin{aligned} u_1 &= \int_0^\infty g_1(x_3,\xi)\bar{t}\cos(\xi x_1)d\xi, \\ u_3 &= \int_0^\infty g_2(x_3,\xi)\bar{t}\sin(\xi x_1)d\xi, \\ \sigma_{13} &= \int_0^\infty g_3(x_3,\xi)\bar{t}\cos(\xi x_1)d\xi, \\ \sigma_{33} &= \int_0^\infty g_4(x_3,\xi)\bar{t}\sin(\xi x_1)d\xi, \end{aligned} \tag{4.9}$$

where

$$\begin{aligned} g_1(x_3,\xi) &= \frac{4(1-\nu)+(3-4\nu)\eta\xi - x_3\xi(2+\mu\xi)}{4\pi\mu\xi\left(1+\kappa_1\xi+\kappa_2\xi^2\right)}e^{-x_3\xi}, \\ g_2(x_3,\xi) &= \frac{2(1-2\nu)+x_3\xi(2+\eta\xi)}{4\pi\mu\xi\left(1+\kappa_1\xi+\kappa_2\xi^2\right)}e^{-x_3\xi}, \\ g_3(x_3,\xi) &= -\frac{2+2(1-\nu)\eta\xi - x_3\xi(2+\eta\xi)}{2\pi\left(1+\kappa_1\xi+\kappa_2\xi^2\right)}e^{-x_3\xi}, \\ g_4(x_3,\xi) &= \frac{(1-2\nu)\eta - x_3(2+\eta\xi)}{2\pi\left(1+\kappa_1\xi+\kappa_2\xi^2\right)}\xi e^{-x_3\xi}. \end{aligned} \tag{4.10}$$

The surface stress and displacement components can be directly obtained from Eqs. (4.9) and (4.10) by setting $x_3 = 0$. The results read

$$
\begin{aligned}
u_1\big|_{x_3=0} &= \frac{1-\nu}{\pi\mu}\int_0^\infty \left(\frac{1}{\xi} - \frac{-\frac{3-4\nu}{4-4\nu}\eta + \kappa_1 + \kappa_2\xi}{1+\kappa_1\xi+\kappa_2\xi^2}\right)\bar{t}\cos(\xi x_1)d\xi,\\
u_3\big|_{x_3=0} &= \frac{1-2\nu}{2\pi\mu}\int_0^\infty \left(\frac{1}{\xi} - \frac{\kappa_1 + \kappa_2\xi}{1+\kappa_1\xi+\kappa_2\xi^2}\right)\bar{t}\sin(\xi x_1)d\xi,\\
\sigma_{13}\big|_{x_3=0} &= -\frac{1}{\pi}\int_0^\infty \left[1 - \frac{-(1-\nu)\eta + \kappa_1 + \kappa_2\xi}{1+\kappa_1\xi+\kappa_2\xi^2}\,\xi\right]\bar{t}\cos(\xi x_1)d\xi,\\
\sigma_{33}\big|_{x_3=0} &= \frac{1-2\nu}{2\pi}\int_0^\infty \frac{\eta\xi}{1+\kappa_1\xi+\kappa_2\xi^2}\,\bar{t}\sin(\xi x_1)d\xi.
\end{aligned}
\tag{4.11}
$$

The classical elasticity-based solution be readily recovered from the current solution given in Eq. (4.9) by neglecting the surface effects. For instance, we have $\bar{t} = T$ for a concentrated tangential force of magnitude *T*. Replacing $\bar{t}$ by *T* and setting η, κ_1 and κ_2 equal to zero in Eq. (4.9) one obtains

$$
\begin{aligned}
u_1^c &= -\frac{T}{\pi\mu}\left[(1-\nu)\ln\rho + \frac{x_3^2}{2\rho^2}\right], \quad & u_3^c &= \frac{T}{2\pi\mu}\left[(1-2\nu)\arctan\frac{x_1}{x_3} + \frac{x_1x_3}{\rho^2}\right],\\
\sigma_{13}^c &= -\frac{2Tx_3x_1^2}{\pi\rho^4}, & \sigma_{33}^c &= -\frac{2Tx_1x_3^2}{\pi\rho^4},
\end{aligned}
\tag{4.12}
$$

where $\rho^2 = x_1^2 + x_3^2$. These results recovered from the current solution are the same as the known classical ones (e.g., Johnson, 1985, pp18; Selvadurai, 2000, pp150).

The influence of surface effects for the 2D Cerruti's problem is examined for different values of η and χ. The results depicted in Figure 4.2 show that changing χ has a significant effect on all the surface quantities with the magnitudes of displacements and shear stress decreasing as χ increases. On the other hand, η has a negligible influence on the in-plane displacement and stress (u_1 and σ_{13}), but its impact on the out-of-plane displacement and stress (u_3 and σ_{33}) is noticeable.

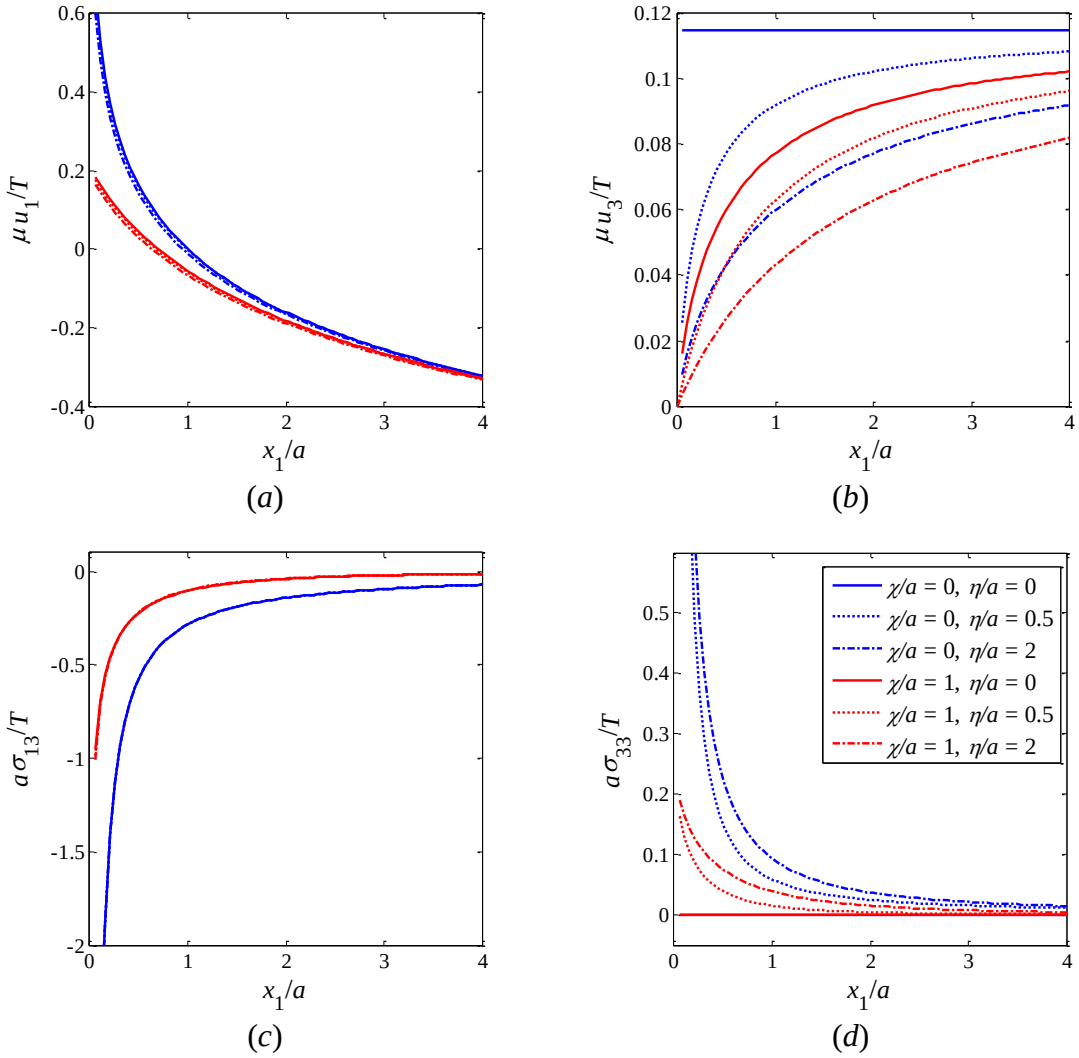

Figure 4.2. Surface displacements and stresses in an elastic half-plane induced by a concentrated tangential force. Herein the parameter *a* can be viewed as a scaling factor.

4.4 Three-Dimensional Cerruti's Problem

4.4.1 Formulation

The potential functions offer many promising features in attacking the Navier's equation with non-standard boundary conditions. In this section, the Papkovitch-Neuber

(P-N) potential functions, consisting of a harmonic vector potential $\boldsymbol{B}$ = (B_1, B_2, B_3) and a harmonic scalar potential B_0, are adopted to formulate the solution. In the absence of body forces, the displacement components in a solid can be expressed in terms of the harmonic potentials as (e.g., Ling *et al*., 2002, pp71)

$$u_i = B_i - \frac{\alpha}{2}(x_j B_j + B_0)_{,i}, \tag{4.13}$$

where $\alpha = \dfrac{\lambda+\mu}{\lambda+2\mu} = \dfrac{1}{2(1-\nu)}$.

For a semi-infinite solid subjected to unidirectional forces acting in the x_1 direction (see Figure 4.1b), the vector potential $\boldsymbol{B}$ takes the form (B_1, 0, B_3) (e.g. Mindlin, 1953; Barbot and Fialko, 2010). Using $\boldsymbol{B}$ = (B_1, 0, B_3) in Eq. (4.13) yields

$$\begin{aligned}
u_1 &= -\frac{\alpha}{2}\left[(-3+4\nu)B_1 + x_1 B_{1,1} + x_3 B_{3,1} + B_{0,1}\right],\\
u_2 &= -\frac{\alpha}{2}\left(x_1 B_{1,2} + x_3 B_{3,2} + B_{0,2}\right),\\
u_3 &= -\frac{\alpha}{2}\left[(-3+4\nu)B_3 + x_3 B_{3,3} + x_1 B_{1,3} + B_{0,3}\right],
\end{aligned} \tag{4.14}$$

and based on Hooke's law the stress components are then found to be

$$\begin{aligned}
\sigma_{13} &= \alpha\mu\left[(1-2\nu)\left(B_{3,1} + B_{1,3}\right) - x_1 B_{1,13} - x_3 B_{3,13} - B_{0,13}\right],\\
\sigma_{23} &= \alpha\mu\left[(1-2\nu)B_{3,2} - x_1 B_{1,23} - x_3 B_{3,23} - B_{0,23}\right],\\
\sigma_{33} &= \alpha\mu\left[(2-2\nu)B_{3,3} + 2\nu B_{1,1} - x_1 B_{1,33} - x_3 B_{3,33} - B_{0,33}\right].
\end{aligned} \tag{4.15}$$

For a semi-infinite solid, the harmonic functions B_1 and B_3 in the Fourier domain take the solution form

$$\bar{B}_1 = b_1 e^{-x_3|\xi|}, \quad \bar{B}_3 = b_3 e^{-x_3|\xi|}, \tag{4.16}$$

where $\xi^2 = \xi_\alpha \xi_\alpha$, and b_1, b_3 are unknowns to be determined from the imposed BCs.

With the help of identities $F[x_\alpha f] = \mathrm{i} d\bar{f} / d\xi_\alpha$ and $F[f_{,\alpha}] = \mathrm{i}\xi_\alpha \bar{f}$ [§§], one finds after taking Fourier transforms on Eqs. (4.14) and (4.15)

$$\begin{aligned}
\bar{u}_1 &= \frac{\alpha}{2}\left[4(1-\nu)b_1 - \mathrm{i}\, x_3\xi_1 b_3 - \mathrm{i}\,\xi_1 b_0\right] e^{-x_3|\xi|}, \\
\bar{u}_2 &= -\frac{\alpha}{2}\mathrm{i}\,\xi_2\left(x_3 b_3 + b_0\right) e^{-x_3|\xi|}, \\
\bar{u}_3 &= \frac{\alpha}{2}|\xi|^{-1}\left[(3-4\nu)|\xi| b_3 + x_3\xi^2 b_3 + \mathrm{i}\,\xi_1 b_1 + \xi^2 b_0\right] e^{-x_3|\xi|},
\end{aligned} \tag{4.17}$$

and

$$\begin{aligned}
\bar{\sigma}_{13} &= \mu\left[(1-\alpha)\mathrm{i}\,\xi_1 b_3 - |\xi|^{-1}(\xi^2 + \alpha\xi_1^2) b_1 + \mathrm{i}\,\alpha\xi_1|\xi|(x_3 b_3 + b_0)\right] e^{-x_3|\xi|}, \\
\bar{\sigma}_{23} &= \mu\xi_2\left[\mathrm{i}(1-\alpha) b_3 - \alpha|\xi|^{-1}\xi_1 b_1 + \mathrm{i}\,\alpha|\xi|(x_3 b_3 + b_0)\right] e^{-x_3|\xi|}, \\
\bar{\sigma}_{33} &= -\mu\left(|\xi| b_3 + x_3\alpha\xi^2 b_3 + \mathrm{i}\,\xi_1 b_1 + \alpha\xi^2 b_0\right) e^{-x_3|\xi|}.
\end{aligned} \tag{4.18}$$

It follows from Eq. (4.17) that

$$\begin{aligned}
(\mu_0 + \lambda_0)\bar{u}_{\beta,\beta 1}\big|_{x_3=0} + \mu_0\,\bar{u}_{1,\beta\beta}\big|_{x_3=0} &= \mathrm{i}\frac{\alpha}{2} b_0(2\mu_0 + \lambda_0)\xi_1\xi^2 - b_1\left[(\mu_0 + \lambda_0)\xi_1^2 + \mu_0\xi^2\right], \\
(\mu_0 + \lambda_0)\bar{u}_{\beta,\beta 2}\big|_{x_3=0} + \mu_0\,\bar{u}_{2,\beta\beta}\big|_{x_3=0} &= \mathrm{i}\frac{\alpha}{2} b_0(2\mu_0 + \lambda_0)\xi_2\xi^2 - b_1(\mu_0 + \lambda_0)\xi_1\xi_2, \\
\bar{u}_{3,\beta\beta}\big|_{x_3=0} &= -\frac{\alpha}{2}|\xi|\left[\xi^2 b_0 + \mathrm{i}\,\xi_1 b_1 + (3-4\nu)|\xi| b_3\right].
\end{aligned} \tag{4.19}$$

Next, we substitute Eqs. (4.18) and (4.19) into Eq. (4.1) and obtain the three unknowns from the resulting equations:

[§§] These two identities hold when the Fourier transform pair is given by

$$\bar{f}(\xi) = \int_{-\infty}^{\infty} f(x) e^{-\mathrm{i}\xi x} dx \text{ and } f(x) = \frac{1}{2\pi}\int_{-\infty}^{\infty} \bar{f}(\xi) e^{\mathrm{i}\xi x} d\xi .$$

$$b_1 = \frac{\overline{t}}{\mu|\xi| + \mu_0 \xi^2}, \quad b_0 = -\mathrm{i}\frac{\xi_1}{\xi^2} C_0(\xi) b_1, \quad b_3 = -\mathrm{i}\,\xi_1 C_3(\xi) b_1, \tag{4.20}$$

where

$$\begin{aligned} C_0(\xi) &= \frac{a_0 + a_1|\xi| + a_2\xi^2}{c_0 + c_1|\xi| + c_2\xi^2}, \\ C_3(\xi) &= \frac{1}{1-2\nu}\left[\frac{\mu_0 + \lambda_0}{\alpha\mu} + \frac{1}{|\xi|} - \left(\frac{2\mu_0 + \lambda_0}{2\mu} + \frac{1}{|\xi|}\right) C_0(\xi)\right], \end{aligned} \tag{4.21}$$

with coefficients a_i and c_i defined by

$$\begin{aligned} a_0 &= 2\nu, \quad a_1 = \frac{\tau_0}{2\mu} + \frac{\mu_0 + \lambda_0}{\alpha\mu}, \quad a_2 = \left(\frac{1}{\alpha} - \frac{1}{2}\right)\frac{\tau_0}{\mu}\frac{\mu_0 + \lambda_0}{\mu}, \\ c_0 &= \alpha, \quad c_1 = \frac{\tau_0}{2\mu} + \frac{2\mu_0 + \lambda_0}{2\mu}, \quad c_2 = \frac{2-\alpha}{4}\frac{\tau_0}{\mu}\frac{2\mu_0 + \lambda_0}{\mu}. \end{aligned} \tag{4.22}$$

The parameters $\frac{\tau_0}{\mu}$, $\frac{\mu_0}{\mu}$ and $\frac{\lambda_0}{\mu}$ have dimensions of length and can be regarded as intrinsic length parameters.

Up till here we have actually completed the solution to the 3D Cerruti's problem, inasmuch as what remains is no more than transforming the stresses and displacements given in Eqs. (4.17) and (4.18) into the space domain using the obtained results for b_0, b_1 and b_3.

For simplicity we shall focus our discussion on $\overline{t}$ that is function of ξ only, which is the case when the magnitude of tangential traction is axisymmetric. The displacements and stresses can be derived by inverse Fourier transform of Eqs. (4.17) and (4.18). With the aid of transform identities outlined in Section 3 one finally gets on the plane $x_3 = 0$

$$
\begin{aligned}
u_1\big|_{x_3=0} &= \frac{1}{4\pi}\int_0^\infty \left\{\left[2S_0(\xi)-S_1(\xi)\right]J_0(\xi r)+\left(2x_1^2r^{-2}-1\right)S_1(\xi)J_2(\xi r)\right\}\bar{t}d\xi,\\
u_2\big|_{x_3=0} &= \frac{x_1x_2}{2\pi r^2}\int_0^\infty S_1(\xi)J_2(\xi r)\bar{t}d\xi,\\
u_3\big|_{x_3=0} &= -\frac{x_1}{2\pi r}\int_0^\infty S_2(\xi)J_1(\xi r)\bar{t}d\xi,
\end{aligned}
\tag{4.23}
$$

and

$$
\begin{aligned}
\sigma_{13}\big|_{x_3=0} &= -\frac{\mu}{4\pi}\int_0^\infty \left\{\left[2S_0(\xi)-S_3(\xi)\right]J_0(\xi r)+\left(2x_1^2r^{-2}-1\right)S_3(\xi)J_2(\xi r)\right\}\xi\bar{t}d\xi,\\
\sigma_{23}\big|_{x_3=0} &= -\mu\frac{x_1x_2}{2\pi r^2}\int_0^\infty S_3(\xi)\xi J_2(\xi r)\bar{t}d\xi,\\
\sigma_{33}\big|_{x_3=0} &= -\mu\frac{x_1}{2\pi r}\int_0^\infty S_4(\xi)\xi J_1(\xi r)\bar{t}d\xi,
\end{aligned}
\tag{4.24}
$$

where $r^2 = x_1^2 + x_2^2$, and

$$
\begin{aligned}
&S_0(\xi) = (\mu+\mu_0\xi)^{-1}, \quad S_1(\xi) = \frac{\alpha}{2}C_0(\xi)S_0(\xi),\\
&S_2(\xi) = \frac{\alpha}{2}\left[1-C_0(\xi)-(3-4\nu)C_3(\xi)\xi\right]S_0(\xi),\\
&S_3(\xi) = \left[\alpha(C_0-1)+(1-\alpha)C_3(\xi)\xi\right]S_0(\xi),\\
&S_4(\xi) = \left[\alpha C_0(\xi)-1+C_3(\xi)\xi\right]S_0(\xi).
\end{aligned}
\tag{4.25}
$$

The above results will be greatly simplified if the surface elastic constants are set equal to zero. That is, letting $\mu_0 = \lambda_0 = 0$ in Eq. (4.23) gives the surface displacements as

$$
\begin{aligned}
u_1\big|_{x_3=0}^{\mu_0=\lambda_0=0} &= -\frac{1}{8\pi\mu}\int_0^\infty \bar{t}\left[\frac{2\nu-4+(\alpha-4)\kappa\xi}{1+\kappa\xi}J_0(\xi r)-\frac{2\nu+\kappa\alpha\xi}{1+\kappa\xi}\left(2x_1^2r^{-2}-1\right)J_2(\xi r)\right]d\xi,\\
u_2\big|_{x_3=0}^{\mu_0=\lambda_0=0} &= \frac{x_1x_2}{4\pi\mu r^2}\int_0^\infty \bar{t}\,\frac{2\nu+\kappa\alpha\xi}{1+\kappa\xi}J_2(\xi r)d\xi,\\
u_3\big|_{x_3=0}^{\mu_0=\lambda_0=0} &= \frac{x_1}{4\pi\mu r}\int_0^\infty \bar{t}\,\frac{1-2\nu}{1+\kappa\xi}J_1(\xi r)d\xi,
\end{aligned}
\tag{4.26}
$$

where $\kappa = (1-\nu)\tau_0 / \mu$. It is of interest to note that the surface displacements given by Eq. (4.26) are independent of surface residual stress for incompressible solids (ν = 0.5), which agrees with the observation made by He and Lim's (2006).

4.4.2 Illustrative Examples

To demonstrate the analytical solutions derived in the preceding sections, two representative problems, one with a concentrated tangential force and another with uniformly distributed uni-directional tangential traction, are quantitatively studied here.

4.4.2.1 Concentrated Tangential Force

In the presence of surface effects, the solution of the Cerruti's problem is readily obtained by setting $\bar{t} = T$ in Eqs. (4.23) and (4.24). If the surface effects are ignored, i.e. setting κ = 0 in Eq. (4.26) leads to the classical solutions (e.g. Johnson, 1985, pp69; Ling *et al*., 2000, pp88):

$$u_1^c\big|_{x_3=0} = \frac{T}{2\mu\pi}\left[\frac{1-\nu}{r} + \nu\frac{x_1^2}{r^3}\right], \quad u_2^c\big|_{x_3=0} = \frac{\nu x_1 x_2}{2\pi\mu r^3}T, \quad u_3^c\big|_{x_3=0} = \frac{(1-2\nu)}{4\mu\pi}\frac{x_1}{r^2}T. \quad (4.27)$$

Figure 4.3 shows the displacement and stress components along the x_1-axis (u_2 and σ_{23} vanish on the plane x_2 = 0 and hence they are not displayed).

The classical elasticity solutions are recovered as a special case in which $\tau_0 = \mu_0 = \lambda_0 = 0$, and they are represented by the solid blue lines in Figure 4.3. It is seen that the in-plane surface displacements are insensitive to the change in the surface residual stress, τ_0 and they depend decisively on the surface elastic constants, μ_0 and λ_0, particularly for those points near the point of application of force. However, the out-of-plane displacement exhibits strong dependence on all surface parameters and decreases with

increasing values of μ_0, λ_0, or τ_0. As reflected in Figure 4.3, the consideration of surface effects results in decreased magnitudes of the surface displacements, which implies material hardening.

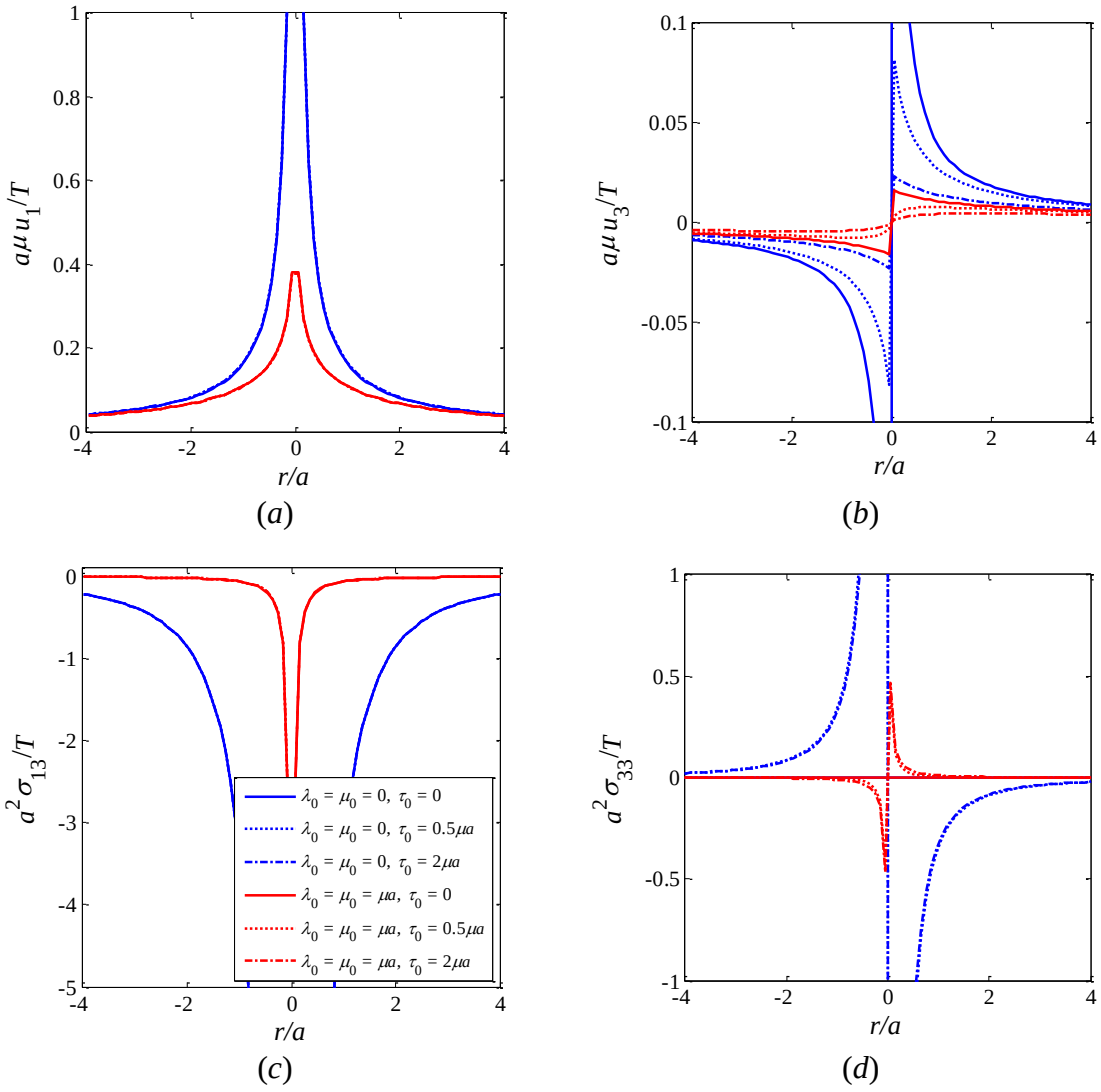

Figure 4.3. Displacements and stresses along the x_1-axis of an elastic half space subjected to a concentrated surface tangential force (Herein a is a scaling factor).

4.4.2.2 Uniformly Distributed Tangential Force

Next we consider a half-plane loaded by a uniform traction of intensity t_0 acting tangentially on the surface of an elastic half space over a circular region of radius a. In the transformed domain, we have

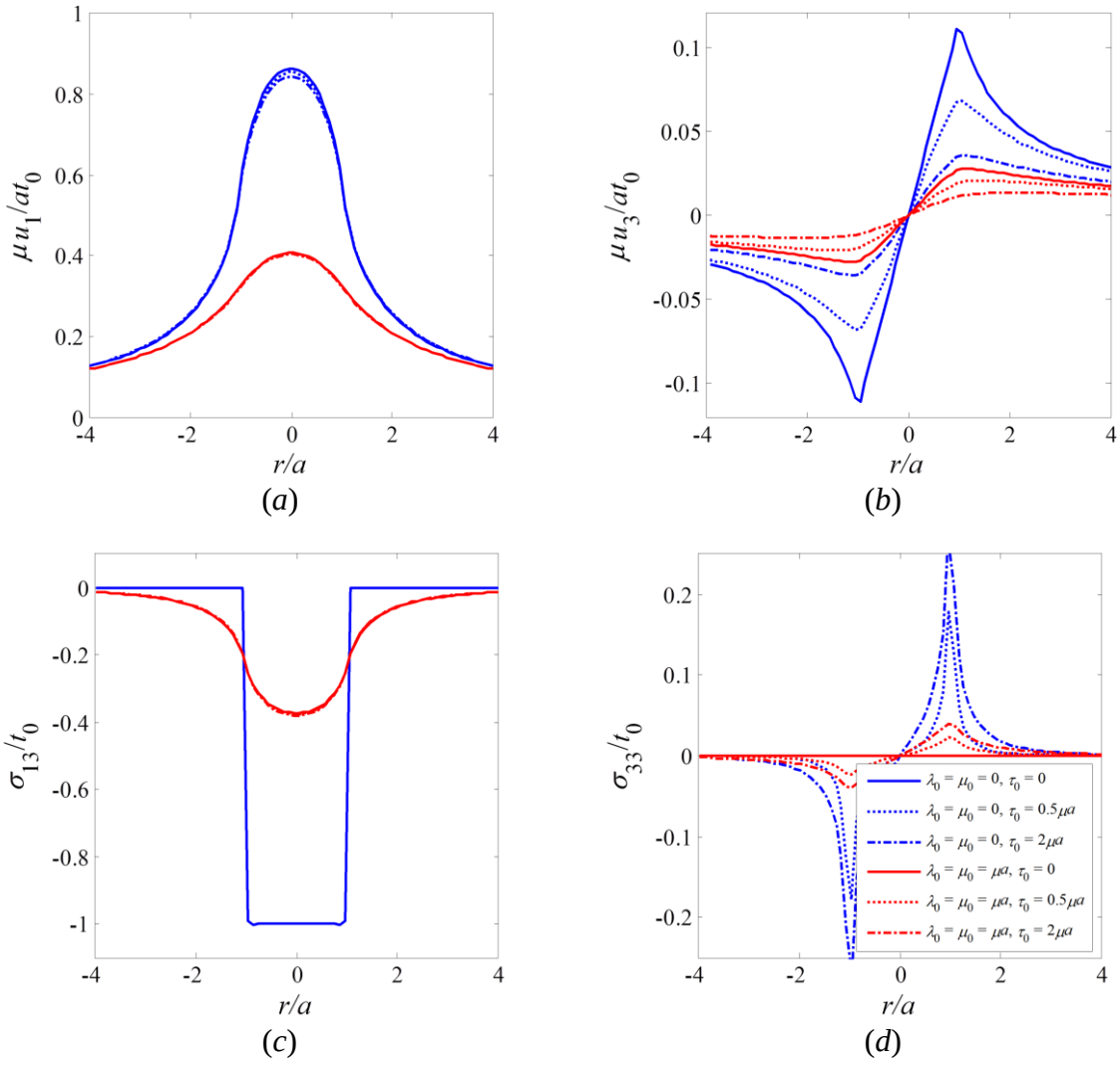

Figure 4.4. Surface displacements and stresses along the x_1-axis of a half space under uniformly distributed surface tangential forces acting in a circular region of radius a.

$$\bar{t} = 2\pi t_0 a\xi^{-1} J_1(a\xi). \tag{4.28}$$

The surface stresses and displacements can then be obtained by using Eq. (4.28) in Eqs. (4.23) and (4.24).

The numerical results shown in Figure 4.4 reveal analogous observations on the surface effects. Besides, we notice a smooth change in the shear stress profile across the loading boundary as long as the surface elastic constants (τ_0 and μ_0) are non-zero. That is, the jump in the shear stress existing in the classical solution disappears when the very problem is examined in the context of surface elasticity.

4.5 Summary

In this section the solution for the elastic field in a homogeneous elastic half-space subject to a surface tangential traction is derived using the theory of surface elasticity of Gurtin and Murdoch (1975, 1978). The formulation is based on the Fourier transform method and makes use of stress functions – Airy's stress function for the half-plane problem and P-N functions for the half-space. This technique enables one to obtain the analytical solution to the Navier's equation with the non-standard BCs in integral forms. The newly derived solution includes material length scale parameters that are characterized by the surface residual stress and surface elastic constants, and the classical elasticity solution can be reproduced as a particular solution in which the surface effects are ignored.

The derived general solution is applied to few illustrative examples to assess the possible impact of the surface effects on the elastic field of the half-space induced by the

surface tangential forces. The numerical results show substantial departure between the classical results and the newly derived ones in the vicinity of the loading area. For the generalized Cerruti's problem considered, the current solution predicts a much smoother elastic field and smaller deformation. Therefore, the material hardening effect can be captured by the current solution which incorporates the surface effects.

5. STRAIN GRADIENT SOLUTIONS OF SEMI-INFINITE INDENTATION PROBLEMS

5.1 Introduction

Due to the lack of intrinsic material lengths the classical continuum mechanics cannot describe size-effects exhibited by many materials at micron and nanometer scales. At such scales, the effects of surface energy, defects and microstructure, and internal strain become significant and need to be considered in the modeling of material behaviors. Augmented higher-order continuum theories have been developed to interpret the micro-structure dependent phenomena, which include the Cosserat elasticity (Cosserat and Cosserat, 1909), couple stress theory (e.g., Toupin, 1962, 1964; Kioter, 1964; Mindlin, 1962, 1963), higher order strain gradient elasticity (e.g., Mindlin, 1964, 1965), surface elasticity (e.g., Gurtin and Murdoch, 1975, 1978), and strain gradient plasticity (e.g., Fleck and Hutchinson, 1993; Flect *et al*., 1994).

A common approach to incorporate the effects of microstructure is to enrich the classical equations with additional higher-order derivatives. In the early 20^{th} century, the Cosserat brothers (Cosserat and Cosserat, 1909) took into account the micro-rotation and included the couple stress (energetically conjugated to the micro-rotation) in the equilibrium equations. The framework of the couple stress theory and gradient theories were mainly developed in the 1960s with essential contributions from Mindlin (1962, 1964, 1965), Toupin (1962, 1964) and Kioter (1964). In gradient theories, the micro-structure features are demonstrated through the micro-deformations and the material

characteristic lengths enter the constitutive equations through the strain energy function.

The work of Mindlin and coworkers (Mindlin, 1964, 1965; Mindlin and Eshel, 1968) is especially valuable in the development of strain gradient theories. In a landmark paper, Mindlin (1964) developed a strain gradient theory with 18 material constants for isotropic materials. Mindlin's original theories contain many material constants that are challenging to be quantified experimentally (Exadaktylos and Vardoulakis, 1998; Askes and Aifantis, 2011). Difficulties also arise from the mathematical manipulations of the associated equilibrium equations and constitutive relations. Due to these and other reasons, Mindlin's original theory has not been widely applied in the modeling of size-dependent phenomena.

Simplified strain gradient elasticity theories (SSGETs) have been suggested (e.g., Vardoulakis *et al*., 1996; Exadaktylos *et al*., 1996; Altan and Aifantis, 1992, 1997). Vardoulakis' model contains two additional constants associated with volume and surface energy terms, whereas that of Altan and Aifantis (1992, 1997) includes one additional material constant corresponding to the volume strain energy. These simplified models are mathematically more tractable and are very desirable due to the formidable experimental efforts in determining the extra material constants.

These simplified versions of Mindlin's strain gradient elasticity theory have been employed to analyze various problems, such as fracture (Exadaktylos, 1998; Shi *et al*., 2000; Georgiadis, 2003), mechanics of defects (Lazar and Maugin, 2005), thick-walled shell problem (Gao *et al*., 2009) and Eshelby type inclusion problems (Gao and Ma, 2009, 2010a,b). The two-dimensional (2D) and three-dimensional (3D) problems of a

point force in an infinite elastic body have been well studied in strain gradient elasticity (e.g., Karlis *et al*., 2010). However, the problems of a half-plane and of a half-space subjected to a concentrated force, e.t. the Flamant and Boussinesq problems, have not been satisfactorily addressed using strain gradient elasticity theories. The Flamant problem was analyzed by Zhou and Jin (2003) and Li *et al*. (2004) employing the simplified versions of Vardoulakis kind (Vardoulakis *et al*., 1996) and Altan and Aifantis (1997), respectively. However, these solutions are not exact in that the boundary conditions (BCs) used are not variationally consistent with those derived in Bleustein (1967), Mindlin and Eshel (1968) and Gao and Park (2007). The Flamant problem was recently re-examined by Georgiadis and Anagnostou (2008) using the correct BCs. Following Zhou and Jin (2003) and Li *et al*. (2004), they also utilized the Fourier transform method to directly solve the displacement-equation of motion, which are forth order partial differential equations (PDEs).

In the present work the Flamant and Boussinesq problems are solved in a unified manner using the simplified strain gradient elasticity theory. The SSGET based solutions are derived by using the Fourier transform method along with the stress functions of Mindlin (1965).

5.2 Displacement Function Method

5.2.1 Simplified Strain Gradient Elasticity

In classical elastic theory the strain energy density, w, is a function of strains only, whereas in the context of the strain gradient elasticity the strain energy density

depends, additionally, on the gradient of strains, e.t.,

$$w = w(\varepsilon_{ij}, \kappa_{kij}), \tag{5.1}$$

where ε_{ij} and κ_{kij} are, respectively, the infinitesimal strain and strain gradient defined by

$$\varepsilon_{ij} = \frac{1}{2}\left(u_{i,j} + u_{j,i}\right), \quad \kappa_{kij} = \varepsilon_{ij,k}, \tag{5.2}$$

with u_i being the displacement component.

For an isotropic, linearly elastic material, the expression of w can be written as (Mindlin, 1964, Eqs. (9.11) and (11.3); Mindlin and Eshel, 1968, Eqs. (2.4-2.5))

$$\begin{aligned} w = {} & \frac{1}{2}\lambda\varepsilon_{ii}\varepsilon_{jj} + \mu\varepsilon_{ij}\varepsilon_{ij} + a_1\kappa_{iik}\kappa_{kjj} \\ & + a_2\kappa_{ijj}\kappa_{ikk} + a_3\kappa_{iik}\kappa_{jjk} + a_4\kappa_{ijk}\kappa_{ijk} + a_5\kappa_{ijk}\kappa_{kji}, \end{aligned} \tag{5.3}$$

where (a_1, a_2, a_3, a_4, a_5) are material constants in addition to Lamé's constants μ and λ.

In Eqs. (5.1-5.3) and through this section the summation convention and standard index notation are used with the Greek indices running from 1 to 2 and the Latin ones taking 1 through 3, unless otherwise indicated.

Considering the case in which

$$a_1 = a_3 = a_5 = 0, \quad a_2 = \frac{1}{2}\lambda l^2, \quad \text{and} \quad a_4 = \mu l^2, \tag{5.4}$$

Eq. (5.3) then becomes

$$w = \frac{1}{2}\lambda\varepsilon_{ii}\varepsilon_{jj} + \mu\varepsilon_{ij}\varepsilon_{ij} + l^2\left(\frac{1}{2}\lambda\varepsilon_{ii,k}\varepsilon_{jj,k} + \mu\varepsilon_{ij,k}\varepsilon_{ij,k}\right), \tag{5.5}$$

which corresponds to the SSGET suggested by Altan and Aifantis (1997, Eq. (5)). Consequently, in the standard variational manner we can define the associated Cauchy stress, τ_{ij}, and the double stress, μ_{ijk}, as

$$\tau_{ij} = \frac{\partial w}{\partial \varepsilon_{ij}} = \lambda \varepsilon_{ll} \delta_{ij} + 2\mu \varepsilon_{ij} = \tau_{ji},$$
$$\mu_{kij} = \frac{\partial w}{\partial \kappa_{kij}} = l^2 \left(\lambda \varepsilon_{ll,k} \delta_{ij} + 2\mu \varepsilon_{ij,k} \right) = l^2 \tau_{ij,k}. \tag{5.6}$$

The total stress, σ_{ij}, is related to the Cauchy stress through

$$\sigma_{ij} = \tau_{ij} - \mu_{kij,k} = (1 - l^2 \nabla^2) \tau_{ij}. \tag{5.7}$$

The displacement-equation of motion is then obtained by inserting Eqs. (5.6) and (5.7) into the equilibrium equations (Mindlin and Eshel, 1968; Bleustein, 1967)

$$\sigma_{ji,j} + f_i = 0 \tag{5.8}$$

where f_i is the body force components. In the absent of the body forces, the equilibrium equation can be written in terms of displacements as (e.g., Altan and Aifantis, 1997; Gao and Park, 2007)

$$(1 - l^2 \nabla^2) \left[(\lambda + 2\mu) \nabla \nabla \cdot \mathbf{u} - \mu \nabla \times \nabla \times \mathbf{u} \right] = \mathbf{0}, \tag{5.9}$$

which is a special case of the general displacement-equation of motion provided in Mindlin and Eshel (1968).

5.2.2 Displacement Functions of Mindlin

According to Mindlin (1964), the equations of equilibrium in terms of displacements can have the form (Mindlin, 1964, Eqs. (9.31), (10.8) and (13.1))

$$(\lambda + 2\mu)(1 - l_1^2 \nabla^2) \nabla \nabla \cdot \mathbf{u} - \mu (1 - l_2^2 \nabla^2) \nabla \times \nabla \times \mathbf{u} = \mathbf{0}. \tag{5.10}$$

Herein l_1 and l_2 are two intrinsic material length scale parameters, which can characterize a cell size, e.g., a crystallite of a polycrystalline or a grain of a granular

material. The two parameters l_1 and l_2 can be related to the material constant a_i by[***] (Karlis *et al*., 2010; Shodja and Tehranchi, 2010)

$$l_1^2 = \frac{2(a_1 + a_2 + a_3 + a_4 + a_5)}{\lambda + 2\mu}, \quad l_2^2 = \frac{1}{2\mu}(a_3 + 2a_4 + a_5). \tag{5.11}$$

Apparently, Eq. (5.10) reduces to Eq. (5.9) when $l_1 = l_2 = l$.

Based on the Helmholtz decomposition of breaking a displacement vector into the gradient of a scalar potential and the curl of a vector potential, Mindlin (1964) showed that any solution **u** of Eq. (5.10) can be represented by

$$\mathbf{u} = \mathbf{B} - l_2^2 \nabla\nabla\cdot\mathbf{B} - \frac{1}{2}(\alpha - l_1^2\nabla^2)\nabla\left[\mathbf{r}\cdot(1 - l_2^2\nabla^2)\mathbf{B} + B_0\right], \tag{5.12a}$$

where $\alpha = 1/(2-2\nu)$, **r** is a position vector, and **B** is a vector function and B_0 a scalar function satisfying

$$\begin{aligned} \mu(1 - l_2^2\nabla^2)\nabla^2\mathbf{B} &= \mathbf{0}, \\ \mu(1 - l_1^2\nabla^2)\nabla^2 B_0 &= 0. \end{aligned} \tag{5.12b,c}$$

Clearly, when both length parameters are set equal to zero Eq. (5.10) reduces to the Navier equations of equilibrium in classical elasticity and the displacement functions (**B** and B_0) become the well-known Papkovitch-Neuber functions. Particular, when l_1 = 0, Equation (5.10) and its corresponding solution given in Eq. (5.12) reduce to those derived in Mindlin and Tiersten (1962, Eq. (11.1) and (11.17-19)), e.t.,

$$\mu\nabla^2\mathbf{u} + (\lambda + \mu)\nabla\nabla\cdot\mathbf{u} + \mu l^2\nabla^2\nabla\times\nabla\times\mathbf{u} = \mathbf{0}, \tag{5.13}$$

and

[***] The expression $l_2^2 = 2(a_3 + a_4)/\mu$ as found in Mindlin (1964) is seen to be inconsistent with Eq. (5.9) when Eq. (5.4) is used in Eq. (5.10).

$$\mathbf{u} = \mathbf{B} - l^2 \nabla \nabla \cdot \mathbf{B} - \frac{\alpha}{2} \nabla \left[\mathbf{r} \cdot (1 - l^2 \nabla^2) \mathbf{B} + B_0 \right],$$
$$\mu (1 - l^2 \nabla^2) \nabla^2 \mathbf{B} = \mathbf{0}, \tag{5.14}$$
$$\mu \nabla^2 B_0 = 0.$$

Equation (5.10) has been used by Dhaliwal (1973) and Exadaktylos (1999) to solve axisymmetric contact problems and the problems of a half-plane subjected to arbitrary surface loads, respectively.

Note that Eqs. (5.9) and (5.10) are identical if $l_1 = l_2$. Hence, the solution to Eq. (5.9) can be obtained by setting $l_1 = l_2 = l$ in Eq. (5.12):

$$\mathbf{u} = \mathbf{B} - l^2 \nabla \nabla \cdot \mathbf{B} - \frac{1}{2} (\alpha - l^2 \nabla^2) \nabla \left[\mathbf{r} \cdot (1 - l^2 \nabla^2) \mathbf{B} + B_0 \right], \tag{5.15a}$$

where

$$(1 - l^2 \nabla^2) \nabla^2 \mathbf{B} = \mathbf{0},$$
$$(1 - l^2 \nabla^2) \nabla^2 B_0 = 0. \tag{5.15b,c}$$

The displacement functions **B** and B_0 will be determined from the imposed boundary conditions. This displacement function method will be adopted in the current study along with the integral transforms to solve the non-standard boundary value problems involving high order partial differential equations (PDEs). This problem solving technique is more advisable than the Fourier transform method commonly employed by others (e.g., Zhou and Jin, 2003; Li *et al.*, 2004; Georgiadis and Anagnostou, 2008).

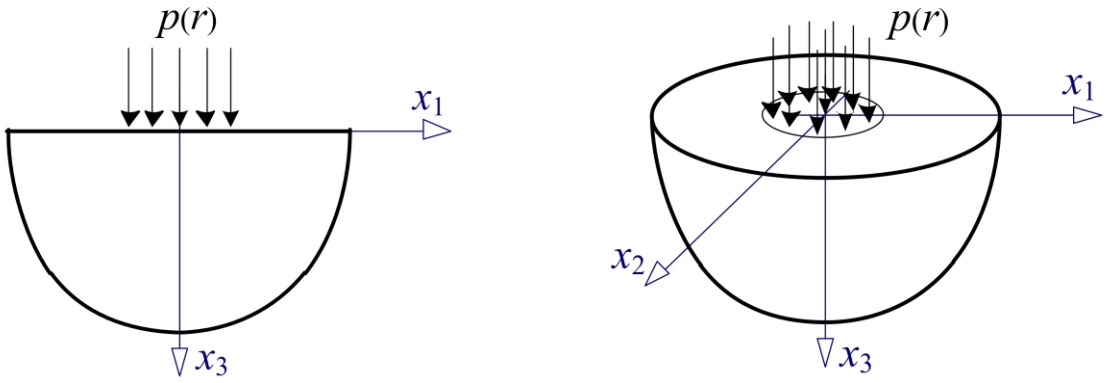

(a) (b)

Figure 5.1. Schematics of a half-plane (a) and half-space (b) subjected to normal forces applied on the surface.

5.3 Formulation

Problems of a semi-infinite elastic solid subjected to normal loads applied on its bounding surface are analytically solved using the simplified strain gradient elasticity theory. The half-plane and half-space problems being considered are schematically shown in Figure 5.1, and the body forces and body double forces are assumed to be absent.

For a half-space (occupying $x_3 > 0$) subjected to normal forces, the vector function **B** takes the form [0, 0, B_3] and the scalar function B_0 is non-vanishing (e.g. Mindlin, 1953; Dhaliwal, 1973). As a result, by Eq. (5.15) the displacement components are now written as

$$\begin{aligned} u_\beta &= -l^2 B_{3,3\beta} - \frac{1}{2}(\alpha - l^2\nabla^2)\left[x_3(1-l^2\nabla^2)B_3 + B_0\right]_{,\beta}, \\ u_3 &= B_3 - l^2 B_{3,33} - \frac{1}{2}(\alpha - l^2\nabla^2)\left[x_3(1-l^2\nabla^2)B_3 + B_0\right]_{,3}, \end{aligned} \tag{5.16}$$

with

$$(1-l^2\nabla^2)\nabla^2 B_3 = 0,$$
$$(1-l^2\nabla^2)\nabla^2 B_0 = 0. \tag{5.17}$$

5.3.1 Boundary Conditions

The BCs in strain gradient theories were firstly formulated in Mindlin (1964) based on variational principle and were further clarified by Bleustein (1967). The natural BCs were well summarized in a paper by Mindlin and Eshel (1968) based on conservation principle. The readers can also refer to Polyzos *et al*. (2003) and Gao and Park (2007) for detailed derivation regarding the BCs for form II of Mindlin's theory.

The natural BCs for the linear strain gradient theory are (e.g., Gao and Park, 2007)

$$n_j(\tau_{jk} - \mu_{ijk,i}) - (n_i\mu_{ijk})_{,j} + n_j(n_l n_i \mu_{ijk})_{,l} = t_k,$$
$$n_j n_i \mu_{ijk} = q_k, \tag{5.18}$$

where t_i and q_i are the surface traction and the surface double traction components, respectively. These BCs are variationally consistent and hence should be adopted in solving relevant problems. However, incomplete BCs have been used in literature (e.g., Dhaliwal, 1973; Exadaktylos, 1999; Zhou and Jin, 2003; Li *et al*., 2004; Lazar and Maugin, 2005) and the corresponding solutions are not exact.

By using Eq. (5.6) in Eq. (5.18) one obtains the BCs for a semi-infinite solid under prescribed normal forces as

$$
\begin{aligned}
0 &= p + (1 - l^2\nabla^2)\tau_{33}, \\
0 &= (1 - l^2\nabla^2)\tau_{3\alpha} - l^2(\tau_{\alpha 1,31} + \tau_{\alpha 2,32}), \quad \text{on } x_3 = 0 \\
0 &= l^2\tau_{3i,3},
\end{aligned}
\tag{5.19}
$$

where $p = p(r)$ denotes the normal pressure distribution. In arriving at Eq. (5.19a), use has been made of Eq. (5.19c). Apparently, when $l = 0$ Eqs. (5.19a,b) reduce to the conventional BCs.

For a half-plane problem, Eq. (5.19) becomes, after setting derivative with respect to x_2 equal to zero,

$$
\begin{aligned}
0 &= p + (1 - l^2\nabla^2)\tau_{33}, \\
0 &= (1 - l^2\nabla^2)\tau_{31} - l^2\tau_{11,31}, \\
0 &= l^2\tau_{31,3}, \\
0 &= l^2\tau_{33,3},
\end{aligned}
\quad \text{on } x_3 = 0 \tag{5.20}
$$

which are identical to the BCs used in Georgiadis and Anagnostou (2008).

The BCs listed in Eqs. (5.19) and (5.20) will be used to determine the constants involved in the stress function **B** and B_0 defined by Eq. (5.17).

5.3.2 Solutions by Fourier Transform Method

The Fourier transforms and Hankel transforms are widespread techniques used to solve boundary value problems (BVPs). These techniques are especially powerful when they are used along with certain potential functions. For example, an elegant treatment of contact problems was presented by Harding and Sneddon (1945) using Hankel transforms. As demonstrated in Selvadurai (2000, pp131-132), the use of Airy stress functions under Fourier transform is very advantageous in solving 2D elastic problems and this method is borrowed by Zhao and Rajapakse (2009) to solve half-plane problems

with surface energy effects. More recently, Barbot and Fialko (2010) solved a 3D non-classical BVP by using Fourier transforms and potential functions.

In this section, the Fourier transform method is employed along with the use of displacement functions of Mindlin to solve the semi-infinite contact problems using SSGET. The ordinary Fourier transform pair and double Fourier transform pair will be used, respectively, for the half-plane and half-space problems.

The ordinary Fourier transform pair is given by

$$\begin{aligned} \overline{f}(\xi) &= \int_{-\infty}^{\infty} f(x) e^{-\mathrm{i}\xi x} dx, \\ f(x) &= \frac{1}{2\pi} \int_{-\infty}^{\infty} \overline{f}(\xi) e^{\mathrm{i}\xi x} d\xi, \end{aligned} \tag{5.21}$$

whereas the double Fourier transform pair reads

$$\begin{aligned} \overline{f}(\xi_1, \xi_2) &= \int_{-\infty}^{\infty} \int_{-\infty}^{\infty} f(x_1, x_2) e^{-\mathrm{i}\xi_\alpha x_\alpha} dx_1 dx_2, \\ f(x_1, x_2) &= \frac{1}{4\pi^2} \int_{-\infty}^{\infty} \int_{-\infty}^{\infty} \overline{f}(\xi_1, \xi_2) e^{\mathrm{i}\xi_\alpha x_\alpha} d\xi_1 d\xi_2, \end{aligned} \tag{5.22}$$

where the overhead bar denotes the function in the transformed space.

The solutions to the displacement functions can be readily identified in the Fourier domain, e.t., by Eq. (5.17) we have

$$\begin{aligned} (1 + l^2\xi^2 - l^2 d^2)(d^2 - \xi^2)\overline{B}_3 &= 0, \\ (1 + l^2\xi^2 - l^2 d^2)(d^2 - \xi^2)\overline{B}_0 &= 0, \end{aligned} \tag{5.23}$$

where $d = \partial_3$ is the derivative operator, and $\xi^2 = \xi_\alpha \xi_\alpha$ (it equals to ξ_1^2 and $\xi_1^2 + \xi_2^2$ for the ordinary and double Fourier transforms, respectively).

If the stress components are to vanish at $x_3 \to \infty$, the solutions for Eq. (5.23) have forms

$$\begin{aligned}\bar{B}_0 &= Ae^{-x_3|\xi|} + Be^{-x_3\zeta},\\ \bar{B}_3 &= Ce^{-x_3|\xi|} + De^{-x_3\zeta},\end{aligned} \tag{5.24}$$

in which $\zeta \equiv \sqrt{\xi^2 + l^{-2}}$ and *A*, *B*, *C* and *D* are unknowns to be determined from the imposed BCs.

Performing Fourier transforms on Eq. (5.16) and using Eq. (5.24) yield

$$\begin{aligned}\bar{u}_\beta &= -\frac{\mathrm{i}}{2}\xi_\beta\left[\alpha\left(Cx_3 + A\right)e^{-x_3|\xi|} - \left(B - \alpha B + 2Dl^2\zeta\right)e^{-x_3\zeta}\right],\\ \bar{u}_3 &= \frac{1}{2}\left[(2-\alpha)C + \alpha|\xi|(Cx_3 + A)\right]e^{-x_3|\xi|} - \frac{1}{2}\left[(1-\alpha)B\zeta + 2Dl^2\xi^2\right]e^{-x_3\zeta}.\end{aligned} \tag{5.25}$$

In a similar fashion, the transformed Cauchy stress components in the transformed space are obtained to be

$$\begin{aligned}\frac{\bar{\tau}_{\beta 3}}{\mu} &= \mathrm{i}\xi_\beta\left\{\left[(1-\alpha)C + \alpha(Cx_3 + A)|\xi|\right]e^{-x_3|\xi|} - \left[(1-\alpha)B\zeta + D\left(1 + 2l^2\xi^2\right)\right]e^{-x_3\zeta}\right\},\\ \frac{\bar{\tau}_{12}}{\mu} &= \xi_1\xi_2\left\{\alpha(Cx_3 + A)e^{-x_3|\xi|} - \left[(1-\alpha)B + 2Dl^2\zeta\right]e^{-x_3\zeta}\right\},\\ \frac{\bar{\tau}_{\beta\beta}}{\mu} &= \alpha\left[-2C\nu|\xi| + (Cx_3 + A)\xi_\beta^2\right]e^{-x_3|\xi|} + \left\{B\left[\nu\alpha l^{-2} - (1-\alpha)\xi_\beta^2\right] - 2Dl^2\xi_\beta^2\zeta\right\}e^{-x_3\zeta},\\ \frac{\bar{\tau}_{33}}{\mu} &= -\left[C|\xi| + \alpha(Cx_3 + A)\xi^2\right]e^{-x_3|\xi|} + \left\{B\left[\tfrac{1}{2}l^{-2} + (1-\alpha)\xi^2\right] + 2l^2\xi^2\zeta D\right\}e^{-x_3\zeta}.\end{aligned} \tag{5.26}$$

Note no summation is implied on β in Eq. (5.26c)

Equations (5.25) and (5.26) provide the expressions of the stress and displacement components in the Fourier domain. These expressions also hold for the half-plane problem by replacing ξ_1 with ξ:

$$\begin{aligned}\bar{u}_1 &= -\frac{\mathrm{i}}{2}\xi\left[\alpha\left(Cx_3+A\right)e^{-x_3|\xi|}-\left(B-\alpha B+2Dl^2\zeta\right)e^{-x_3\zeta}\right],\\ \bar{u}_3 &= \frac{1}{2}\left[(2-\alpha)C+\alpha|\xi|(Cx_3+A)\right]e^{-x_3|\xi|}-\frac{1}{2}\left[(1-\alpha)B\zeta+2Dl^2\xi^2\right]e^{-x_3\zeta},\end{aligned} \tag{5.27}$$

and

$$\begin{aligned}\frac{\bar{\tau}_{13}}{\mu} &= \mathrm{i}\xi\left\{\left[(1-\alpha)C+\alpha(Cx_3+A)|\xi|\right]e^{-x_3|\xi|}-\left[(1-\alpha)B\zeta+D\left(1+2l^2\xi^2\right)\right]e^{-x_3\zeta}\right\},\\ \frac{\bar{\tau}_{11}}{\mu} &= \alpha\left[-2C\nu|\xi|+(Cx_3+A)\xi^2\right]e^{-x_3|\xi|}+\left\{B\left[\nu\alpha l^{-2}-(1-\alpha)\xi^2\right]-2Dl^2\xi^2\zeta\right\}e^{-x_3\zeta},\\ \frac{\bar{\tau}_{33}}{\mu} &= -\left[C|\xi|+\alpha(Cx_3+A)\xi^2\right]e^{-x_3|\xi|}+\left\{B\left[\tfrac{1}{2}l^{-2}+(1-\alpha)\xi^2\right]+2Dl^2\xi^2\zeta\right\}e^{-x_3\zeta}.\end{aligned} \tag{5.28}$$

Insertion of Eq. (5.26) (for a half-space) and Eq. (5.28) (for a half-plane), respectively, in Eq. (5.19) and Eq. (5.20) leads to the corresponding BCs in the Fourier domain. These BCs, which happen to be the same for the half-space and half-plane problems, have the form

$$\begin{aligned}0 &= -\bar{p}+\alpha\mu\xi^2A+\mu|\xi|(1+2\alpha l^2\xi^2)C,\\ 0 &= \alpha|\xi|l^2\zeta^2A+\left[\alpha\nu+(\alpha-1)l^2\xi^2\right]\zeta B+(1-\alpha)l^2\zeta^2C-2l^4\xi^2\zeta^2D,\\ 0 &= \alpha|\xi|^3l^2A-\left[\tfrac{1}{2}+(1-\alpha)l^2\xi^2\right]\zeta B+(1-\alpha)l^2\xi^2C-2l^4\xi^2\zeta^2D,\\ 0 &= -\alpha\xi^2A+(1-\alpha)\zeta^2B+(2\alpha-1)|\xi|C+(1+2l^2\xi^2)\zeta D.\end{aligned} \tag{5.29}$$

where $\bar{p}$ is the normal load in the Fourier domain. In matrix form they can be written as

$$\begin{bmatrix}\alpha|\xi| & 0 & 1+2\alpha l^2\xi^2 & 0\\ \alpha|\xi|l^2\zeta^2 & \left[\alpha\nu+(\alpha-1)l^2\xi^2\right]\zeta & (1-\alpha)l^2\zeta^2 & -2l^4\xi^2\zeta^2\\ \alpha|\xi|^3l^2 & -\left[\tfrac{1}{2}+(1-\alpha)l^2\xi^2\right]\zeta & (1-\alpha)l^2\xi^2 & -2l^4\xi^2\zeta^2\\ -\alpha\xi^2 & (1-\alpha)\zeta^2 & (2\alpha-1)|\xi| & (1+2l^2\xi^2)\zeta\end{bmatrix}\begin{Bmatrix}A\\B\\C\\D\end{Bmatrix}=\begin{Bmatrix}\dfrac{\bar{p}}{\mu|\xi|}\\0\\0\\0\end{Bmatrix}.$$

Solving Eq. (5.29) gives

$$
\begin{aligned}
A &= -\frac{2\bar{p}(1-\nu)}{\mu\xi^2\varphi(\xi)}\left[(1-2\nu)(1-\nu+2l^4\xi^2\zeta^2)+4\nu l^4\zeta|\xi|^3\right],\\
B &= \frac{4\bar{p}(1-\nu)l^4\xi^2}{\mu\varphi(\xi)},\\
C &= \frac{2\bar{p}(1-\nu)}{\mu|\xi|\varphi(\xi)}\left[1-\nu+2l^4\xi^2\zeta\left(\zeta-|\xi|\right)\right],\\
D &= -\frac{\bar{p}(1-\nu)}{\mu\zeta\varphi(\xi)}\left(1+2l^2\xi^2\right),
\end{aligned}
\tag{5.30}
$$

in which $\varphi(\xi)=(1-\nu)(1+2l^2\xi^2)+2l^6\zeta^2\xi^2(\zeta-|\xi|)^2$. It is of interest to note that *A*, *B*, *C* and *D* are all even functions of ξ and $\varphi(\xi)\geq 1-\nu$ regardless of the value of ξ.

5.4 General Solutions

General expressions for the displacements and Cauchy stresses are provided here in integral forms. For simplicity the pressure distribution for the half-plane and half-space problems are assumed to be symmetric and axisymmetric, respectively. This assumption enables the use of Fourier sine/cosine transforms as for the 2D problems and Hankel transforms for the 3D problems.

5.4.1 2D Solutions

For a symmetrically distributed contact pressure profile $\bar{p}$ is an even function of ξ. Accordingly, $\bar{u}_1$ and $\bar{\tau}_{13}$ are odd functions of ξ, while $\bar{u}_3$, $\bar{\tau}_{11}$ and $\bar{\tau}_{33}$ are even functions of ξ. Substituting Eq. (5.30) into Eqs. (5.27) and (5.28), and making use of Fourier sine/cosine transforms defined by

$$f(x)=\frac{1}{2\pi}\int_{-\infty}^{\infty}\overline{f}(\xi)e^{\mathrm{i}\xi x}d\xi=\begin{cases}\dfrac{\mathrm{i}}{\pi}\displaystyle\int_0^{\infty}\overline{f}(\xi)\sin(\xi x)d\xi, & \text{if } \overline{f} \text{ is odd,}\\[2ex] \dfrac{1}{\pi}\displaystyle\int_0^{\infty}\overline{f}(\xi)\cos(\xi x)d\xi, & \text{if } \overline{f} \text{ is even,}\end{cases} \tag{5.31}$$

we obtain the displacements in a half-plane as

$$\begin{aligned}u_1&=-\frac{1}{2\pi\mu}\int_0^{\infty}\frac{\overline{p}}{\xi\varphi(\xi)}\left(h_{11}e^{-x_3\xi}+h_{12}e^{-x_3\zeta}\right)\sin(\xi x_1)d\xi,\\ u_3&=\frac{1}{2\pi\mu}\int_0^{\infty}\frac{\overline{p}}{\xi\varphi(\xi)}\left(h_{21}e^{-x_3\xi}+h_{22}e^{-x_3\zeta}\right)\cos(\xi x_1)d\xi,\end{aligned} \tag{5.32}$$

and the Cauchy stress components are

$$\begin{aligned}\tau_{11}&=-\int_0^{\infty}\frac{\overline{p}}{\pi\varphi(\xi)}\left(g_{11}e^{-x_3\xi}+g_{12}e^{-x_3\zeta}\right)\cos(\xi x_1)d\xi,\\ \tau_{13}&=\int_0^{\infty}\frac{\overline{p}}{\pi\varphi(\xi)}\left(g_{21}e^{-x_3\xi}+g_{22}e^{-x_3\zeta}\right)\sin(\xi x_1)d\xi,\\ \tau_{33}&=-\int_0^{\infty}\frac{\overline{p}}{\pi\varphi(\xi)}\left(g_{31}e^{-x_3\xi}+g_{32}e^{-x_3\zeta}\right)\cos(\xi x_1)d\xi,\end{aligned} \tag{5.33}$$

where

$$\begin{aligned}h_{11}&=1-\nu+2l^4\xi^2\zeta^2+(2\nu+x_3\xi)\left[\nu-1+2l^4\xi^2\zeta(\xi-\zeta)\right],\\ h_{12}&=-2l^2\xi^2\left(1-\nu+l^2\xi^2\right),\\ h_{21}&=2(1-\nu)\left(1-\nu+\tfrac{1}{2}x_3\xi+2l^4\xi^2\zeta^2\right)+2l^4\xi^3\zeta\left[2\nu-3+x_3(\zeta-\xi)\right],\\ h_{22}&=2l^2\xi^3\zeta^{-1}\left(l^2\xi^2+\nu\right),\end{aligned} \tag{5.34}$$

and

$$\begin{aligned}g_{11}&=(1-\nu+2l^4\xi^2\zeta^2)(1-x_3\xi)+2x_3l^4\xi^4\zeta,\\ g_{12}&=-2l^4\xi^2\zeta^2,\\ g_{21}&=x_3\xi(\nu-1)+2l^4\xi^3\zeta(1+x_3\xi-x_3\zeta),\end{aligned} \tag{5.35a-c}$$

$$g_{22} = -\xi\zeta^{-1}(1-\nu+2l^4\xi^2\zeta^2),$$
$$g_{31} = (1-\nu+2l^4\xi^2\zeta^2)(1+x_3\xi) - 2(2+x_3\xi)l^4\xi^3\zeta, \tag{5.35d-f}$$
$$g_{32} = 2l^4\xi^4.$$

By setting x_3 = 0 in Eqs. (5.32) and (5.33), the displacement and stress components on the bounding surface can be readily obtained as

$$u_1\big|_{x_3=0} = -\frac{1}{2\mu\pi}\int_0^\infty \frac{\bar{p}}{\xi\varphi(\xi)}\left[(1-\nu)(1-2\nu) - 2\nu l^4\xi^2(\zeta-\xi)^2\right]\sin(\xi x)d\xi,$$
$$u_3\big|_{x_3=0} = \frac{1-\nu}{\mu\pi}\int_0^\infty \frac{\bar{p}}{\xi\varphi(\xi)}\left[1-\nu-l^2\xi^3\zeta^{-1}+2l^4\xi^2\zeta(\zeta-\xi)\right]\cos(\xi x)d\xi, \tag{5.36}$$

and

$$\tau_{11}\big|_{x_3=0} = -\frac{1-\nu}{\pi}\int_0^\infty \frac{\bar{p}}{\varphi(\xi)}\cos(\xi x)d\xi,$$
$$\tau_{13}\big|_{x_3=0} = -\frac{1-\nu}{\pi}\int_0^\infty \frac{\xi\bar{p}}{\zeta\varphi(\xi)}\sin(\xi x)d\xi, \tag{5.37}$$
$$\tau_{33}\big|_{x_3=0} = -\frac{1}{\pi}\int_0^\infty \frac{\bar{p}}{\varphi(\xi)}\left[1-\nu+2l^4\xi^2(\zeta-\xi)^2\right]\cos(\xi x)d\xi.$$

5.4.2 3D Solutions

For an axisymmetric contact pressure distribution, Hankel transforms can be applied. By using the formulae derived in Section 3:

$$F^{-1}[\bar{f}(\xi)] = \frac{1}{2\pi}\int_0^\infty \bar{f}(\xi)\xi J_0(\xi r)d\xi,$$
$$F^{-1}[\bar{f}(\xi)\xi_\alpha] = \mathrm{i}\frac{x_\alpha}{2\pi r}\int_0^\infty \bar{f}(\xi)\xi^2 J_1(\xi r)d\xi,$$
$$F^{-1}[\bar{f}(\xi)\xi_1\xi_2] = -\frac{x_1x_2}{2\pi r^2}\int_0^\infty \bar{f}(\xi)\xi^3 J_2(\xi r)d\xi, \tag{5.38}$$
$$F^{-1}[\bar{f}(\xi)\xi_\alpha^2] = \frac{1}{4\pi}\int_0^\infty \bar{f}(\xi)\xi^3\left[J_0(\xi r) - \left(2x_\alpha^2 r^{-2}-1\right)J_2(\xi r)\right]d\xi,$$

the expressions for the displacement and Cauchy stress components are found to be

$$u_\beta = -\frac{x_\beta}{4\mu\pi r}\int_0^\infty \frac{\bar{p}}{\xi\varphi(\xi)}\left(h_{11}e^{-x_3\xi}+h_{12}e^{-x_3\zeta}\right)\xi J_1(\xi r)d\xi,$$
$$u_3 = \frac{1}{4\pi\mu}\int_0^\infty \frac{\bar{p}}{\xi\varphi(\xi)}\left(h_{21}e^{-x_3\xi}+h_{22}e^{-x_3\zeta}\right)\xi J_0(\xi r)d\xi, \tag{5.39}$$

and

$$\tau_{\beta 3} = \frac{x_\beta}{2r}\int_0^\infty \frac{\bar{p}}{\pi\varphi(\xi)}\left(g_{21}e^{-x_3\xi}+g_{22}e^{-x_3\zeta}\right)\xi J_1(\xi r)d\xi,$$
$$\tau_{33} = -\frac{1}{2}\int_0^\infty \frac{\bar{p}}{\pi\varphi(\xi)}\left(g_{31}e^{-x_3\xi}+g_{32}e^{-x_3\zeta}\right)\xi J_0(\xi r)d\xi. \tag{5.40}$$

On the loading surface, Eqs. (5.39) and (5.40) give

$$u_\beta\big|_{x_3=0} = -\frac{x_\beta}{4\mu\pi r}\int_0^\infty \frac{\bar{p}}{\varphi(\xi)}\left[(1-\nu)(1-2\nu)-2\nu l^4\xi^2(\zeta-\xi)^2\right]J_1(\xi r)d\xi,$$
$$u_3\big|_{x_3=0} = \frac{1-\nu}{2\mu\pi}\int_0^\infty \frac{\bar{p}}{\varphi(\xi)}\left[1-\nu-l^2\xi^3\zeta^{-1}+2l^4\xi^2\zeta(\zeta-\xi)\right]J_0(\xi r)d\xi, \tag{5.41}$$

and

$$\tau_{\beta 3}\big|_{x_3=0} = -\frac{1-\nu}{2\pi r}x_\beta\int_0^\infty \frac{\xi\bar{p}}{\zeta\varphi(\xi)}\xi J_1(\xi r)d\xi,$$
$$\tau_{33}\big|_{x_3=0} = -\frac{1}{2\pi}\int_0^\infty \frac{\bar{p}}{\varphi(\xi)}\left[1-\nu+2l^4\xi^2(\zeta-\xi)^2\right]\xi J_0(\xi r)d\xi. \tag{5.42}$$

From Eqs. (5.36), (5.37), (5.41) and (5.42) it can be observed that

1) The SSGET-based solution predicts smaller in-plane displacements, u_α, and Cauchy stress, $\tau_{\alpha 3}$, than the classical solution.

2) According to the newly derived solution, the surface shear stresses are non-vanishing, which is similar to the observation made by using the theory of surface elasticity in Section 3.

5.5 Illustrative Examples

The general solutions derived in the preceding section are in integral forms and their closed form solutions are typically not available. These integrals are evaluated numerically for simple load distributions – concentrated force and uniform pressure distribution – to demonstrate the possible departure between the SSGET-based solution and the classical one.

5.5.1 Point Force

The classical problems of a semi-infinite elastic solid acted by a concentrated force and by a line force are known as Boussinesq problem and Flamant problem, respectively. These two fundamental problems are studied using the SSGET-based solutions derived in the preceding section. For a concentrated force of magnitude *P*, we shall have $\bar{p} = P$ in the Fourier domain. The displacement and stress components for the 2D and 3D problems can then be obtained by replacing $\bar{p}$ with *P* in Eqs. (5.36) and (5.37) and Eqs. (5.41) and (5.42), respectively.

For the Flamant problem, the current SSGET-based solution gives, using Eqs. (5.36) and (5.37), the surface displacements as

$$\begin{aligned} u_1\big|_{x_3=0} &= -\frac{P}{2\mu\pi}\int_0^\infty \frac{1}{\xi\varphi(\xi)}\Big[(1-\nu)(1-2\nu)-2\nu l^4\xi^2(\zeta-\xi)^2\Big]\sin(\xi x)d\xi, \\ u_3\big|_{x_3=0} &= \frac{1-\nu}{\mu\pi}P\int_0^\infty \frac{1}{\xi\varphi(\xi)}\Big[1-\nu-l^2\xi^3\zeta^{-1}-2l^4\xi^2\zeta(\xi-\zeta)\Big]\cos(\xi x)d\xi, \end{aligned} \tag{5.43}$$

and the surface Cauchy stresses as

$$\tau_{11}\big|_{x_3=0} = -\frac{1-\nu}{\pi} P\int_0^\infty \frac{1}{\varphi(\xi)}\cos(\xi x)d\xi,$$

$$\tau_{13}\big|_{x_3=0} = -\frac{1-\nu}{\pi} P\int_0^\infty \frac{\xi}{\zeta\varphi(\xi)}\sin(\xi x)d\xi, \tag{5.44}$$

$$\tau_{33}\big|_{x_3=0} = -\frac{P}{\pi}\int_0^\infty \frac{1}{\varphi(\xi)}\left[1-\nu+2l^4\xi^2(\zeta-\xi)^2\right]\cos(\xi x)d\xi.$$

Regarding the Boussinesq problem, the use of Eqs. (5.41) and (5.42) leads to

$$u_\beta\big|_{x_3=0} = -\frac{Px_\beta}{4\mu\pi r}\int_0^\infty \frac{1}{\varphi(\xi)}\left[(1-\nu)(1-2\nu)-2\nu l^4\xi^2(\zeta-\xi)^2\right]J_1(\xi r)d\xi,$$

$$u_3\big|_{x_3=0} = \frac{1-\nu}{2\mu\pi} P\int_0^\infty \frac{1}{\varphi(\xi)}\left[1-\nu-l^2\xi^3\zeta^{-1}+2l^4\xi^2\zeta(\zeta-\xi)\right]J_0(\xi r)d\xi, \tag{5.45}$$

and

$$\tau_{\beta 3}\big|_{x_3=0} = -\frac{1-\nu}{2\pi r} Px_\beta\int_0^\infty \frac{\xi^2 J_1(\xi r)}{\zeta\varphi(\xi)}d\xi,$$

$$\tau_{33}\big|_{x_3=0} = -\frac{P}{2\pi}\int_0^\infty \frac{\xi J_0(\xi r)}{\varphi(\xi)}\left[1-\nu+2l^4\xi^2(\zeta-\xi)^2\right]d\xi. \tag{5.46}$$

Note that the current SSGET-based solutions include the classical Flamant and Boussinesq solutions as special cases. Setting $l = 0$ and $\bar{p} = P$ in Eqs. (5.32) and (5.33) yield the following classical elasticity solution (e.g., Ling *et al*., 2002, pp95-96):

$$u_{1,1}^c = -\frac{P}{2\pi\mu}\int_0^\infty (1-2\nu-x_3\xi)e^{-x_3\xi}\cos(\xi x_1)d\xi = -\frac{P}{2\pi\mu}\frac{x_3}{r^2}\left[1-2\nu-\frac{x_3^2-x_1^2}{r^2}\right],$$

$$u_{3,1}^c = -\frac{P}{\pi\mu}\int_0^\infty \left(1-\nu+\tfrac{1}{2}x_3\xi\right)e^{-x_3\xi}\sin(\xi x_1)d\xi = -\frac{P}{\pi\mu}\left[(1-\nu)\frac{x_1}{r^2}+x_3^2\frac{x_1}{r^4}\right], \tag{5.47}$$

and

$$\tau_{11}^{c} = -\frac{P}{\pi}\int_0^{\infty}(1-x_3\xi)e^{-x_3\xi}\cos(\xi x_1)d\xi = -\frac{2P}{\pi}\frac{x_3x_1^2}{r^4}$$

$$\tau_{13}^{c} = -\frac{P}{\pi}\int_0^{\infty}x_3\xi e^{-x_3\xi}\sin(\xi x_1)d\xi = -\frac{2P}{\pi}\frac{x_1x_3^2}{r^4}, \tag{5.48}$$

$$\tau_{33}^{c} = -\frac{P}{\pi}\int_0^{\infty}(1-x_3\xi)e^{-x_3\xi}\cos(\xi x_1)d\xi = -\frac{2P}{\pi}\frac{x_3^2}{r^4}.$$

The classical solution for the displacements obtained from Eq. (5.47) is discontinuous and unbounded at the loading point.

By evaluating the integrals in Eqs. (5.43) and (5.44), the variations of the surface displacements and Cauchy stresses are examined to assess the influence of the intrinsic material length scale parameter *l*. These results are shown in Figure 5.2 and 5.3. A Poisson's ratio of 0.27 is used in the numerical simulations.

According to the classical Flamant solution, the in-plane displacement, u_1, is discontinuous and the out-of-plane displacement, u_3, is unbounded at the point of application of force. However, such discontinuity and singularity are not predicted by the current SSGET-based solution for the same problem. As shown in Figure 5.2, u_1 vanishes at the loading point (and thus is continuous), and u_3 is well-defined at that point. The current solutions for u_1 and u_3 gradually converge to the classical ones at far distance from the loading point. Such mechanical responses are believed to be more natural than the singular behavior predicted by the classical solution (e.g., Georgiadis and Anagnostou, 2008). In addition, the newly derived strain gradient solution deviates significantly from the classical one in the immediate vicinity of the loading point and the discrepancy between the two solutions increases as the characteristic length *l* increases.

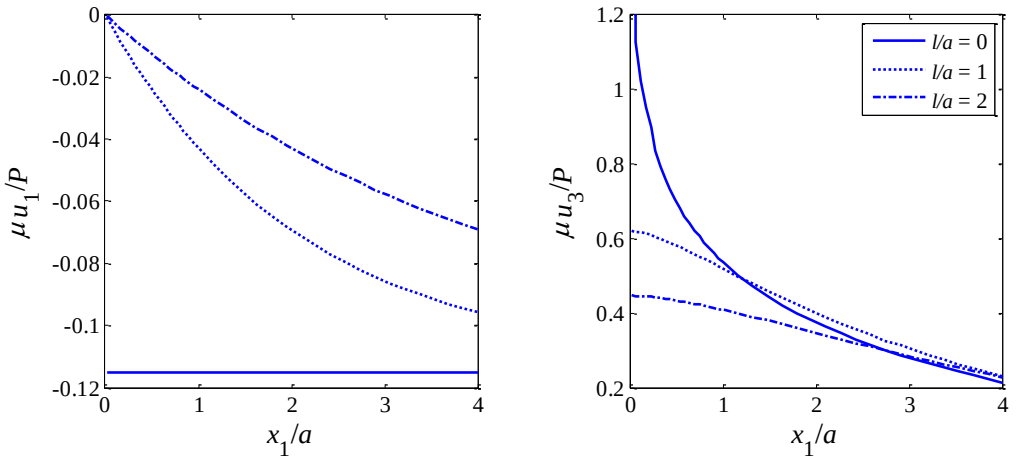

Figure 5.2. Surface displacements of a half-plane loaded by a concentrated normal force (assuming $u_3 = 0$ at $x_1 = 10a$).

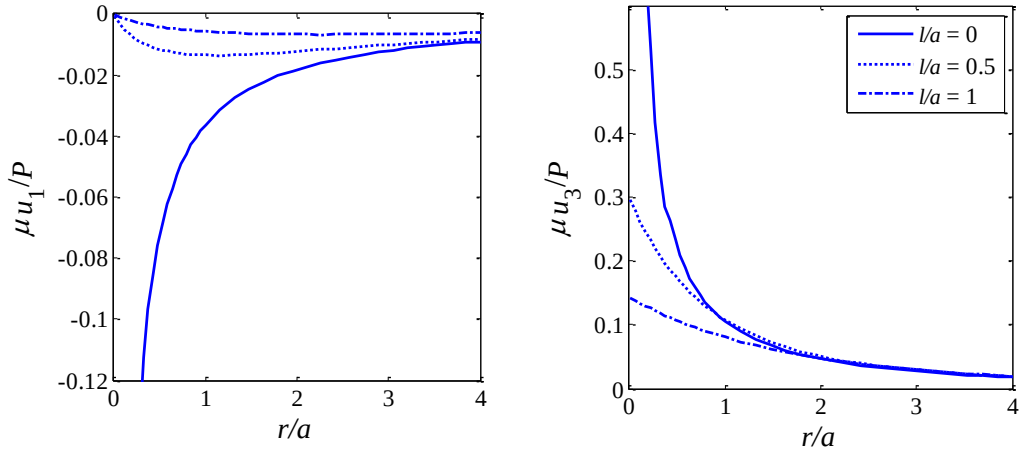

Figure 5.3. Surface displacements along $x_2 = 0$ of a half-space loaded by a concentrated normal force (assuming $u_3 = 0$ at $x_1 = 10a$).

5.5.2 Uniformly Distributed Load

When there is a uniformly distributed load of intensity q_0 applied over the region $-a < x < a$ in the bonding surface of a half-plane, the Fourier cosine transform can be

applied to obtain

$$\bar{p} = 2\int_0^a q_0 \cos(\xi x)dx = 2q_0\xi^{-1}\sin(\xi a). \tag{5.49}$$

For a half-space, if the uniform pressure is distributed over the region $r < a$, then it follows that (refer to Section 3 for detailed derivation)

$$\bar{p} = 2\pi a q_0 \xi^{-1} J_1(a\xi). \tag{5.50}$$

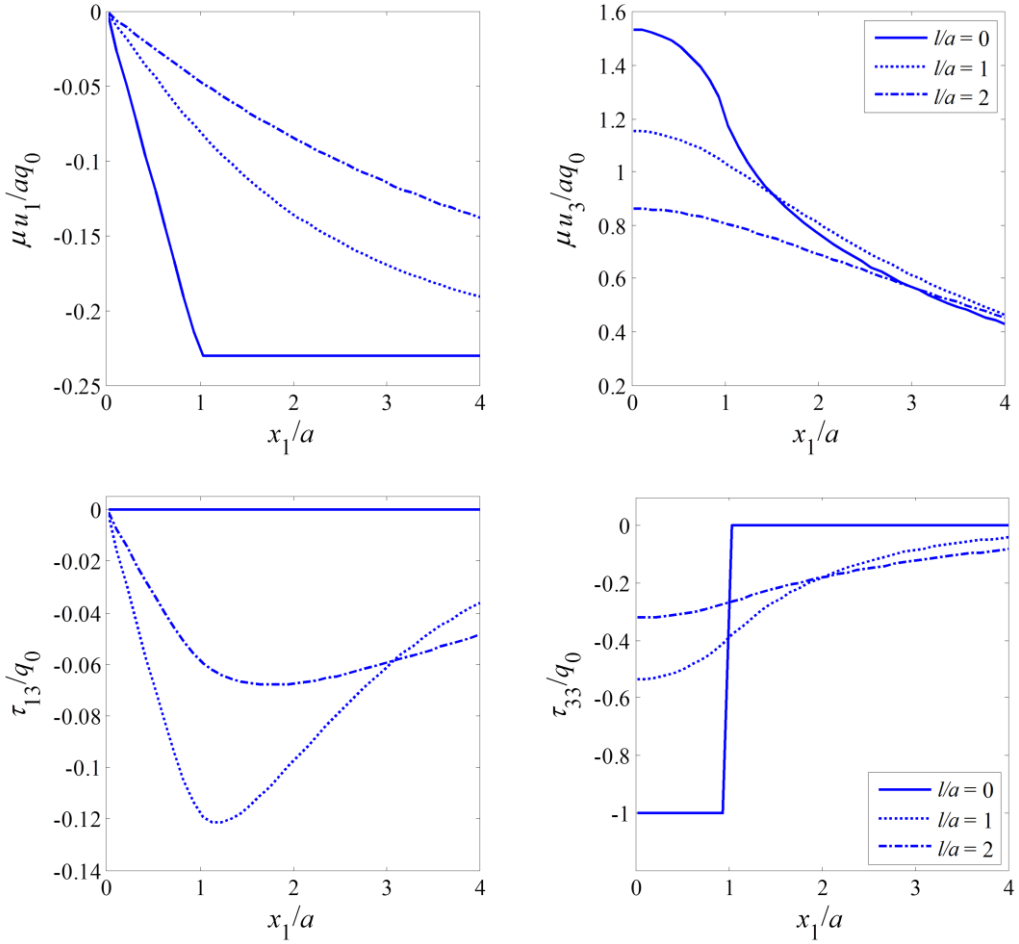

Figure 5.4. Surface displacements and Cauchy stresses of a half-plane loaded by a uniform pressure on the bounding surface.

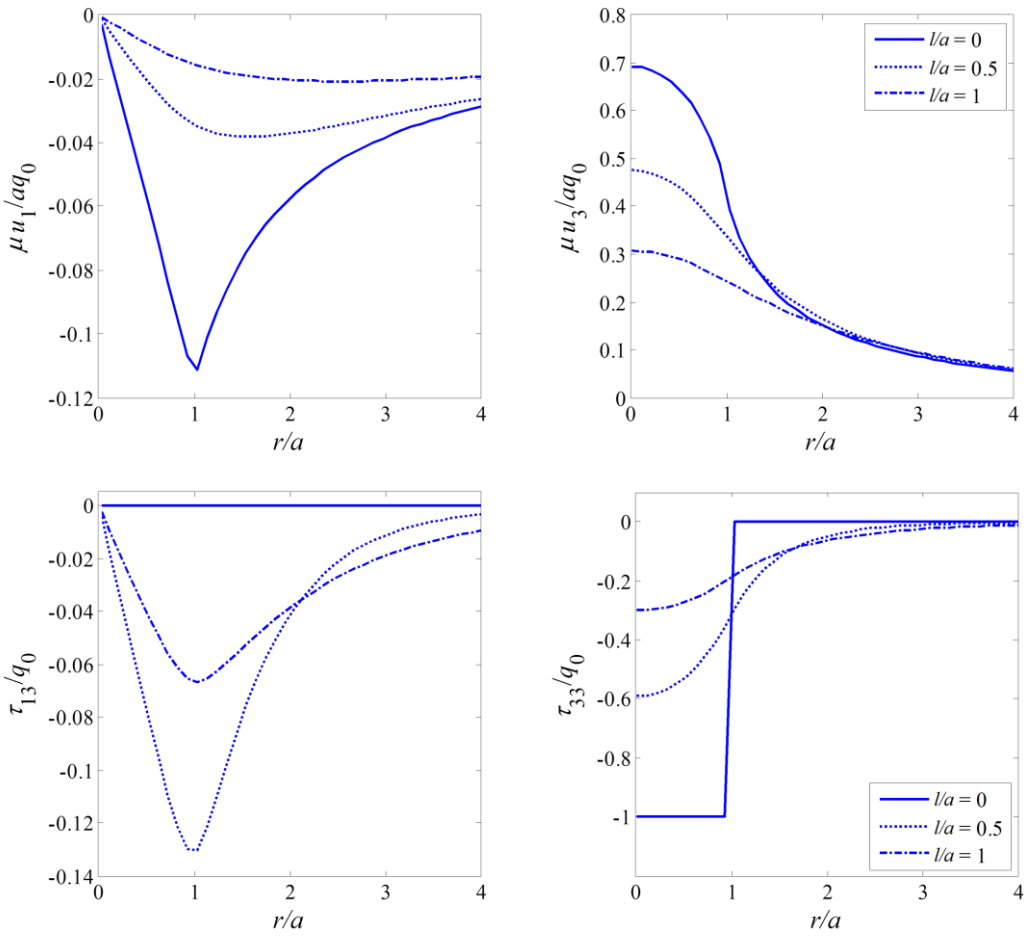

Figure 5.5. Surface displacements and Cauchy stresses along $x_2 = 0$ of a half-space loaded by a uniform pressure on its bounding surface.

Using Eqs. (5.49) and Eq. (5.50), respectively, in Eqs. (5.36-5.37) and Eqs. (5.41 -5.42) immediately leads to the analytical solutions for the displacements and stresses for the 2D and 3D problems.

As reflected in Figures 5.4 and 5.5, the influence of the material length l on the displacement field is analogous to that observed in the previous section. It is worth

noting that the SSGET-based solutions are smoother – both u_1 and τ_{33} change smoothly across the loading periphery – than the classical ones which show sharp angles, and converge to the classical solutions at a distance far from the loading zone. A similar observation was made for the near-tip displacement in the 2D crack problem (e.g., Shi *et al*., 2000 and Georgiadis, 2003) which closes more smoothly if a strain gradient theory is used to describe the material behavior. Also it should be noticed that the surface shear stress is non-vanishing according to the SSGET-based solution.

5.6 Indentation Problems

The analysis of the state of stress and strain in an elastic body indented by a punch is of significant practical interest. There have been extensive studies in this respect (e.g., Johnson, 1985) since the late 1800s when the problems of a semi-infinite elastic solid indented by a flat-ended punch and by a spherical punch were solved, respectively, by Boussinesq (1885) and Hertz (1882).

However, the well-established classical contact mechanics cannot explain non-conventional mechanical behaviors in micron and nanometer ranges such as size-dependent indentation hardness (e.g., Stelmashenko *et al*., 1993; De Guzman *et al*., 1993; Ma and Clarke, 1995). This is due to the lack of any material length scale parameter.

In this section, the axisymmetric contact problems are investigated using the newly derived solutions which contains one material length scale parameter and can be used to model substrates with significant microstructures. Several types of load

distributions are selected to illustrate the possible deviation from the predictions by classical continuum theory.

5.6.1 Flat-Ended Punch

The problem of an elastic half-space indented by a rigid flat-ended punch was first solved by Boussinesq (1885) using the classical theory of elasticity. According to Boussinesq's solution the pressure profile under the punch takes the form (e.g., Barber, 2002):

$$p_\infty(r) = q_0(a^2 - r^2)^{-1/2}, \tag{5.51}$$

where a is the radius of the punch, and the subscripts '∞', '1', and '2' denote the flat-ended, conical and spherical punch profile, respectively (e.g., S.-S Zhou *et al*., 2011). Taking Fourier transform on Eq. (5.51) gives

$$\bar{p}_\infty(\xi) = \begin{cases} q_0 \pi J_0(a\xi), & 2D, \\ 2\pi q_0 \xi^{-1} \sin(a\xi), & 3D. \end{cases} \tag{5.52}$$

The displacements and stresses can be readily obtained by using Eq. (5.52) in the general solutions for the half-plane or half-space problem. For contact problems the indentation depth δ (or the depth of penetration of the punch tip) is an important quantity highly concerned (S.-S Zhou *et al*., 2011). Substituting Eq. (5.52b) into Eq. (5.41) and taking $r = 0$ yield

$$\delta_\infty^{3D} = q_0 \frac{1-\nu}{\mu} \int_0^\infty \frac{\phi(\xi)}{\xi \varphi(\xi)} \sin(a\xi) d\xi = q_0 \frac{1-\nu}{\mu} \int_0^\infty \frac{\phi(\frac{t}{a})}{t\varphi(\frac{t}{a})} \sin t dt, \tag{5.53}$$

where $\phi(\xi) = 1 - \nu - l^2\xi^3\zeta^{-1} + 2l^4\xi^2\zeta(\zeta - \xi)$ and $\varphi(\xi)$ is defined near Eq. (5.30).

Figures 5.6 and 5.7 show the variations of surface displacements and Cauchy

stresses of the half-plane and half-space problems for different values of l/a. The particular solution with $l = 0$ corresponds to the classical solution and is displayed for comparison purpose. The displacements of strain gradient theory are considerably smaller in and near the loading zone than those of the classical solutions. Also, it is observed that the Cauchy stress τ_{33} given by the current solution is well-defined and smooth, unlike that predicted by the classical solution.

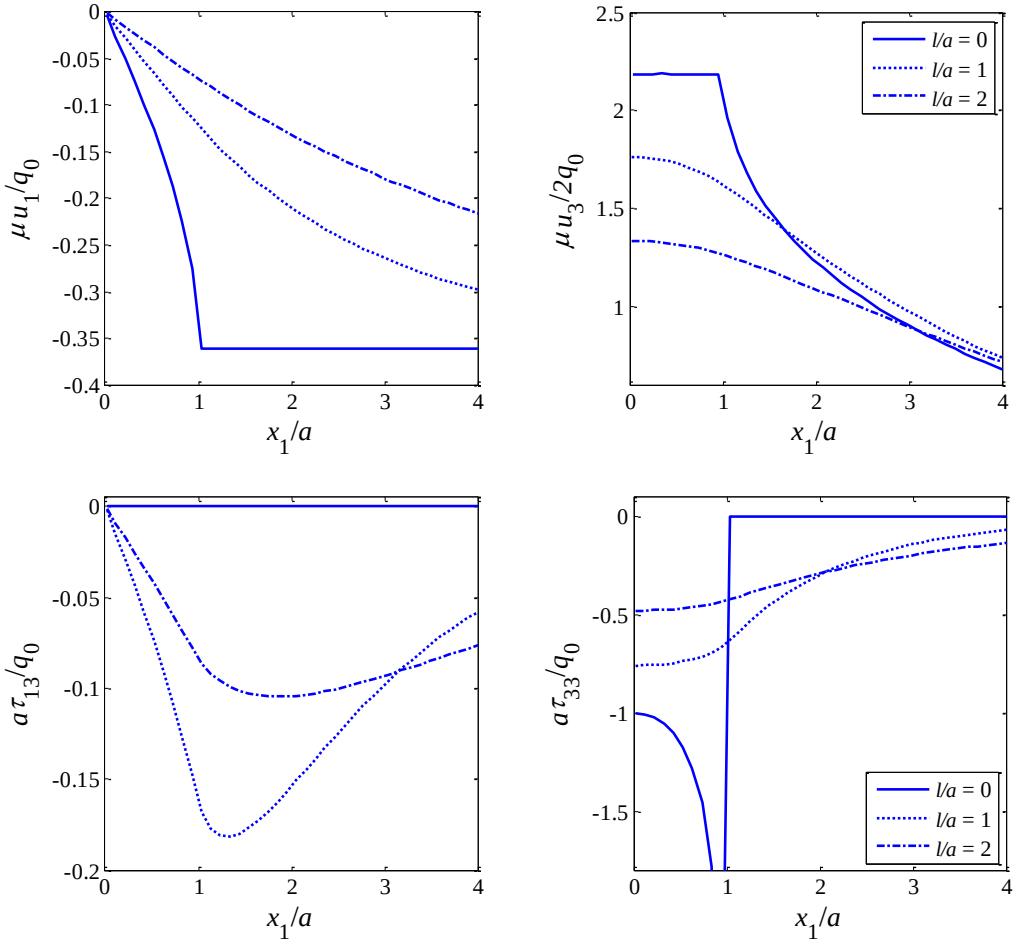

Figure 5.6. Variations of displacements and Cauchy stresses on $x_3 = 0$ of a half-plane subjected to the Boussinesq pressure distribution.

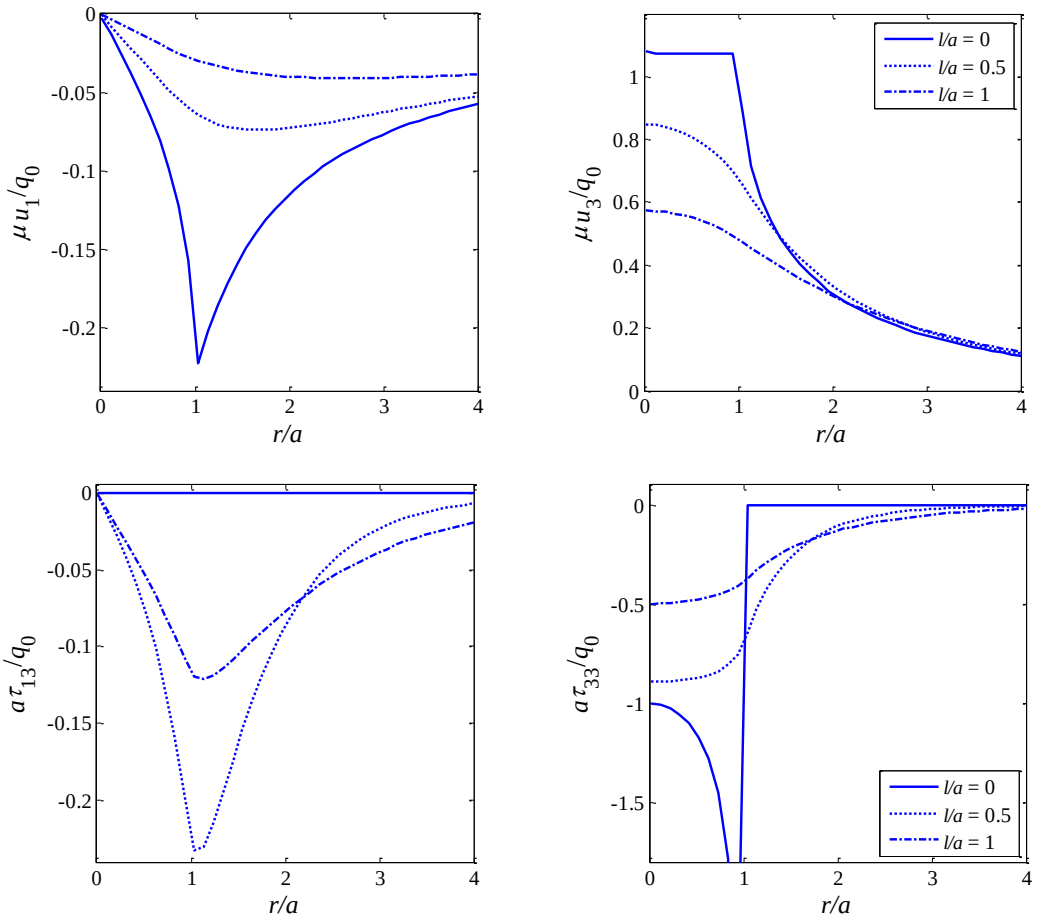

Figure 5.7. Variations of the displacements and Cauchy stresses along $x_2 = 0$ of a half-space subjected to the Boussinesq pressure distribution.

5.6.2 Spherical Punch

The Hertz's solution (1882) for the frictionless and non-adhesive contact problems of two elastic spheres is one of the most prestigious models in contact mechanics. According to Hertz's solution, the pressure distribution under the indenter is given by

$$p_2(r) = q_0\sqrt{a^2 - r^2}, \tag{5.54}$$

and the corresponding Fourier transform yields

$$\bar{p}_2(\xi) = \begin{cases} \pi q_0 a \xi^{-1} J_1(a\xi), & 2D, \\ 2\pi q_0 \xi^{-3}\left[\sin(a\xi) - a\xi\cos(a\xi)\right], & 3D. \end{cases} \tag{5.55}$$

Using Eq. (5.55b) in Eq. (5.41b) leads to

$$\delta_2^{3D} = q_0 \frac{1-\nu}{\mu} \int_0^\infty \frac{a^2 \phi(\frac{t}{a})}{t^3 \varphi(\frac{t}{a})} \left(\sin t - t\cos t\right) dt, \tag{5.56}$$

where the definitions for ϕ and φ can be found near Eq. (5.53).

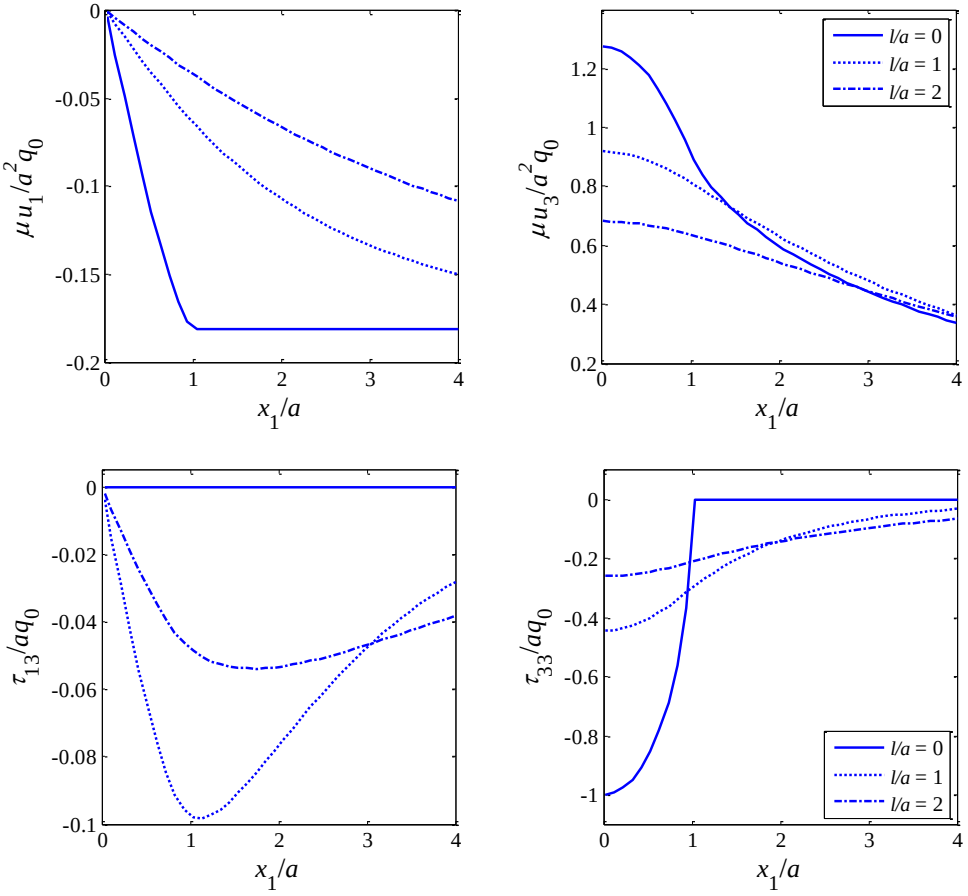

Figure 5.8. Surface displacements and Cauchy stresses in a half-plane subjected to the Hertzian pressure distribution.

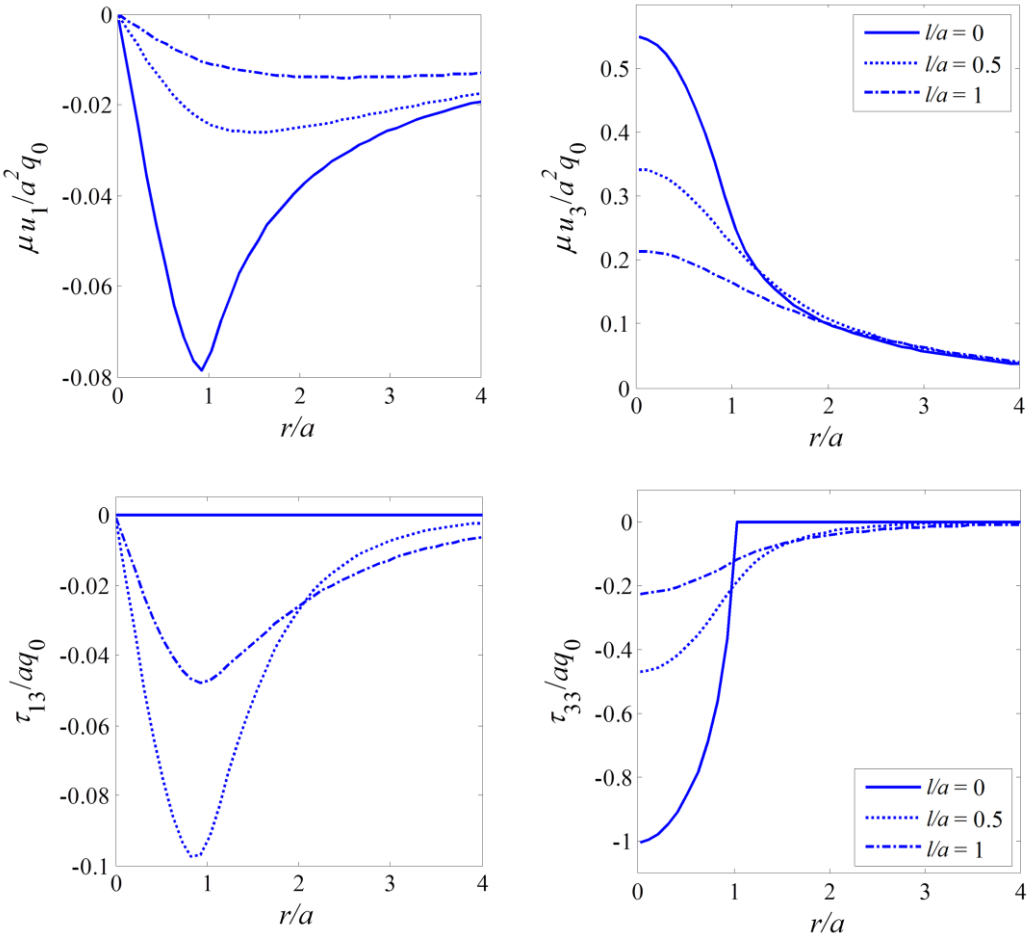

Figure 5.9. Surface displacements and Cauchy stresses of a half-space subjected to the Hertzian pressure distribution.

The displacement field and state of stress in the half-plane and half-space are displayed in Figures 5.8 and 5.9. The effect of the strain gradient on the displacement and stress components is analogous to the discussion for the flat-ended punch problem.

5.6.3 Conical Punch

The conical shaped indenters are frequently used in indentation tests. According to the classical elasticity-based solution, the pressure distribution in the contact zone has

the form (Sneddon, 1965)

$$p_1(r) = q_0 \cosh^{-1}\frac{a}{r}, \tag{5.57}$$

and it is found in the Fourier domain

$$\bar{p}_1(\xi) = 2\pi q_0 \xi^{-2}\left[1-\cos(\xi a)\right], \quad 3D. \tag{5.58}$$

Consequently, by using Eq. (5.58) in Eq. (5.41b) we find

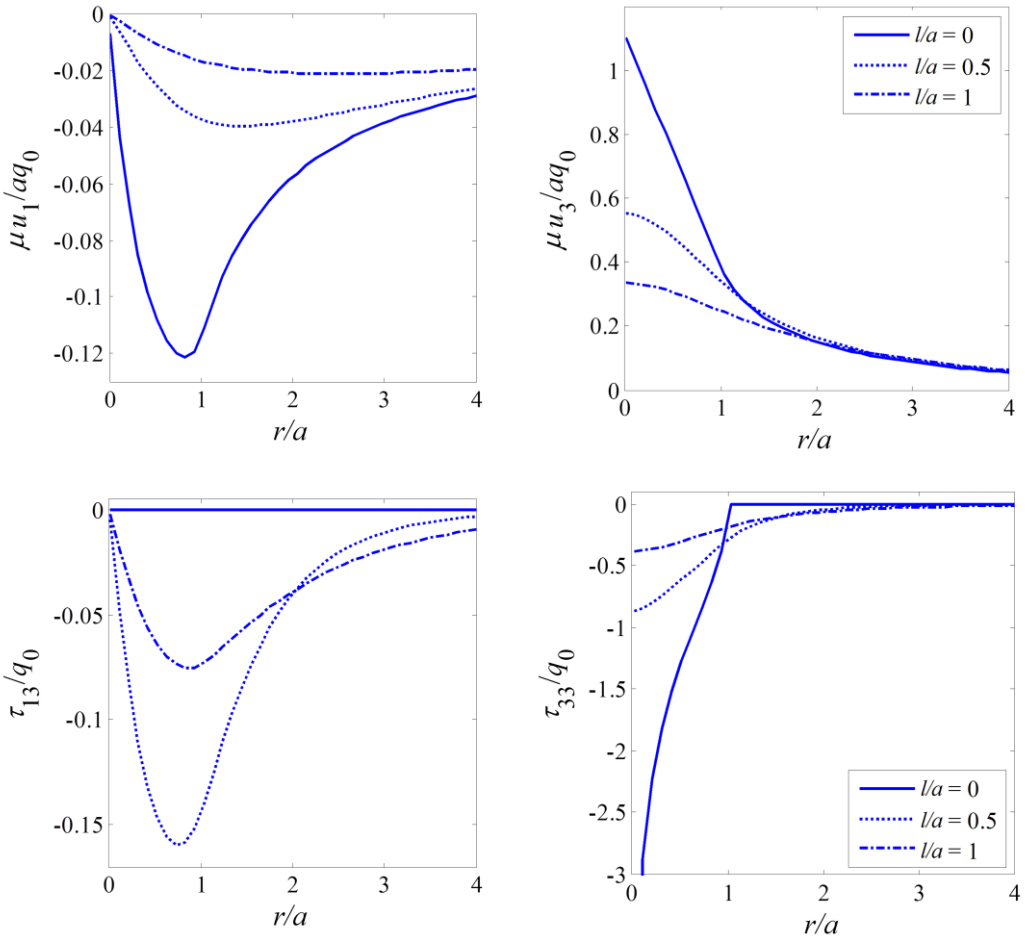

Figure 5.10. Surface displacements and Cauchy stresses of a half-space subjected to the conical punch pressure distribution.

$$\delta_1^{3D} = q_0 \frac{1-\nu}{\mu} \int_0^{\infty} \frac{a\phi(\frac{t}{a})}{t^2 \varphi(\frac{t}{a})} (1-\cos t)\, dt. \tag{5.59}$$

The numerical results for the conical punch indentation are shown in Figure 5.10.

5.6.4 Depth-Dependent Hardness

In contact mechanics, the indentation depth δ and total applied load P are of significant practical interest. The resultant forces P for the Boussinesq pressure distribution (flat-ended punch), the Hertzian pressure profile (spherical punch) and the conical punch pressure distribution have been calculated in Section 3 to be, respectively,

$$P_{\infty} = 2\pi a q_0,\ P_2 = \frac{2}{3}\pi a^3 q_0 \text{ and } P_1 = \pi a^2 q_0. \tag{5.60}$$

The indentation hardness adopted here is defined to be (e.g., Wang and Feng, 2007)

$$H = \frac{P}{\delta}. \tag{5.61}$$

In the absence of the strain gradient effect, use of Eq. (5.53), (5.56) or (5.59) and Eq. (5.60) in Eq. (5.61) yield

$$H_{\infty}^c = \frac{4\mu a}{1-\nu}, \quad H_2^c = \frac{8\mu a}{3(1-\nu)}, \quad H_1^c = \frac{2\mu a}{1-\nu}. \tag{5.62}$$

The newly derived solution for indentation hardness relates to the conventional indentation hardness through

$$\frac{H_{\infty}^c}{H_{\infty}} = 1 - \frac{2}{\pi} \int_0^{\infty} \psi(a,t) t^{-1} \sin t dt, \tag{5.63a}$$

for the Boussinesq pressure distribution,

$$\frac{H_2^c}{H_2} = 1 - \frac{4}{\pi}\int_0^\infty \psi(a,t) t^{-3} \left(\sin t - t\cos t\right) dt, \tag{5.63b}$$

for the Hertzian pressure profile, and

$$\frac{H_1^c}{H_1} = 1 - \frac{2}{\pi}\int_0^\infty \psi(a,t) t^{-2} \left(1 - \cos t\right) dt, \tag{5.63c}$$

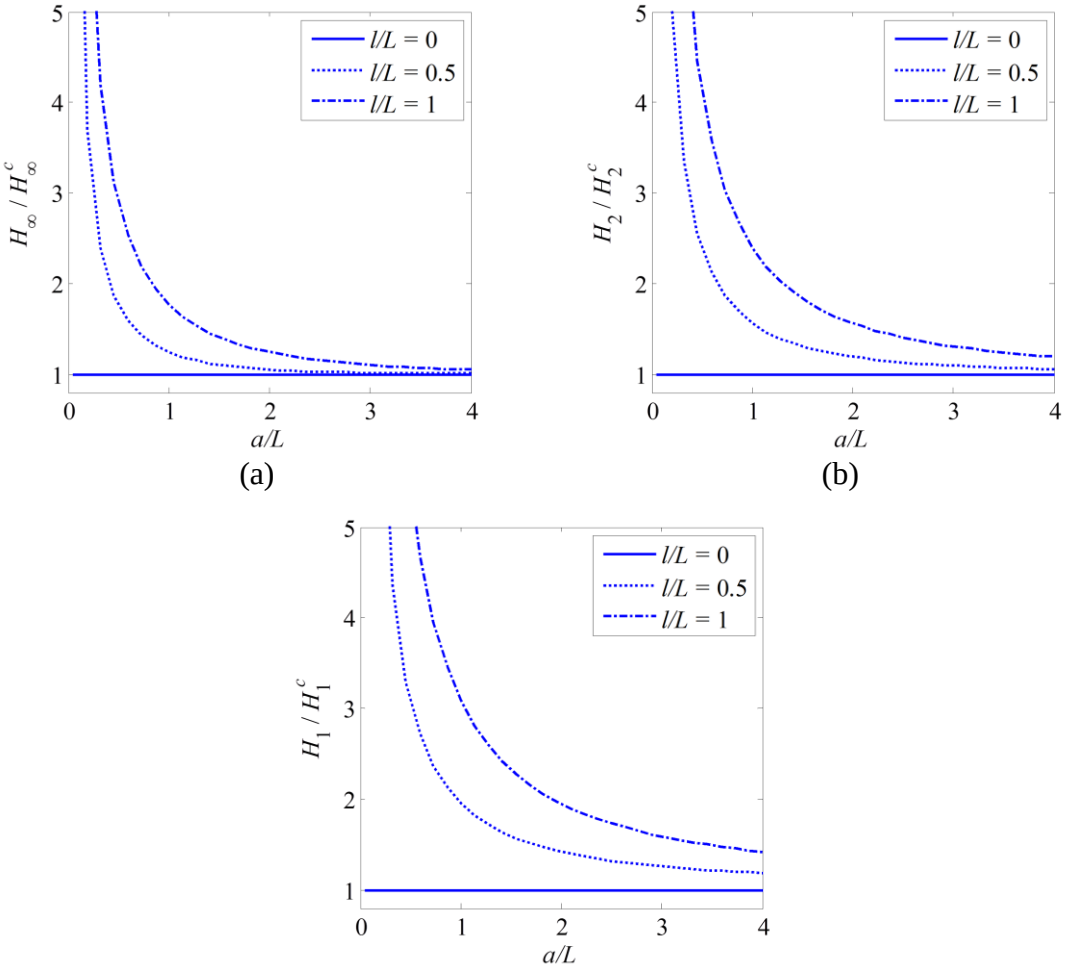

Figure 5.11. Indentation hardness versus the contact radius for different punch profiles: (a) flat-ended, (b) spherical, and (c) conical (L is a scaling parameter).

for the pressure distribution of a conical punch. In Eq. (5.63)

$$\psi(a,t)=1-\frac{\phi(\frac{t}{a})}{\varphi(\frac{t}{a})}=\tilde{l}^2t^2\,\frac{2(1-\nu)+t\tilde{\zeta}^{-1}-2\tilde{l}^4t\tilde{\zeta}(\tilde{\zeta}-t)^2}{(1-\nu)(1+2\tilde{l}^2t^2)+2\tilde{l}^6\tilde{\zeta}^2t^2(\tilde{\zeta}-t)^2}, \tag{5.63d}$$

with $\tilde{l}=\dfrac{l}{a}$ and $\tilde{\zeta}=\sqrt{1+\tilde{l}^2t^2}$.

If the strain gradient effect is neglected (that is, l = 0) we have from Eq. (5.63d) ψ (a, t) = 0 and thus $H_1^c=H_1$, $H_2^c=H_2$ and $H_\infty^c=H_\infty$. That is, the indentation hardness given by the current SSGET-based solution reduces to that by the classical solution in each of the three indentation problems considered. The microstructural effect is significant when the contact radius a is close to the value of l, and in case a >> l (e.g., indentation at macro scale) one has ψ (a, t) → 0 and the current solution converges to the classical one.

The numerical results displayed in Figures 5.11 and 5.12 show the variation of

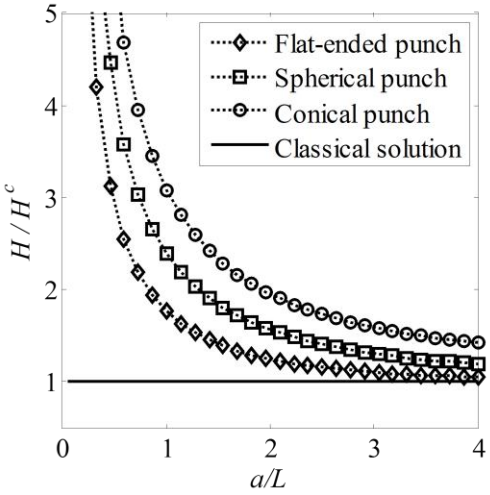

Figure 5.12. H-curves for different pressure distributions with l / L = 1.

the indentation hardness against contact radius a. For each type of the pressure distribution we examined, the ratio of H to H^c increases with decreasing contact radius a and increases as l increases. In addition, we noticed that the H to H^c ratios are different for different pressure profiles at given values of l and a.

5.7 Summary

The contact problems of a half-plane/space subjected to boundary normal forces are analyzed using the simplified strain gradient elasticity theory (SSGET). The general SSGET-based solutions for the half-plane and half-space problems are derived in a unified manner by use of the potential function method of Mindlin (1964) and integral transforms. The current solution incorporates the microstructural effects into the modeling of material responses and contains material length scale parameter that is capable of capturing material size effect at small length scales. The classical elasticity solution is regenerated as a special/limiting case in which the strain gradient effects are disregarded or the contact radius is much larger than the length scale parameter.

For the 2D and 3D fundamental problems, the numerical results show that the displacement singularity and discontinuity as exist in the classical solutions are removed when the same problems are examined under SSGET. The established general solution is also applied to study the contact problems with pressure distributions produced by a flat-ended, spherical and conical punch indenting an elastic half-space. The newly derived solution is found to deviate considerably from the classical predictions within and near the loading zone, and converge to the classical solution at increasing distances away

from the loading area. The departure between the two solutions increases with increasing material length scale parameter. The size-dependency of indentation hardness is studied by using the general solution and the indentation hardness predicted by the current solution is markedly higher than the classical results.

At this point we need to point out that the SSGET-based solution is suitable for modeling substrate materials with significant micro-structures, e.g., polycrystalline or granular materials; while the surface elasticity based model presented in Section 3 is oriented to substrates with distinct surface properties, e.g., substrate with a coated thin film or peened surface. Both of the two solutions are derived for contact problems involving an elastic, homogeneous and isotropic semi-infinite solid, and do not consider material anisotropy and inhomogeneity.

6. SUMMARY

6.1 Summary of Major Findings

This dissertation is intended to study the size-dependent material responses observed at micron and submicron levels, which cannot be satisfactorily explained by classical continuum theories due to the lack of inherent material length scale parameters. A number of enriched-continuum models are employed to examine the mechanical behavior of a semi-infinite solid subjected to normal and tangential boundary forces. The size effects are well predicted when the associated problems are examined by each of the three theories being used – adhesive contact mechanics, surface elasticity and strain gradient elasticity.

By employing the cohesive contact model pioneered by Johnson *et al*. (1971) and Derjaguin *et al*. (1975), and elaborated by Maugis (1992) we studied in Section 2 the elastic field of a half-space indented by a rigid punch and the relations between applied load, contact radius and depth of penetration. The use of harmonic functions – Green and Zerna potentials – permits an easy calculation of normal load and stress intensity factor, and effectively resolves the axisymmetric contact problems. The general solution we established is applicable to the adhesive contact problems involving an arbitrary punch shape and an adhesive interaction force distribution, and links many existing solutions/models for axisymmetric non-adhesive and adhesive contact problems like the Hertz solution, Sneddon's solution, the JKR, DMT and M-D models. It is demonstrated that the adhesive interaction forces could contribute significantly to the mechanical

behaviors of elastic solids under light load. It is because of the presence of the adhesive forces that in the absence of applied load the contact radius of solids under intimate contact is non-vanishing and a pull-off force is required to separate the solids.

The theory of surface elasticity of Gurtin and Murdoch (1975, 1978) is adopted in Sections 3 and 4 to study the mechanical behaviors of the generalized problems of Boussinesq and Cerruti, respectively. The technique of Fourier transform and certain types of potential functions are employed in attacking the problems of Boussinesq and Cerruti. The corresponding numerical results for each of the three problems studied show substantial deviation from their classical counterparts near the area of application of load, and the newly derived solution predicts a smoother elastic field and smaller deformation. The material hardening/stiffening effect is clearly predicted by the current solution which incorporates the surface effects. Note that these outlined solutions are also applicable to describe the behaviors of a considerably thick substrate with coated thin film (distinct surface properties) or with peened surface (high residual surface stress).

Regarding the generalized Boussinesq's and Cerruti's problems, it is observed that the discontinuity and singularity of the elastic field which exist in the classical theory are markedly alleviated when the surface effects are considered. Unlike the classical solution, surface elasticity based solution predicts non-vanishing out-of plane normal stress and in plane shear stresses outside the loading zone. Application of the generalized solution to the axisymmetric contact problems reveals that the indentation hardness predicted by the current solution is considerably higher than the classical result

at small length scales. For a half-region under normal loads, the out-of plane displacement and stress as well as the indentation hardness are shown to primarily depend on the residual surface stress, whereas the influence of the surface elastic constants is only significant on the in-plane displacements and stresses. On the other hand, for a half-region acted by surface tangential forces the surface material constants have a dominating impact on the elastic field, while the influence of residual surface stress is relatively insignificant.

In Section 5 we re-examined the Boussinesq's problem using the strain gradient elasticity theory, which is a more refined continuum theory that incorporates material microstructure and is capable to capture size effects. By using the displacement functions of Mindlin (1964) we were able to obtain solutions to the problems of a half-space (3D) and half-plane (2D) subjected to normal loads in a unified fashion based on Fourier transforms. The 2D and 3D fundamental solutions as well as surface Green's functions are provided and they regenerate the classical solutions if the microstructural effects are disregarded. Various load distributions are investigated to demonstrate the possible deviation from the classical results as well as to show the size-dependent phenomena. The displacements and stresses are found to change very smoothly (smoother than those obtained in Section 3 using surface elasticity) if the mechanical behavior of material is governed by gradient elasticity. Most importantly, the singularities and discontinuities as encountered in classical solutions are eliminated when the same problems are studied in the context of strain gradient elasticity.

6.2 Recommendations for Future Works

In this dissertation we examined a series of fundamental problems involving an elastic half-region within the context of several enriched-continuum theories and derived the point load solutions which form the basis of solutions to complex loading problems. However, limited applications of the formulated solutions have been investigated in the current study and extension of the generalized solutions to more general problems shall be a suitable topic for future studies in this field. Besides, the fundamental solutions outlined in this work can be used by researchers specializing on numerical analysis to develop programs that can be embed in the finite element method (FEM) or boundary element method (BEM).

The integral transform is a wide-spread technique frequently adopted in literature and this method is employed in many sections of this dissertation – standard Fourier transforms are used in solving 2D problems and double Fourier transforms for 3D problems. The connections between the double Fourier transforms and Hankel transforms are established and used to calculate the displacement and stress components of axisymmetric contact problems. The advantage of the integral transform approach is that it enables one to obtain analytical solutions to the PDEs with prescribed BCs by manipulating algebraic equations.

Of special importance is the use of various potential functions suggested by different authors which automatically satisfy the displacement-equation of motion and effectively break the associated high-order PDEs into tractable potentials. The stress functions are extremely powerful when they are appropriately used in association with

the method of integral transforms in that their analytical solutions can be readily determined in the transformed domain. The potential functions are very desirable and sometimes indispensible in solving problems in the framework of non-conventional continuum theories. The difficulties arisen from the non-classical BCs (such as the problems examined under theory of surface elasticity) or very higher order PDEs (e.g. the strain gradient elasticity) can all be satisfactorily addressed once certain types of potential functions are employed. Such advantages are highlighted in many parts in this study:

In Section 2 the harmonic functions suggested by Green and Zerna (1968) are used to solve axisymmetric adhesive contact problems. Based on this approach, one is able to calculate the normal load and stress intensity factor in an easy manner. Therefore, this method can be applied to solve axisymmetric crack problems in which the evaluation of stress intensity factor usually involves formidable efforts.

The Papkovitch-Neuber functions are employed in Section 3 and 4 to attack the BVPs in the context of surface elasticity. The methodology outline in these sections can be adopted to solve problems of similar kind in which the material behaviors are governed by the classical elastic theory while the BCs are non-classical. The models and corresponding results in each of these two sections are derived by using the general formulations of Gurtin and Murdoch (1975, 1978) which includes the surface elastic constants and residual stress. The fundamental studies and associated methodologies in these sections can be adopted to investigate surface energy effects which are gaining increased attention in recent years.

The displacement functions propounded by Mindlin (1964) can be viewed as generalized P-N functions that contain intrinsic material lengths and they effectively reduce the high-order PDEs in SSGET into to tractable potential functions. The Mindlin's stress functions have not been well-recognized and can be widely applied to solve pertinent problems under strain gradient elasticity. The theory we employed in Section 5 is the most simplified version, however, the same methodology can be applied to solve the same problem by using the more general theory, such as the one containing two material lengths (e.g., Mindlin, 1964).

Both the surface elasticity based and SSGET-based solutions are derived for semi-infinite contact problems involving elastic, homogeneous and isotropic solids. However, this idealized condition might deviate from the materials used in micro/nano-indentation, which typically exhibit certain degrees of inhomogeneity and/or anisotropy. Refined models are needed to include material anisotropy and/or inhomogeneity, and thereby yield more accurate results.

REFERENCES

Abramowitz, M., Stegun, I.A., 1964. Handbook of Mathematical Functions with Formulas, Graphs, and Mathematical Tables. Courier Dover Publications, New York.

Adamson, A.W., 1967. Physical Chemistry of Surface, 2nd edition. Wiley (Interscience), New York.

Altan, B.S., Aifantis, E.C., 1992. On the structure of the mode III crack-tip in gradient elasticity. Scripta Met. 26, 319–324.

Altan, B.S., Aifantis, E.C., 1997. On some aspects in the special theory of gradient elasticity. J. Mech. Behav. Mater. 8, 231–282.

Askes, H, Aifantis, E.C., 2011. Gradient elasticity in statics and dynamics: An overview of formulations, length scale identification procedures, finite element implementations and new results. Int. J. Solids Struct. 48, 1962–1990.

Attard, P., 2000. The interaction and deformation of elastic bodies the origin of adhesion hysteresis. J. Phys. Chem. 104, 10635–10641.

Attard, P., Parker, J.L., 1992. Deformation and adhesion of elastic bodies in contact. Phys. Rev. A 46, 7959–7971.

Barber, J.R., 1983. The solution of elasticity problems for the half-space by the method of Green and Collins. Appl. Sci. Res. 40, 135–157.

Barber, J.R., 2002. Elasticity, 2nd edition. Kluwer Academic Publishers, The Netherlands.

Barbot, S., Fialko, Y., 2010. Fourier-domain Green's function for an elastic semi-infinite solid under gravity, with applications to earthquake and volcano deformation. Geophys. J. Int. 182, 568–582.

Barthel, E., 1998. On the description of the adhesive contact of spheres with arbitrary interaction potentials. J. Colloid Interface Sci. 200, 7–18.

Barthel, E., 2008. Adhesive elastic contacts: JKR and more. J. Phys. D: Appl. Phys. 41, 163001, 1–20.

Bei, H., George, E.P., Hay, J.L., Pharr, G.M., 2005. Influence of indenter tip geometry on elastic deformation during nanoindentation. Phys. Rev. Lett. 95, 045501.

Bleustein, J.L., 1967. A note on the boundary conditions of Toupin's strain-gradient theory. Int. J. Solids Struct. 3, 1053–1057.

Borodich, F.M., Keer, L.M., Korach, C.S., 2003. Analytical study of fundamental nanoindentation test relations for indenters of non-ideal shapes. Nanotechnology 14, 803–808.

Boussinesq, J., 1885. Application des potentiels à l'étude de l'équilibre et du mouvement des solides élastiques. Gauthiers-Villars, Paris.

Bradley, R.S., 1932. The cohesive force between solid surfaces and the surface energy of solids. Phil. Mag. 13, 853–862.

Cammarat. R.C., 1994. Surface and interface stress effects in thin films. Prog. Surf. Sci. 46, 1–38.

Cammarata, R.C., Sieradzki, K., 1994. Surface and interface stresses. Annu. Rev. Mater. Sci. 24, 215–234.

Casal, P., 1961. La capillarite interne. Cahier du Groupe Francais d'Etudes de Rheologie C. N. R. S., VI, 31–37.

Chaiyat, S., Jin, X., Keer, L.M., Kiattikomol, K., 2008. Analytical and numerical evaluation of crack-tip plasticity of an axisymmetrically loaded penny-shaped crack. C. R. Mecanique 336, 54–68.

Chen, S., Gao, H., 2006a. Generalized Maugis-Dugdale model of an elastic cylinder in non-slipping adhesive contact with a stretched substrate. Int. J. Mater. Research 97, 584–593.

Chen, S., Gao, H., 2006b. Non-slipping adhesive contact of an elastic cylinder on stretched substrates. Proc. R. Soc. A 462, 211–228.

Chen, S., Gao, H., 2007. Bio-inspired mechanics of reversible adhesion: Orientation-dependent adhesion strength for non-slipping adhesive contact with transversely isotropic elastic materials. J. Mech. Phys. Solids 55, 1001–1015.

Chen, W.R., Keer, L.M., 1993. Mixed-Mode Fatigue Crack Propagation of Penny-Shaped Cracks. ASME J. Eng. Mater. Technol. 115, 365–372.

Collins, W.D., 1959. On the solution of some axisymmetric boundary value problems by means of integral equations, II: Further problems for a circular disc and a spherical cap. Mathematika, 6, 120–133.

Collins, W.D., 1963. On the solution of some axisymmetric boundary value problems by means of integral equations: VIII. Potential problems for a circular annulus. Proc. Edinburgh Math. Soc. 13, 235–246.

Cosserat, E., Cosserat, F., 1909. Théorie des corps déformables. A. Hermann et fils, Paris.

de Boer, J. H., 1936. The influence of van der Waals' forces and primary bonds on binding energy, strength and orientation, with special reference to some artificial resins. Trans. Faraday Soc. 32, 10–37.

De Guzman, M.S., Neubauer, G., Flinn, P., Nix, W.D., 1993. The role of indentation depth on the measured hardness of materials. Mater. Res. Sympos. Proc. 308, 613–618.

Derjaguin, B.V., 1934. Untersuchungen über die reibung und adhesion. IV Kolloid–Z. 69, 55–164.

Derjaguin, B.V., Muller, V.M., Toporov, Y.P., 1975. Effect of contact deformations on the adhesion of particles. J. Colloid Interface Sci. 53, 314–326.

Dhaliwal, R.S., 1973. The axisymmetric Boussinesq problem for a semi-space in couple-stress theory.Int. J. Eng. Sci. 11, 1161–1174.

Dingrevillea, R., Qu, J., Cherkaouib, M., 2005. Surface free energy and its effect on the elastic behavior of nano-sized particles, wires and films. J. Mech. Phys. Solids 53, 1827–1854.

Doerner, M.F., Nix, W.D., 1986. A method for interpreting the data from depth sensing indentation experiments. J. Mater. Res. 1, 601–609.

Duan, H.L., Wang, J., Huang, Z.P., Karihaloob, B.L., 2005. Size-dependent effective elastic constants of solids containing nano-inhomogeneities with interface stress. J. Mech. Phys. Solids 53, 1574–1596.

Dupré, M. A., 1869. Théorie mécanique de la chaleur. Gauthier-Villars, Paris.

Eringen, A.C., 1966. Linear theory of micropolar elasticity. J. Math. Mech. 15, 909–923.

Eringen, A.C., 1983. On differential equations of nonlocal elasticity and solutions of screw dislocation and surface waves. J. Appl. Phys. 54, 4703–4710.

Eringen, A.C., 1999. Microcontinuum Field Theories I: Foundations and Solids. Springer–Verlag, New York.

Exadaktylos, G. E., 1999. Gradient elasticity with surface energy: Mode-I crack problem. Int. J. Solids Struct. 35, 421–456.

Exadaktylos, G. E., Vardoulakis, I. 1998. Surface instability in gradient elasticity with surface energy. Int. J. Solids Struct. 35, 2251–2281.

Exadaktylos, G. E., Vardoulakis, I., Aifantis, E. C., 1996. Cracks in gradient elastic bodies with surface energy. Int. J. Fracture 79, 107–119.

Fargesa, G., Degouta, D., 1989. Interpretation of the indentation size effect in vickers microhardness measurements-absolute hardness of materials. Thin Solid Films 181, 365–374.

Feng, G., Nix, W.D., 2004. Indentation size effect in MgO. Scr. Mater. 51, 599–603.

Fleck, N.A., Hutchinson, J.W., 1993. A phenomenological theory for strain gradient effects in plasticity. J. Mech. Phys. Solids 41, 1825–1857.

Fleck, N.A., Muller, G.M., Ashby, M.F., Hutchinson, J.W., 1994. Strain gradient plasticity: theory and experiment. Acta Metall. Mater. 42, 475–487.

Gao, X.-L., 2006a. An expanding cavity model incorporating strain-hardening and indentation size effects. Int. J. Solids Struct. 43, 6615–6629.

Gao, X.-L., 2006b. A new expanding cavity model for indentation hardness including strain-hardening and indentation size effects. J. Mater. Research 21, 1317–1326.

Gao, X.-L., Jing, X.N., Subhash, G., 2006. Two new expanding cavity models for indentation deformations of elastic strain-hardening materials. Int. J. Solids Struct. 43, 2193–2208.

Gao, X.-L., Ma, H. M., 2009. Green's function and Eshelby's tensor based on a simplified strain gradient elasticity theory. Acta Mech. 207, 163–181.

Gao, X.-L., Ma, H. M., 2010a. Solution of Eshelbys inclusion problem with a bounded domain and Eshelbys tensor for a spherical inclusion in a finite spherical matrix based on a simplified strain gradient elasticity theory. J. Mech. Phys. Solids 58, 779–797.

Gao, X.-L., Ma, H. M., 2010b. Strain gradient solution for Eshelby's ellipsoidal inclusion problem. Proc. R. Soc. A 466, 2425–2446.

Gao, X.-L., Park, S.K., 2007. Variational formulation of a simplified strain gradient elasticity theory and its application to a pressurized thick-walled cylinder problem. Int. J. Solids Struct. 44, 7486–7499.

Gao, X.-L., Park, S.K., Ma, H.M., 2009. Analytical solution for a pressurized thick-walled spherical shell based on a simplified strain gradient elasticity theory. Math. Mech. Solids 14, 747–758.

Georgiadis, H.G., 2003. The mode-III crack problem in microstructured solids governed by dipolar gradient elasticity: Static and dynamic analysis. J. Appl. Mech. 70, 517–530.

Georgiadis, H.G., Anagnostou, D.S., 2008. Problems of the Flamant–Boussinesq and Kelvin Type in Dipolar Gradient Elasticity. J. Elast. 90, 71–98.

Gerberich, W.W., Tymiak, N.I., Grunlan, J.C., Horstemeyer, M.F., Baskes, M.I., 2002. Interpretations of indentation size effects. J. Appl. Mech. 69, 433–442.

Germain, P., 1972. Sur l'application de la méthode des puissances virtuelles en mécanique des milieuxcontinus. C. R. Acad. Sci. Paris 274, 1051–1055.

Germain, P., 1973a. La méthode des puissances virtuelles en mécanique des milieux continus. I. Théorie du second gradient. J. Mécanique 12, 235–274.

Germain, P., 1973b. The method of virtual power in Continuum Mechanics. Part 2: Microstructure. SIAM J. Appl. Math. 25, 556–575.

Gibbs, J.W., 1876. On the equilibrium of heterogeneous substances. Conn. Acad. Trans. 3, 108–248, 343–524. Or in The Scientific Papers of J. Willard Gibber: N.Y., Dover Pub., Inc., 1961, 79–82.

Goryacheva, I.G., Makhovskaya, Y.Y., 2001. Adhesive interaction of elastic bodies. J. Appl. Math. Mech. 65, 273–282.

Graham, M.A., Grasley, Z.C., Abu Al-Rub, R.K., 2010. The effect of atomic force microscope probe size on indentation tests simulated using realistic surface forces. Int. J. Mater. Struct. Integrity 4, 160–169.

Green, A.E., 1949. On Boussinesq's problem and penny-shaped cracks. Proc. Cambridge Phil. Soc. 45, 251–257.

Green, A.E., Zerna, W, 1968. Theoretical Elasticity, 2nd edition. Oxford University Press, London.

Greenwood, J.A., 1997. Adhesion of elastic spheres. Proc. R. Soc. London A 453, 1277–1297.

Greenwood, J.A., Johnson, K.L., 1981. The mechanics of adhesion of viscoelastic solids.Phil. Mag. 43, 697–711.

Greenwood, J.A., Johnson, K.L., 1998. An alternative to the Maugis model of adhesion between elastic spheres. J. Phys. D: Appl. Phys. 31, 3279–3290.

Gurtin, M.E., Murdoch, A.I., 1975. A continuum theory of elastic material surfaces. Arch. Rat. Mech. Anal. 57, 291–323. Addenda to our paper A continuum theory of elastic material surfaces. Arch. Rat. Mech. Anal. 59, 389–390.

Gurtin, M.E., Murdoch, A.I., 1978. Surface stress in solids. Int. J. Solids Struct. 14, 431–440.

Gurtin, M.E., Weissmuller, J., Larche, F., 1998. A general theory of curved deformable interfaces in solids at equilibrium.Phil. Mag. A 78, 1093–1109.

Hamaker, H.C., 1937. The London-van der Waals attraction between spherical particles. Physica 4, 1058–1072.

Harding, J.W., Sneddon, I.N., 1945. The elastic stresses produced by the indentation of the plane surface of a semi-infinite elastic solid by a rigid punch. Proc. Cambridge Philos. Soc. 41, 16–26.

Hayes, W.C., Keer, L.M., Herrmann, G., Mockros, L.F., 1972. A mathematical analysis for indentation tests of articular cartilage. J. Biomech. 5, 541–551.

He, L.H., Lim, C.W., 2006. Surface Green Function for a Soft Elastic Half-Space: Influence of Surface Stress. Int. J. Solids Struct. 43, 132–143.

He, L.H., Lim, C.W., Wu, B.S., 2004. A continuum model for size-dependent deformation of elastic films of nano-scale thickness. Int. J. Solids Struct. 41, 847–857.

He, L.H., Li, Z.R., 2006. Impact of surface stress on stress concentration. Int. J. Solids Struct. 43, 6208–6219.

Herring, C., 1951. Some Theorems on the Free Energies of Crystal Surfaces. Phys. Rev. 82, 87–93.

Hertz, H., 1882. Über die Berührung fester elastischer Körper. J. Reine Angew. Math. 92, 156–171.

Hong, S., Weil, R., 1996. Low cycle fatigue of thin copper foils. Thin Solid Films 283, 175–181.

Huang, Y.J., Shen, J.S., Sun Y., Sun, J.F., 2010. Indentation size effect of hardness of metallic glasses. Mater. Des. 31, 1563–1566.

Huang, Y., Zhang, F., Hwang, K.C., Nix, W.D., Pharr, G.M., Feng, G., 2006. A model of size effects in nano-indentation, J. Mech. Phys. Solids 54, 1668–1686.

Hughes, B.D., White, L.R., 1979. Soft contact problems in linear elasticity. Q. J. Mech. Appl. Math. 32, 445–471.

Jakata, K., Every, A., 2008. Determination of the dispersive elastic constants of the cubic crystals Ge, Si, GaAs, and InSb. Phys. Rev. B. 77, 174301.

Jin, X., Chaiyat, S., Keer, L.M., Kiattikomol, K., 2008. Refined Dugdale plastic zones of an external circular crack. J. Mech. Phys. Solids 56, 1127–1146.

Johnson, K.L., Kendall, K., Roberts, A.D., 1971. Surface energy and the contact of

elastic solids. Proc. R. Soc. London A 324, 301–313.

Johnson, K.L., 1982. One hundred years of Hertz contact. Proc. Instn. Mech. Engrs. 196, 363–378.

Johnson, K.L., 1985. Contact Mechanics. Cambridge University Press, London.

Johnson, K.L., Greenwood, J.A., 1997. An adhesion map for the contact of elastic spheres. J. Colloid Interface Sci. 192, 326–333.

Judelewicz, M., Künzi, H.U., Merk, N., Ilschner, B., 1994. Tensile and fatigue strength of ultrathin copper films. Mater. Sci. Eng. A 186 , 135–142.

Karlis, G. F., Charalambopoulos, A., Polyzos, D., 2010. An advanced boundary element method for solving 2D and 3D static problems in Mindlin's strain-gradient theory of elasticity. Int J. Numer. Method Eng. 83, 1407–1427.

Kassir, M.K., Sih, G.C., 1975. Mechanics of Fracture, Vol. 2: Three-Dimensional Crack Problems. Noordhoff International Publishing, Leyden, The Netherlands.

Keer, L.M., 1964. A class of non-symmetrical punch and crack problems. Q. J. Mech. Appl. Math. 17, 423–436.

Kendall, K., 1969. Ph.D. dissertation, Cambridge University, England.

Kendall, K., 1973. Shrinkage and peel strength of adhesive joints. J. Phys. D.: Appl. Phys. 6, 1782–1787.

Kendall, K., 1975a. A. Control of Cracks by Interfaces in Composites. Proc. R. Soc. London A 341, 409–428.

Kendall, K., 1975b. Thin-film peeling-the elastic term. J. Phys. D: Appl. Phys. 8, 1449–1452.

Kendall, K., 1976. Interfacial cracking of a composite: Part 1 Interlaminar shear and tension. J. Mater. Sci. 11, 638–644.

Kim, K.-S., McMeeking, R.M., Johnson, K.L., 1998. Adhesion, slip, cohesive zones and energy fluxes for elastic spheres in contact. J. Mech. Phys. Solids 46, 243–266.

Koch, R. 1994. The intrinsic stress of polycrystalline and epitaxial thin metal films. J. Phys.: Condens. Matter 6, 9519.

Koguchi, H., 2007. Effects of Surface Stresses on Elastic Fields near Surface and Interface. J. Solid Mech. Mater. Eng. 1, 152–168.

Koiter, W.T., 1964. Couple-stresses in the theory of elasticity, I & II. Proc. K. Ned. Akad. Wet. (B) 67, 17–44.

Kroner, E. 1967 Elasticity theory of materials with long-range cohesive forces. Int. J. Solids Struct. 3, 731–742.

Lazar, M., Maugin, G.A., 2005. Nonsingular stress and strain fields of dislocations and disclinations in first strain gradient elasticity. Int. J. Eng. Sci. 43, 1157–1184.

Li, S., Miskioglu, I., Altan, B. S., 2004. Solution to line loading of a semi-infinite solid in gradient elasticity. Int. J. Solids Struct. 41, 3395–3410.

Lim, C.W., He, L.H., 2004. Size-dependent nonlinear response of thin elastic films with nano-scale thickness. Int. J. Mech. Sci. 46, 1715–1726.

Ling, F.F., Lai, W.M., Lucca, D.A., 2002. Fundamentals of Surface Mechanics with Applications. Springer-Verlag, New York.

Lowengrub, M., Sneddon, I.N., 1965. The distribution of stress in the vicinity of an external crack in an infinite elastic solid. Int. J. Eng. Sci. 3, 451–460.

Ma, Q., Clarke, D.R., 1995. Size dependent hardness of silver single crystals. J. Mater. Res. 10, 853–863.

Marangantia, R., Sharma, P., 2007. A novel atomistic approach to determine strain-gradient elasticity constants: Tabulation and comparison for various metals, semiconductors, silica, polymers and the (Ir) relevance for nanotechnologies. J. Mech. Phys. Solids 55, 1823–1852.

Maugis, D., 1992. Adhesion of spheres: the JKR-DMT transition using a Dugdale model. J. Colloid Interface Sci. 150, 243–269.

Maugis, D., 2000. Contact, Adhesion, and Rupture of Elastic Solids. Springer, Berlin.

Maugis, D., Barquins, M., 1978. Fracture mechanics and the adherence of viscoelastic bodies. J. Phys. D.: Appl. Phys. 11, 1989–2023.

McElhaney, K.W., Vlassak, J.J., Nix, W.D., 1998. Determination of indenter tip geometry and indentation contact area for depth-sensing indentation experiments. J. Mater. Res. 13, 1300–1306.

Miller, R.E., Shenoy, V.B., 2000. Size dependent elastic properties of nanosized structural elements. Nanotechnology 11, 139–147.

Mindlin, R., 1936. Note on the Galerkin and Papkovich stress functions, Bull. Am. Math. Soc. 42, 373–376.

Mindlin, R., 1953. Force at a point in the interior of a semi-infinite solid. 1st Midwestern Conf. Solid Mech. 56–59.

Mindlin, R.D., 1963. Influence of couple-stresses on stress concentrations. Exp. Mech. 3, 1–7.

Mindlin, R.D., 1964. Micro-structure in linear elasticity. Arch. Ration. Mech. Anal. 16, 51–78.

Mindlin, R.D., 1965. Second gradient of strain and surface tension in linear elasticity. Int. J. Solids Struct. 1, 417–438.

Mindlin, R.D., Eshel, N.N., 1968. On first strain-gradient theories in linear elasticity. Int. J. Solids Struct. 4, 109–124.

Mindlin, R.D., Tiersten, H.F., 1962. Effects of couple-stresses in linear elasticity. Arch. Rat. Mech. Anal. 11, 415–448.

Mogilevskaya, S.G., Pyatigorets, A.V., Crouch, S. L., 2011. Green function for the problem of a plane containing a circular hole with surface effects. J. Appl. Mech. 78, 021008.

Muller, V.M., Yushchenko, V.S., Derjaguin, B.V., 1980. On the influence of molecular forces on the deformation of an elastic sphere and its sticking to a rigid plane. J. Colloid Interface Sci. 77, 91–101.

Muller, V.M., Yushchenko, V.S., Derjaguin, B.V., 1982. General theoretical considerations on the influence of surface forces on contact deformations. J. Colloid Interface Sci. 92, 92.

Muller, V.M., Derjaguin, B.V., Toporov, Yu. P. 1983. On two methods of calculation of the force of sticking of an elastic sphere to a rigid plane. Colloids Surf. 7, 251–259.

Nicolson. M.M., 1955. Surface Tension in Ionic Crystals. Proc. R. Soc. A 228, 490–510.

Nix, W.D., Gao, H., 1998. Indentation size effects in crystalline materials: a law for

strain gradient plasticity. J. Mech. Phys. Solids, 46, 411–425.

Nowinki, J. L., 1992. On the three-dimensional Cerruti problem for an elastic nonlocal half-space. J. Appl. Math. Mech. 72, 243–249.

Orowan, E., 1970. Surface Energy and Surface Tension in Solids and Liquids. Proc. R. Soc. A 316, 473–491.

Pashley, M.D., 1984. Further consideration of the DMT model for elastic contact. Colloids Surf. 12, 69–77.

Polyzos D, Tsepoura KG, Tsinopoulos SV, Beskos DE, 2003. A boundary element method for solving 2-d and 3-d static gradient elastic problems. Part I: integral formulation. Comput. Methods Appl. Mech. Engrg. 192, 2845–2873.

Povstenko, Y.Z., 1993. Theoretical investigation of phenomena caused by heterogeneous surface tension in solids. J. Mech. Phys. Solids 41, 1499–1514.

Qu, S., Huang, Y., Nix, W.D., Jiang, H., Zhang, F., Hwang, K.C., 2004. Indenter tip radius effect on the Nix–Gao relation in micro- and nanoindentation hardness experiments. J. Mater. Res. 19, 3423–3434.

Read, D.T., 1998. Tension-tension fatigue of copper thin films. Int. J. Fatigue 20, 203–209.

Roberts, A.D., 1968. Ph.D. dissertation, Cambridge University, England.

Segedin, C.M., 1957. The relation between load and penetration for a spherical punch. Mathematika 4, 156–161.

Selvadurai, A.P.S., 2000. Partial Differential Equations in Mechanics 2- the Biharmonic Equation Poisson Equation. Springer-Verlag, Berlin Heidelburg.

Selvadurai, A.P.S., 2007. The analytical method in geomechanics. Appl. Mech. Rev. 60, 87–106.

Sharma, P., Ganti, S., 2004. Size-dependent Eshelby's tensor for embedded nano-inclusions incorporating surface/interface energies. J. Appl. Mech. 71, 663–671.

Sharma, P., Ganti, S., Bhate, N., 2003. Effect of surfaces on the size-dependent elastic state of nano-inhomogeneities. Appl. Phys. Lett. 82, 535–537.

Shchukin, V.A., Bimberg, D., 1999. Spontaneous ordering of nanostructures on crystal surfaces. Rev. Mod. Phys. 71, 1125–1171.

Shenoy, V.B., 2002. Size-dependent rigidities of nanosized torsional elements. Int. J. Solids Struct. 39, 4039–4052.

Shi, M.X., Huang, Y., Hwang, K.C., 2000. Fracture in the higher-order elastic continuum. J. Mech. Phys. Solids 48, 2513–2538.

Shodja, H.M., Tehranchi, A., 2010. A formulation for the characteristic lengths of fcc materials in first strain gradient elasticity via the Sutton–Chen potential. Phil. Mag. 90, 1893–1913.

Shuttleworth, R., 1950. The surface tension of solids. Proc. Phys. Soc. A 63, 444–457.

Sneddon, I.N., 1965. The relation between load and penetration in the axisymmetric Boussinesq problem for a punch of arbitrary profile. Int. J. Eng. Sci. 3, 47–57.

Spence, D.A., 1968. Self similar solutions to adhesive contact problems with incremental loading. Proc. Roy. Soc. A 305, 55–80.

Stelmashenko, N.A., Walls, M.G., Brown, L.M., Milman, Yu.V., 1993. Microindentation on W and Mo oriented single crystals: an STM study. Acta

Metall. Mater. 41, 2855–2865.

Sternberg, E., 1960. On the integration of the equations of motion in the classical theory of elasticity. Arch. Rat. Mech. Anal. 6, 34–50.

Streitz, F.H., Cammarata, R.C., Sieradzki, K., 1994. Surface-stress effects on elastic properties. I. Thin metal films. Phys. Rev. B 49, 10699–10706.

Swadener, J.G., George, E.P., Pharr, G.M., 2002. The correlation of the indentation size effect measured with indenters of various shapes. J. Mech. Phys. Solids 50, 681–694.

Tabor, D., 1977. Surface forces and surface interactions. J. Colloid Interface Sci. 58, 2–13.

Tabor, D., Winterton, R.H.S., 1969. The direct measurement of normal and retarded van der waals forces. Proc. R. Soc. Lond. A 312, 435–450.

Thomson, R., Chuang, T.-J., Lin, I.-H., 1986. The role of surface stress in fracture. Acta Metallurgica 34, 1133–1143.

Toupin, R.A., 1962. Elastic materials with couple-stress. Arch. Ration. Mech. Anal.11, 385–414.

Toupin, R.A., 1964. Theory of elasticity with couple-stresses. Arch. Rat. Mech. Anal. 17, 85–112.

Truesdell, C., 1959. Invariant and complete stress functions for general continua. Arch. Rat. Mech. Analysis 4, 1–29.

Tymiak, N.I., Kramer, D.E., Bahr, D.F., Gerberich,W.W., 2001. Plastic strain and strain gradients at very small indentation depths. Acta Mater. 49, 1021–1034.

Vardoulakis, I., Exadaktylos, G., Aifantis, E., 1996: Gradient elasticity with surface energy: Mode-III crack problem. Int. J. Solids Struct. 33, 4531–4559.

Wang, G. F., Feng, X. Q., 2007. Effects of surface stresses on contact problems at nanoscale. J. Appl. Phys. 101, 013510.

Woirgard, J., Audurier, V., Tromas, C., 2008. Elastic stress field beneath an arbitrary axisymmetric punch. Phil. Mag. 88, 1511–1523.

Xue, Z., Huang, Y., Hwang, K.C., Li, M., 2002. The influence of indenter tip radius on the micro-indentation hardness. J. Eng. Mater. Technol. 124, 371–379.

Yang, F.Q., 2004. Size dependent effective modulus of elastic composite materials: spherical nanocavities at dilute concentrations. J. Appl. Phys. 95, 3516–3520.

Yao, H., Ciavarella, M., Gao, H., 2007. Adhesion maps of spheres corrected for strength limit. J. Colloid Interface Sci. 315, 786–790.

Yvonnet, J., Quang, H.Le, He, Q.-C., 2008. An XFEM/level set approach to modelling surface/interface effects and to computing the size-dependent effective properties of nanocomposites. Comput. Mech. 42,119–131.

Zhang, G.P., Sun, K.H., Zhang, B., Gong, J., Sun, C., Wang, Z.G., 2008. Tensile and fatigue strength of ultrathin copper films. Mater. Sci. Eng. A 483–484, 387–390.

Zhao, X.J., Rajapakse, R.K.N.D., 2009. Analytical solutions for a surface-loaded isotropic elastic layer with surface energy effects. Int. J. Eng. Sci. 47, 1433–1444.

Zheng, Z., Yu, J., 2007. Using the Dugdale approximation to match a specific interaction in the adhesive contact of elastic objects. J. Colloid Interface Sci. 310, 27–34.

Zhou, D., Bo Jin, B., 2003. Boussinesq–Flamant problem in gradient elasticity with surface energy. Mech. Res. Commun. 30, 463–468.

Zhou, S.-S., Gao, X.-L., He, Q.-C., 2011. A unified treatment of axisymmetric adhesive contact problems using the harmonic potential function method. J. Mech. Phys. Solids 59, 145–159.

APPENDIX

For axisymmetric contact problems, by defining $\xi_1 = \xi\cos\theta$, $\xi_2 = \xi\sin\theta$, $x_1 = r\cos\varphi$, and $x_2 = r\sin\varphi$ one has $\xi_\alpha x_\alpha = \xi r\cos(\theta-\varphi)$. Accordingly the double Fourier transform can be rewritten as

$$f(x,y) = \frac{1}{4\pi^2}\int_0^\infty\int_0^{2\pi} \bar{f}(\xi,\theta)\xi e^{\mathrm{i}\xi r\cos(\theta-\varphi)}d\theta d\xi. \tag{A.1}$$

For a function $\bar{f}$ that is θ-independent, we obtain by using the periodic nature

$$F^{-1}[\bar{f}(\xi)] = \frac{1}{4\pi^2}\int_0^\infty\int_0^{2\pi} \bar{f}(\xi)\xi e^{\mathrm{i}\xi r\cos\theta}d\theta d\xi. \tag{A.2}$$

The integral definition for Bessel function of the first kind is (Abramowitz and Stegun, 1964, pp360)

$$J_n(x) = \frac{\mathrm{i}^{-n}}{\pi}\int_0^\pi e^{\mathrm{i}x\cos\theta}\cos(n\theta)\mathrm{d}\theta, \tag{A.3}$$

and application of the periodic nature leads to

$$J_n(x) = \frac{\mathrm{i}^{-n}}{2\pi}\int_{-\pi}^{\pi} e^{\mathrm{i}x\cos\theta}\cos(n\theta)\mathrm{d}\theta = \frac{\mathrm{i}^{-n}}{2\pi}\int_0^{2\pi} e^{\mathrm{i}x\cos\theta}\cos(n\theta)\mathrm{d}\theta. \tag{A.4}$$

It follows from Eq. (A.4) that

$$\begin{aligned} J_0(x) &= \frac{1}{2\pi}\int_0^{2\pi} e^{\mathrm{i}x\cos\theta}\,\mathrm{d}\theta, \\ J_1(x) &= -\frac{\mathrm{i}}{2\pi}\int_0^{2\pi} e^{\mathrm{i}x\cos\theta}\cos\theta\mathrm{d}\theta, \\ J_2(x) &= -\frac{1}{2\pi}\int_0^{2\pi} e^{\mathrm{i}x\cos\theta}\cos(2\theta)\mathrm{d}\theta. \end{aligned} \tag{A.5}$$

Use of Eq. (A.5a) in Eq. (A.2) yields

$$F^{-1}[\,\overline{f}(\xi)] = \frac{1}{2\pi}\int_0^{\infty} \overline{f}(\xi)\xi J_0(\xi r)d\xi. \tag{A.6}$$

If a function in Fourier domain can be expressed as $\overline{f}(\xi)\xi_1$, then its inverse Fourier transform is given by

$$\begin{aligned} F^{-1}[\,\overline{f}(\xi)\xi_1] &= \frac{1}{4\pi^2}\int_0^{\infty}\int_0^{2\pi} \overline{f}(\xi)\xi^2 \cos\theta e^{\mathrm{i}\xi r\cos(\theta-\varphi)}d\theta d\xi \\ &= \frac{1}{4\pi^2}\int_0^{\infty} \overline{f}(\xi)\xi^2 \int_{-\varphi}^{2\pi-\varphi} \cos(t+\varphi)e^{\mathrm{i}\xi r\cos t}dtd\xi \\ &= \frac{1}{4\pi^2}\int_0^{\infty} \overline{f}(\xi)\xi^2 \int_{-\varphi}^{2\pi-\varphi} \left(\cos t\cos\varphi - \sin t\sin\varphi\right)e^{\mathrm{i}\xi r\cos t}dtd\xi \\ &= \frac{\cos\varphi}{4\pi^2}\int_0^{\infty} \overline{f}(\xi)\xi^2 \int_{-\varphi}^{2\pi-\varphi} \cos t e^{\mathrm{i}\xi r\cos t}dtd\xi, \end{aligned} \tag{A.7}$$

since $\int_{-\varphi}^{2\pi-\varphi} \sin t e^{\mathrm{i}\xi r\cos t}dt = 0$. Substituting Eq. (A.5b) into Eq. (A.7) one obtains

$$F^{-1}[\,\overline{f}(\xi)\xi_1] = \mathrm{i}\frac{x_1}{2\pi r}\int_0^{\infty} \overline{f}(\xi)\xi^2 J_1(\xi r)d\xi. \tag{A.8}$$

In a similar fashion, one can obtain

$$F^{-1}[\,\overline{f}(\xi)\xi_2] = \mathrm{i}\frac{x_2}{2\pi r}\int_0^{\infty} \overline{f}(\xi)\xi^2 J_1(\xi r)d\xi. \tag{A.9}$$

For $\overline{f}(\xi)\xi_1\xi_2$ and $\overline{f}(\xi)\xi_1^2$ it can been shown that

$$\begin{aligned} F^{-1}[\,f(\xi)\xi_1\xi_2] &= \frac{1}{4\pi^2}\int_0^{\infty}\int_0^{2\pi} \overline{f}(\xi)\xi^3 \cos\theta\sin\theta e^{\mathrm{i}\xi r\cos(\theta-\varphi)}d\theta d\xi \\ &= \frac{1}{8\pi^2}\int_0^{\infty} \overline{f}(\xi)\xi^3 \int_{-\varphi}^{2\pi-\varphi} \left(\sin 2t\cos 2\varphi + \sin 2\varphi\cos 2t\right)e^{\mathrm{i}\xi r\cos t}dtd\xi \\ &= \frac{\sin 2\varphi}{8\pi^2}\int_0^{\infty} \overline{f}(\xi)\xi^3 \int_0^{2\pi} \cos 2t e^{\mathrm{i}\xi r\cos t}dtd\xi, \end{aligned} \tag{A.10}$$

$$
\begin{aligned}
F^{-1}[f(\xi)\xi_1^2] &= \frac{1}{4\pi^2}\int_0^\infty \int_0^{2\pi} \overline{f}(\xi)\xi^3 \cos^2\theta e^{\mathrm{i}\xi r\cos(\theta-\varphi)} d\theta d\xi \\
&= \frac{1}{8\pi^2}\int_0^\infty \overline{f}(\xi)\xi^3 \int_{-\varphi}^{2\pi-\varphi} \left(1+\cos 2t\cos 2\varphi - \sin 2\varphi \sin 2t\right) e^{\mathrm{i}\xi r\cos t} dt d\xi \\
&= \frac{1}{8\pi^2}\int_0^\infty \overline{f}(\xi)\xi^3 \int_0^{2\pi} \left(1+\cos 2t\cos 2\varphi\right) e^{\mathrm{i}\xi r\cos t} dt d\xi \\
&= \frac{1}{8\pi^2}\int_0^\infty \overline{f}(\xi)\xi^3 \int_0^{2\pi} \left[1+\cos 2t\left(2x_1^2 r^{-2}-1\right)\right] e^{\mathrm{i}\xi r\cos t} dt d\xi,
\end{aligned}
\tag{A.11}
$$

where use has been made of the fact that

$$
\int_{-\varphi}^{2\pi-\varphi} \sin 2t e^{\mathrm{i}\xi r\cos t} dt = -2\int_{-\varphi}^{2\pi-\varphi} \cos t e^{\mathrm{i}\xi r\cos t} d\cos t = 0 .
$$

Using Eq. (A.5c) in Eqs. (A.10) and (A.11) yields

$$
F^{-1}[f(\xi)\xi_1\xi_2] = -\frac{x_1 x_2}{2\pi r^2}\int_0^\infty \overline{f}(\xi)\xi^3 J_2(\xi r) d\xi, \tag{A.12}
$$

$$
F^{-1}[f(\xi)\xi_1^2] = \frac{1}{4\pi}\int_0^\infty \overline{f}(\xi)\xi^3 \left[J_0(\xi r) - (2x_1^2 r^{-2}-1) J_2(\xi r)\right] d\xi. \tag{A.13}
$$

Analogous result can be obtained for $F^{-1}[f(\xi)\xi_2^2]$ by replacing x_1 with x_2 in Eq. (A.13).

VITA

Name:	Songsheng Zhou
Address:	Department of Mechanical Engineering Texas A&M University College Station, Texas 77843-3123
Email Address:	songsheng.zhou@gmail.com
Education:	B.Sc. in Automotive Engineering Wuhan University of Technology, China, 2006
	M.Sc., in Automotive Engineering Wuhan University of Technology, China, 2009
	Ph.D. in Mechanical Engineering Texas A&M University, U.S., 2011